Design and Fabrication of Antenna Structures for Wireless Body Area Network and Testing on A Phantom

A Thesis Submitted in Fulfilment of the Requirement for the Award of the Degree of

Doctor of Philosophy

Submitted By

Anupma

Registration No.: 901606027

Under the Supervision of

Dr. Ankush Kansal

Associate Professor, ECED

TIET, Patiala

Dr. Paras Chawla

Professor, ECED

CU, Mohali

THAPAR INSTITUTE
OF ENGINEERING & TECHNOLOGY
(Deemed to be University)

ELECTRONICS AND COMMUNICATION ENGINEERING DEPARTMENT

THAPAR INSTITUTE OF ENGINEERING AND TECHNOLOGY, PATIALA-147004

February 2021

CERTIFICATE

I, Anupma hereby certify that the thesis entitled, **"Design and Fabrication of Antenna Structures for Wireless Body Area Network and Testing on A Phantom"** in fulfilment of the requirement for the award of degree of "Doctor of Philosophy" submitted to the Department of Electronics and Communication Engineering, Thapar Institute of Engineering and Technology, Patiala is an authentic record of work carried out under the supervision of Dr. Ankush Kansal, Associate Professor, ECED, TIET, and Dr. Paras Chawla, Professor, ECED, Chandigarh University.

The matter presented in this thesis has not been submitted either in part or full to any other university or institute for the award of any other degree.

Date: 17-05-2021

Anupma
Reg. No. 901606027

This is to certify that the above statement made by the candidate is correct and true to the best of my knowledge and belief.

Dr. Ankush Kansal,
Associate Professor,
Department of ECE,
TIET, Patiala

Dated: 17-05-2021

Dr. Paras Chawla,
Professor,
Department of ECE,
CU, Chandigarh

Dated: 17-05-2021

ABSTRACT

Wireless Body Area Network (WBAN) is an ongoing research field that enables the transmission of biological signals from human body to an off-body device for further processing and action. Compact antennas with stable on-body behaviour are achieving interest for signal transmission for WBAN applications. Advancements of flexible electronic devices and sensor nodes has demanded conformal antenna structures for the wearable devices. Moreover, human body is a non-planar structure and endures various postures and movements. Use of stiff material for making on-body antenna may cause uneasiness to the user. In addition to this, antenna performance is unavoidably exposed by the user's movement. Thus, antenna must have stable resonance and impedance while structural deformations. Beside this, body tissue is also affected by the exposure of near field radiations which needs to follow safety regulations. The existing on-body antenna structures still grieves from number of challenges like complex and comparatively bigger structures, highly immune to body tissue, low efficiency and gain, narrow bandwidth and unstable performance. The work presented in this thesis has concentrated on the two main aspects of antenna technology: design of new structures for on-body data transfer applications and presenting the applications of antenna in medical sector.

Design, realization and performance evaluations of five antenna topologies for on body and off body communication is presented. In the first design a conformal, wide band, MIMO antenna is proposed for on body and off body data transfer application. Inverted U-shaped slot is deployed at the ground plane for reducing mutual coupling between the two radiators. This antenna has the excellent diversity performance, possess wide bandwidth and it can easily withstand frequency detuning effect due to structural deformation. Antenna has compact planar dimensions of 14 mm × 25 mm and less than -30 dB mutual coupling. In the second structure, dual band resonance with high gain is achieved. Metallic reflector is used to match antenna impedance and for providing isolation between body tissue and antenna radiations. Antenna has stable frequency response along x-axis bending. With metallic back reflector antenna has good radiation characteristics for lower and upper ISM bands. It provides broadside and unidirectional radiation pattern for reliable on body to off body communication. Antenna has gain value of 6.31 dBi and 8.75 dBi. In the third structure, a defected ground patch is designed for on to off body communication. To reduce the coupling effect of body tissue on antenna performance, I-shaped AMC structure is added with the

antenna. It enhances antenna radiation characteristics and reduced the specific absorption rate value. Numerical simulation is done for observing the bending effect on antenna performance. After adding of AMC structure 65% of on-body radiation efficiency is obtained with bandwidth of 600 MHz. Performance of all the antenna structures is validated through lab testing on phantom tissue. Specific absorption rate is evaluated through numerical simulation. as compared to the on-body antennas reported in literature. Flexible antennas have excellent stability of resonance frequency and impedance matching against structural deformation.

Fourth and fifth antenna structures are designed for dual mode operation; on-on and on-off body data transfer. In the fourth design miniaturization and dual band performance is attained through open end slotting. Open end slotted dual mode antenna has omnidirectional and dipole like radiation characteristics at 2.45 GHz and 5.0 GHz which supports dual mode operation. Finally, in the fifth structure, square ring-shaped ground is used to excite multiple resonance mode in the truncated corner radiator. It has covered the bandwidth of ISM, LTE and WLAN bands. It makes antenna more practical for on-body and off-body communication. All the proposed structures are characterized to operate in close proximity of human body, owns smaller footprints, wider -10 dB impedance bandwidth.

Further, an overview of applications of designed antennas in health care domain is presented. Main applications of antennas in close proximity of body are: (a) data transmission from implantable and on-body devices (b) diagnosis of malignant tissue cells by analysing the variation of antenna parameters and (c) treatment of various diseases though thermal ablation therapies. Antenna is the minimally invasive and cost-effective treatment method and amenable to unfavourable tumour locations. A defected ground patch antenna is designed for detection of cancerous cells in breast tissue. Antenna is covering 3.1 GHz to 10.6 GHz UWB spectrum. partial ground plane of conventional patch antenna is modified by etching two slots and adding a narrow vertical strip. A high dielectric constant substrate is added below the antenna, which shows remarkable effect on performance. Backscattered signal variation is processed through ground penetrating radar algorithm to reconstruct microwave image.

Ultimate goal of this research work is to design antennas for different applications in health care system and to improve the overall system performance.

ACKNOWLEDGEMENT

Working on the Ph.D. thesis in the area of antenna technology is one of the most valuable and exciting experiences in my education. The knowledge and experience I gained during the study years will be beneficial for my life. I am greatly indebted to my academic and research advisor, Associate Professor (Dr.) Ankush Kansal, who puts so many efforts in mentoring and helping me in every aspect to complete my thesis on time.

First and foremost, I express my deepest gratitude to my research advisor for his guidance and help throughout my work and for gladly sharing his knowledge and experience. I particularly admire his scientific way of thinking and providing new ideas and extraordinary human qualities. I would like to express my sincere thanks to my co-supervisor, Prof. (Dr.) Paras Chawla, Chandigarh University, for continuous encouragement, guidance, and support through the beautiful academic coursework journey, experiment, and writing the thesis. The insight and vast knowledge of my supervisors guided me to the completion of this research work. Due to their broad research interest, they allowed exploring many exciting applications of antenna for health care systems.

I would like to express my sincere gratitude for the entire administration and management of the Thapar Institute of Engineering and Technology, Patiala, for supporting me in achieving one of the most important goals of my life. I have great pleasure in expressing special thanks and the highest appreciation to my doctoral research committee members Dr. Rajesh Khanna, Professor ECED, Dr. Hari Shankar, Associate Professor, ECED, and Dr. S. Ghosh, Professor, EEID for closely monitoring and sharing their valuable inputs in completing this work. Their watchful way of analytically prompting and monitoring research activities helped me immensely in achieving my objectives.

I express my sincere gratitude to **"Dr. Alpana Aggarwal**" Head of Department, ECED. I am also thankful for the support I received from all the teaching and non-teaching staff for their pleasant cooperation with the students. I want to thank the laboratory staff at Microwave Lab, IIT Kanpur, and Mr. Zamir Ahmad Wani, Research scholar, IIT Delhi, for their valuable support in experimental work.

Finally, I would like to thank all my family members. A special mention to my son Nilesh Kumar and my parents for their moral support, endless care and love under all circumstances. Last but not least, I would not have made till here without the encouragement of my husband, Mr. Vipan Kumar. I am very thankful for motivating me to pursue my higher studies.

ANUPMA

CONTENTS

LIST OF FIGURES

LIST OF TABLES

LIST OF ABBREVIATIONS

2D	Two Dimensional
3D	Three Dimensional
2G	Second Generation
3D	Three Dimensional
3G	Third Generation
7T	Seven Tesla
ADC	Analog to Digital Converter
AMC	Artificial Magnetic Conductor
AP	Access Point
CCL	Channel Capacity Loss
CFT	Copper Foil Tape
CP	Circular Polarization
CPS	Coplanar Strip
CPW	Coplanar Waveguide
CSRR	Complementary Split Ring Resonator
CST	Computer Simulation Technology
CT	Copper Tape
DG	Diversity Gain
DGS	Defected Ground Structure
EBG	Electronic Band Gap
ECC	Envelope Correlation Coefficient
ECG	Electro Cardiograph
EEG	Electroencephalogram
EM	Electromagnetic
ETIS	Electrical Tissue Impedance Spectroscopy
FSS	Frequency Selective Surface
HM	Half Mode
HMSIW	Half Mode Surface Integrated Waveguide
IEEE	Institute of Electrical and Electronics Engineering
IoT	Internet of Things
ISM	Industrial Scientific and Medical

LCP	Liquid Crystal Polymer
LHCP	Left Hand Circular Polarization
LTE	Long Term Evolution
MCU	Microcontroller Unit
MICS	Medical Implant and Communication Systems
MIMO	Multiple Input Multiple Output
MRI	Magnetic Resonance Imaging
MWA	Microwave Ablation
NBR	Nitrile Butadiene Rubber
PAN	Personal Area Network
PBG	Photonic Band Gap
PDMS	Polydimethylsiloxane
PIFA	Planar Inverted-F Antenna
QM	Quasi-Mode
QOS	Quality of Service
QW	Quarter Wave
PCB	Printed Circuit Board
RFA	Radio Frequency Ablation
RHCP	Right Hand Circular Polarization
SAR	Specific Absorption Rate
SHS	Selective Heat Synthering
SIW	Surface Integrated Waveguide
TE	Transverse Electric
TEM	Transverse Electromagnetic
TM	Transverse Magnetic
UHF	Ultra-High Frequency
UWB	Ultra-Wide Band
VNA	Vector Network Analyzer
WBAN	Wireless Body Area Network
WiMAX	Worldwide Interoperability for Microwave Access
WLAN	Wireless Local Area Network
WMI	Microwave Imaging
WMTS	Wireless Medical Telemetry Service

LIST OF SYMBOLS

Symbol	Description
α_{attn}	Attenuation Constant of EM Waves
ε_r	Relative Permittivity
μ	Free space permeability
ε_0	Free space permittivity
ω	Angular Frequency
σ	Conductivity
E	Electric field Intensity
ρ	Tissue Mass Density
$\tan \delta$	Loss Tangent
B0	Static Magnetic Field
χ	Susceptibility
ε_{reff}	Effective Dielectric Constant
ρ_e	Envelope Correlation Coefficient
λo	Free Space Wavelength
π	Pi
$\vec{E}_1(\theta, \phi)$	Radiation Pattern for Port-1
$\vec{E}_2^*(\theta, \phi)$	Complex Conjugate of the Radiation Pattern for Port-2
$K(k_n)$	Elliptical Integral
$K'(k_n)$	Complement of Elliptical Integral
xl	Inductive Reactance
xc	Capacitive Reactance
Q	Quality factor
ε	Absolute Permittivity
c	Speed of Light
ε_{eq}	Equivalent Dielectric Constant
η_{tissue}	Antenna Efficiency on Body Tissue

Chapter-1

INTRODUCTION

1.1 Wireless Body Area Network (WBAN)

WBAN is an emerging technology that aims to simplify design and enhance the communication reliability of sensor nodes deployed in the close locality of the human body. At the beginning of the 20th century, it was the part of Personal Area Network (PAN) protocols [1]. After some years, a Philips's research group marked some distinct features for BAN and unified BAN and PAN as two different networks [2]. Soon, BAN became very popular, and it was found as a critical component of patient-monitoring medical systems [3]. Mobile health project named MobiHealth [4] and research publications by IEEE T-ITB made BAN a well-recognized infrastructure. BAN is extended beyond the sensor connectivity and engrossed with automatic sensing, power scavenging, and intelligent low power microsystems [5]. In this way, BAN emerged as WBAN in 2006 [6].

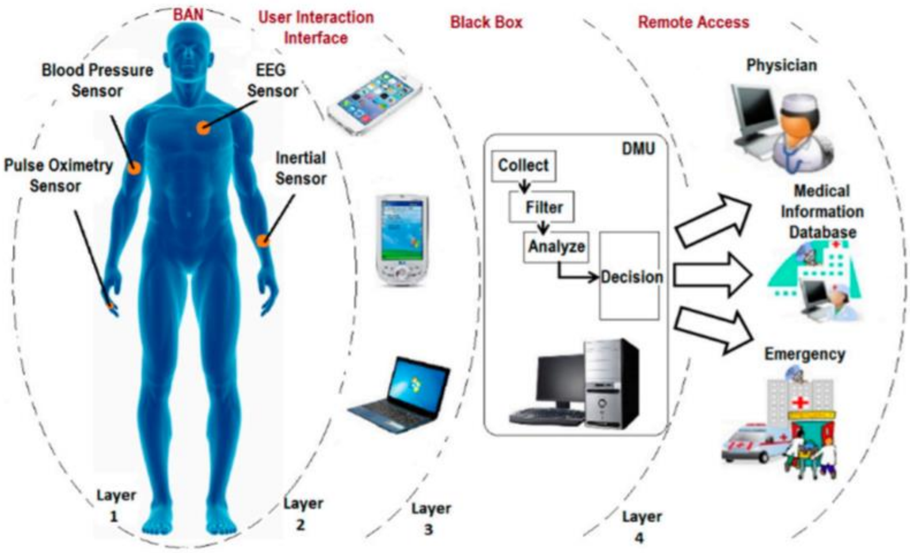

Fig. 1.1 Four-layer communication architecture of WBAN medical system [7]

The concept of WBAN was introduced by Yang [8] and reported it as the most capable technology for providing persistent health monitoring services, early disease detection, and telemedicine design perspective [9]. These services can be accomplished by interconnecting various wireless communication standards and networks with on-body and implanted sensor nodes. The communication architecture of WBAN e-healthcare system is shown in Fig. 1.1. WBAN provides real-time decision-based health information collected by the sensors deployed on or implanted into the human body. WBAN Communication process is divided into four layers:

Layer-1 (Body Area Network): This layer incorporates several sensor nodes inside or outside the body. Physiological parameters like ECG, temperature, heart rate, and glucose level are transmitted from the body sensor node to the external control unit through a short-range, low power wireless link. Based on sensor nodes' functionalities and computation proficiencies, data may require some processing before transmission. Based on the sensors' location, layer-1 communication channels can be categorized into the in-on body, on-on body, and on-off body channels [10]. WBAN communication modes are represented in Fig. 1.2. Signal transmission at layer-1 is exceptionally complex and suffers high attenuation [11].

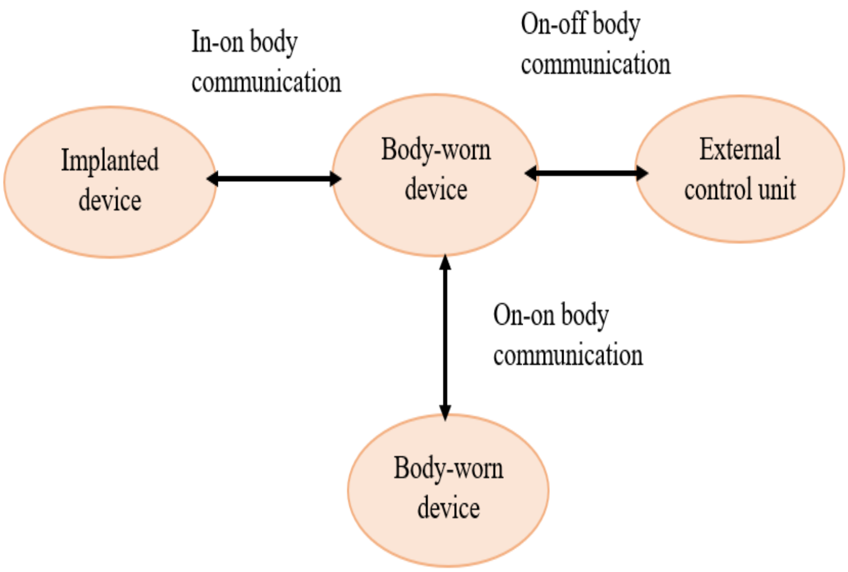

Fig. 1.2 BAN on-body communication modes

Layer-2 (User Interaction Interface): At this communication layer, information stored on a personal server is transmitted to the access points (AP) through Bluetooth, ZigBee, WiMAX, WLAN, and other 3G/4G technologies. Data received at this layer is further sent to the next layer (layer-3) to prepare for future decision making.

Layer-3 (Decision Making Unit): Signal processing of the received data is performed at this layer. The Decision-making unit performs major computation, processes the data, and extracts the information. This information is sent to a hospital where doctors can monitor the patient's health status.

Layer-4 (Remote Access): At this layer, concern doctor has the remote access of patient's health information through a cellular network or the internet. Doctor can determine the health status and provide feedback through intuitive graphical or audio user interface.

1.2 WBAN Standard: IEEE 802.15.6

IEEE 802.15.6 standard is accepted worldwide for body-centric wireless communication. It is attentive towards the short-range transmission with high QOS for in-body or on-body sensor nodes [12]. Maximum allowable transmission power range for WBAN varies from 0.1 mW (-10 dBm) to 1 mW (0 dBm). The bit rate is also limited to 10 Kb/s to 10 Mb/s which restricts the communication range within few meters [13]. Moreover, this standard also defines the safety guidelines (specific absorption rate regulations) to protect the tissue from electromagnetic radiations.

1.3 Applications of WBAN

WBAN covers a wide range of applications. WBAN applications are aimed to improve the user's quality and standard of life. Some medical and non-medical applications of WBAN are listed in Table 1.1.

Table 1.1 Applications of WBAN

Medical Applications	NON- Medical Applications
Blood Pressure, Glucose level & Temperature monitoring	Aiding Professional Sport and military training
Neural Signal Measurement	Entertainment Application
Cardiovascular Diseases	Rescue Operations
Sleep Staging	Location Tracking
Bio-telemetry	Secure Authentication

1.4 Research Motivation

Advanced research of flexible electronic devices and miniaturization of sensor nodes has attained great popularity in the Wireless Body Area Network. Proactive health care and remote health monitoring systems are playing an essential role in our lives because of the fast-living style [14]. These devices can be invasive (implanted inside the body) or non-invasive (worn on the body). Both invasive and non-invasive devices support several applications. Fig. 1.3 shows some applications of implanted devices including brain and gastric stimulators, cochlear and cardiac implants, and insulin pumps etc. [15].

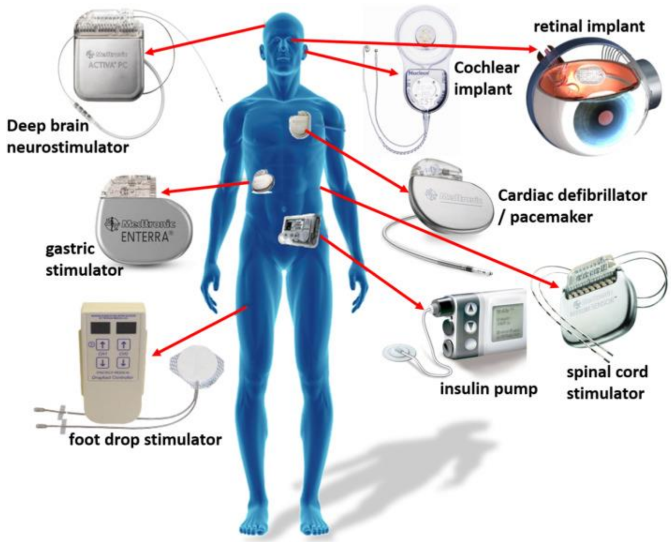

Fig. 1.3 Applications of in-body WBAN devices [15]

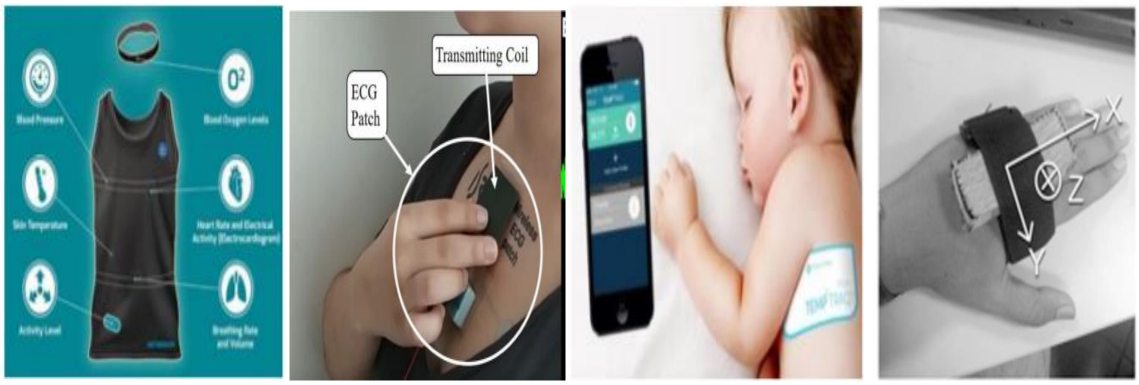

Smart shirt [16] ECG patch [17] Thermometer Patch [18] Motion sensor [19]

Fig. 1.4 Applications of body worn WBAN devices

Fig. 1.4 shows the various applications of body-worn devices include smart shirts, head wearable band for measuring blood pressure, skin temperature, heart, respiration rate [16], tattoo type ECG sensor [17], temperature measuring patch [18], and motion sensors [19]. Information collected by these devices is transmitted to the control unit and send to the doctor through the internet. This process reduces the cost of health care services, saves the time of patient and doctor, and improves the quality of life and comfort level of the user. Antenna is the most critical component of these devices as it establishes a wireless transmission link between on-/in body devices to off-body devices in WBAN.

Communication over the on-body transmission channel is unlike the transmission channel in air. The high conductivity and permittivity of body tissue create a very hostile environment for the transmission of electromagnetic radiations [11].

In WBAN, a large proportion of transmitted power is absorbed by body tissues, the radiated signal gets attenuated, and have high risk of signal lost as compared to the free space communication. Therefore, to establish a reliable communication link, appropriate antenna with prior information of expected on-body channel lost is essentially required. Existing wearable antenna structures are still suffering from some limitations like, large and complex geometrical structures, unstable to structural deformation effects, low bandwidth and poor radiation characteristics. The fast-growing demand for health care devices has stipulated the requirement of flexible, light weight antenna structures with high isolation between body and antenna radiations. Multiband or wideband antenna for on-off body communication mode is the active area of research for improving commercial applications of WBAN and making it more compatible with other communication technologies. The main focus of this thesis is to design conformal, wideband antenna structures for wearable devices and apply in the area of health care systems.

1.5 Antenna Design Issues for On-Body Devices

There are some physical and structural design issues that must be addressed for the on-body wearable antennas. These are summarized as follows:

1.5.1 Tissue Modelling

Ethical and safety issues do not allow antenna testing on an actual human body. Antenna performance is different on bio-tissue, as the human body's electric properties are frequency-dependent and vary dynamic at microwave frequencies. Surrounding body tissues significantly affects the antenna behavior. The antenna's electrical size also the depends on the tissue properties. Also, compared to free space, the resonance frequency is lower on body tissue [20]. Attenuation of electromagnetic radiation varies on different layers of body tissue which also affects antenna radiation characteristics. Attenuation of EM waves (α_{attn} in $\frac{\mathrm{Neper}}{\mathrm{m}}$) on lossy transmission medium is given by [21].

$$\alpha_{attn} = \omega \sqrt{\frac{\mu\varepsilon_0\varepsilon_r}{2}\left(\sqrt{1+\left(\frac{\sigma}{\omega\varepsilon_0\varepsilon_r}\right)^2}-1\right)}$$

(1.1)

Where, ε_0 represents the free space permittivity which is 8.85×10^{-12}F/m, μ represents free space permeability and it is $4\pi\times10^{-7}$ H/m, ε_r represents the relative permittivity of tissue and σ represents the conductivity of tissue in S/m. The values of conductivity and relative permittivity at 2.45 GHz and 5.8 GHz frquencies is given in Table 1.2. Calculated attenuation at 2.45 GHz for fat layer is 75.391 dB/m and for muscle layer is 388.44 dB/m [22]. Large variation in atteuantion level shows that near field radiations of antenna is strongly affected by body.

Table 1.2 Characteristics of tissue layers at 2.4 and 5.8 GHz frequencies [22]

Frequency	Tissue	Loss Tangent	Electrical Permittivity	Conductivity (S/m)
2.4 GHz	Skin	0.28	38	1.44
	Fat	0.14	5.28	0.1
	Muscle	0.24	52.7	1.7
	Bone	0.31	18.6	0.78
5.8 GHz	Skin	0.30	35.7	3.06
	Fat	0.17	4.954	0.24
	Muscle	0.29	48.48	4.96
	Bone	0.4	16	1.84

To characterize the antenna impedance with the human body, the researchers have used different types of the anatomical phantom of real human beings. The body model of a male named Gustav [23] and a female named Ella [24], used for numerical simulation are shown in Fig.1.5. Simulation with the whole body model takes a long time and requires a large system memory. Therefore, the desired part of the phantom body is truncated and used for simulation. In [25], the arm is used for evaluating the on-body antenna performance.

Single and multilayered homogeneous phantom structures with average tissue properties are also modeled to simplify the computational complexity. Fig. 1.6 shows the rectangular [26] and cylindrical [27] shaped canonical geometries of simplified phantoms. The size of the simplified phantom varies from 8.5 mm to 1000 mm [28]. There are several choices for simulation, but restrictions occur during physical testing of the antenna. Tissue-equivalent phantom gels and liquids are prepared to verify the numerically simulated results. Physical phantoms can be prepared for the tissues with high and low permittivity and loss. Tissue with high permittivity (brain, skin, muscle) contains high water content compared to low permittivity tissues like fat and bone [29]. The phantom consists of deionized water, sugar, salt, and flour [30]. Animal tissue is also used for the verification of antenna performance [31]. Physical phantoms used in the literature are displayed in Fig. 1.7 [32,33].

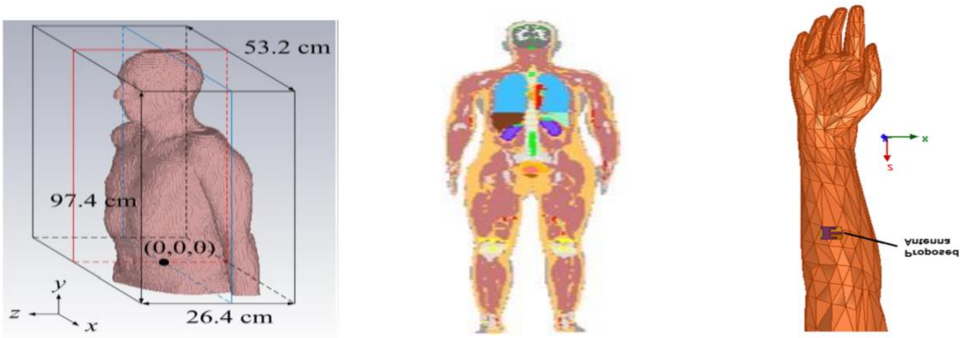

(a) (b) (c)

Fig.1.5 Human model for numeriacl simulations (a) Gutsav model [23] (b) model of Ella [24] (c) truncated hand [25]

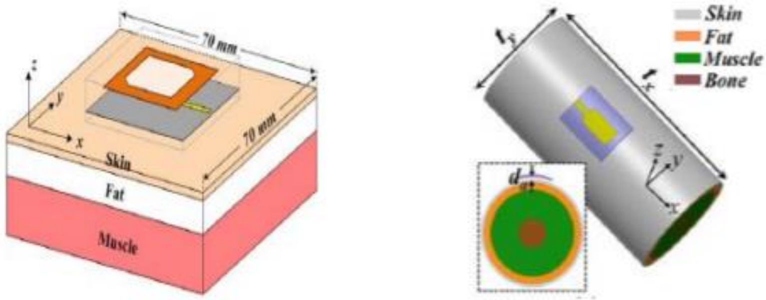

(a) (b)

Fig.1.6 Simplified body phantoms for simulations (a)rectangular [26] (b)cylindrical [27]

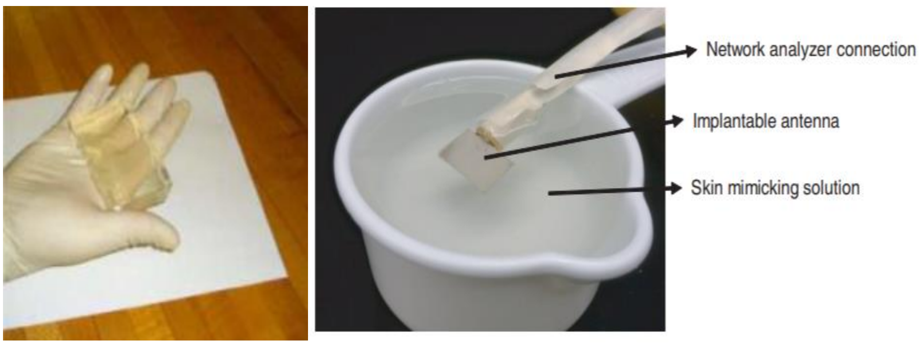

(a) (b)

Fig.1.7 Physical tissue phantoms (a) gel phantom [32] (b) liquid phantom [33]

1.5.2 Frequency Selection

Different authorities have projected different operating frequency bands to adhere to the services of WBAN [8]. In Table 1.3, characteristics of available frequency bands for on-body communication are summarized.

Table1.3 Frequency bands for wireless body area network [8,21,34]

Band Acronym	**Frequency (in MHz)**	**Advantages**	**Restrictions**
Med Radio (Medical Device Radio Communication)	401-406, 413-419, 426-432, 438-444, 451-457	Available globally, quiet channel, good propagation characteristics , only for medical applications	Requires large antenna size and limited bandwidth available
WMTS "(Wireless Medical Telemetry Service)"	608-614, 1395-1400, 1427-1432	Available only for medical applications, good propagation characteristics, medium data rate	Limited spectrum, used heavily, avalable in USA only
ISM (Industrial Scientific and Medical)	433.1-434.8, 868-868.6	Used for general telemetry	Available in Europe only, crowded spectrum, low bandwidth
	2400-2483.5, 5725-5875	Available globally, require small antenna, scalable bandwidth utilization and medium data rate	Coexistence with many other technologies and communication standard
MICS (Medical Implanted Communication Service)	402-405	Available globally, good propagation characteristics	Only for in-body communication, large antenna size and low data rate
UWB (Ultra Wide Band)	3100-10600	Available globally, high data rate, low power requirement and large bandwidth	Coexistence with high data rate network stndards, large attenuation

Frequency selection for on-body communication also has some trade-offs. At lower frequencies, signal attenuation is less with low bandwidth which reduces the data rate. Moreover, at low frequency antenna size is very large. On the other side, high frequencies allow wide bandwidth, high data rate, and smaller antenna geometry. However, these antennas suffer from large attenuation [21]. Based on these trade-offs, frequency range of ISM band is opted for designing the antenna for the present research work.

1.5.3 Wide Bandwidth

Bandwidth specifies the frequency spectrum at which antenna is tuned to radiate the power. Range of frequencies that has below -10 dB reflection coefficient (|S11|) is termed as input impedance bandwidth. Conducting body tissue interacts with the surface current of antenna and disturbs the antenna impedance. In addition, when antenna is operated on different human body, resonance frequency may detune due to varying thickness of tissue layers. Thus, to enhance the practical utilization of on-body antenna, wideband antenna structures with low reflection coefficient need to be designed. Bandwidth can be enhanced by generating multiple resonance paths through etching of slots [35], adding parasitic patch [36], and staircase shape slot excitation of radiator [37].

1.5.4 Stability to Structural Deformation

Human body is a non-planar structure. Antenna with different shapes is required to operate on different body parts. Besides this, several textile materials are used to design the wearable antenna, which are easily subjected to wrinkling and crumpling. Conformal structures should be designed so that antenna can withstand structural deformation along various radii. Stability to structural deformation can be improved by using thin flexible substrates with good mechanical strength such as Rogers 5880 [27], Copper Plated Polyester Textile [38], and Ceramic filled PTFE based RO3010 [39]. The robustness of antenna can be enhanced by designing multi-layered structures [40].

1.5.5 High Gain and Efficiency

Significant power is absorbed by body tissue which reduces antenna gain and efficiency. It limits the transmission range of antenna to a few meters. Also, absorbed power may damage the body tissue. Therefore, an antenna with a wide beam power and gain pattern normal to body surface or with null towards the body tissue should be designed. Unidirectional radiation pattern for off-body transmission mode can be attained by using full ground plane below the antenna [41]. Integration of metamaterial structures [42,43], and placing metallic back reflectors [44] at a distance from the radiator etc. are some of the techniques which enhances the antenna gain and efficiency.

1.5.6 Miniaturization

Limited space is available on the sensor node chip for the antenna. Thus, compact size antenna is required for on-body devices. Researchers have used different miniaturization technique such as use of split ring-shaped radiator geometries [45], adding epsilon-shaped dielectric resonator [46], creating reactance coupling effect [47], etching of slots in patch and ground plane [46,48,49] to reduce the size of in/on body antennas.

1.5.7 Safety Guidelines

To ensure the tissue safety, Specific Absorption Rate (SAR) provides the limit to the maximum allowable incident power to the on-body antenna. Maximum SAR value of 2 W/kg (over 10-g tissue) and 1.6 W/Kg (over 1-g tissue) is stipulated [50, 51] by IEEE regulations. SAR is directly varied with electric field (E), tissue conductivity (σ), and tissue mass density (ρ) which is given by Equation (1.2).

$$\mathrm{SAR} = \int \frac{\sigma(r)|E(r)|^2}{\rho(r)}\, dr \tag{1.2}$$

In [52] radiation pattern is modified by replacing the uniform width spiral patch with a non-uniform width patch. SAR value for the input power of 1W was reduced by 100 W/kg in 1 gram of body tissue. Metamaterial reflector was added in [53] for reducing SAR value and improving gain.

The study of the above-mentioned issues shows that designing an on-body antenna structure is very challenging. Any design issue cannot be separated as performance of one factor is affected by another factor.

1.6 Organization of Thesis

In this thesis, design of the antennas for on body and off body communication mode of WBAN are presented. Also, the applications of antenna technology in the health care systems are addressed. Besides this, antenna design issues are studied and summarized. Based on the issues of data transmission applications, novel, compact and wideband antenna structures are designed in this thesis work. The thesis is organised as summarized below:

Chapter 1: The first chapter gives a brief introduction of wireless body area network architecture and standards. It also describes the application of WBAN, and research motivations. All of the significant factors which affect the performance of on-body wearable antennas are also described briefly.

Chapter 2: This chapter covers the comprehensive literature survey of different types of antenna proposed for on-body devices. It describes the different techniques and methods used to overcome the issues of wearable antennas. It represents the geometrical description, on-body simulation, measurement setup, research contribution, and antenna application. Single and dual-band antennas are reported for on-on and on-off body communication. A wide range of antenna technology like SIW, PIFA, Monopole, Dipole, Patch, and Yagi Uda are referred for wearable devices. Research gaps, restrictions of the reported antennas, objective of the thesis, and research methodologies are also mentioned in this chapter.

Chapter 3: This chapter describes the design, simulation, and testing of a compact, wideband, conformal MIMO antenna structure for on-off body communication. First, a single radiator antenna is designed and characterized by simplified body tissue. The ground of antenna is modified for impedance matching and bandwidth enhancement. Second, a dual radiator MIMO antenna is designed, an inverted U-shaped stub is added as a parasitic resonator to improve the performance of MIMO operation. Assessment of the proposed antenna is carried out on the pork tissue for the flat and bent states. Diversity performance is calculated mathematically from the radiation characteristics.

Chapter 4: The design of two flexible antenna structures with high gain and improved radiation efficiency is presented in this chapter. In first design, L-shaped radiator is excited by a coplanar waveguide feed and an L-shaped ground plane. Antenna is tuned to dual-band resonance with the help of a metallic reflector. In addition, antenna gain and radiation efficiency are also improved by this reflector. In the second design performance of a single band patch antenna is enhanced by using a 2×2 array of AMC unit cell. Significant improvement in gain and reduction in SAR value is achieved with this topology. Both designs have stable impedance matching, unidirectional radiation patterns, and low SAR value.

Chapter 5: This chapter elaborates on the design and performance of two different antenna topologies for dual-band operation. The antenna supports dual-mode communication: the on-on body at 2.45 GHz and on-off body at 5.0 GHz. In first design, an open-end slotted patch antenna, and in second design a ground-coupled radiator-based antenna is designed. Slotting in patch contributes to generate dual-band resonance and perturbates surface current. Ground coupling excited multiple resonance path that enhances antenna bandwidth. The performance of both the designed antennas are evaluated in free space and on the fabricated physical phantom. First design shows omnidirectional and dipole like pattern diversity, and second design shows dipole and broadside radiation pattern for dual-mode operation.

Chapter 6: This chapter covers the basic design fundamentals of anteena design which affects the antenna performance. This chapter also covers the significant roles of antenna in WBAN and medical systems like data transfer from on/in body to off body devices, diagnosis, and treatment. Antenna far-field radiation contributes to transmit the biological signals from invasive and non-invasive sensor nodes to the external devices. Antenna technology provides major benefit of interconnecting wearble sensor nodes wireless. Near field radiations allow sensing of body functioning by observing the variation in antenna parameters on healthy and unhealthy tissue. Moreover, the antenna technology has a successful contribution to curing life-threatening diseases like cancer, tumors, and gastro-oesophageal reflux disease. This survey provides a detailed evaluation of options and challenges for antenna designing required for IoT (Internet of Things) and future wearable and implantable devices. In addition to this a defected ground UWB antenna with dielectric reflector is designed and its performance is analysed for breast cancer detection. Backscattered signal of the propesed antenna structure is used to detect the presence of uhealthy cells in breast. Ground penetrating radar (GPR) algorithm is used to localize the tumour depth of radius 4 mm in breast tissue. The designed antenna has shown considerable performance for the detection of unhealthy cells and can pave the way to save lives.

Chapter 7: Finally, conclusions of the research work performed in this thesis is summarized in this chapter. It also draws the achievement of the designed antenna. The idea for the future scope of antenna technology in wireless body area networks and medical system sensor nodes is included.

Chapter-2

Literature Survey

2.1 Introduction

Wireless body area network is getting more attention in the healthcare domain as people are adapted more to the reckless living style. They are susceptible to incurable ailments due to ignorance of regular health examinations. Therefore, WBAN based proactive health management devices have provided a valuable contribution to improve the quality of life. As it is well known that antenna is an essential part of a wireless system. Several modifications have been performed to enhance antenna performance in terms of miniaturization, bandwidth enhancement, reducing power coupling in body tissue, directivity enhancement, shape determination, and improving biocompatibility. Therefore, to start designing on-body conformal antenna structures, bottomless knowledge of existing antennas is essential. A brief review of different antenna designs/topologies used for WBAN is presented in this chapter.

2.2 Antennas for Bio-telemetry Applications

Wireless telemetry is the way of measuring of signals through the sensor nodes deployed on body and transmitting required data through RF communication link to a base station (phone or personal computer) located at a distance from the body. Further this data is transmitted to the doctor or concern person via internet for diagnosis and to advice the patient accordingly. Fig. 2.1 represents the block diagram of a BAN sensor module. Physiological signals obtained by using sensors are post processed and transmitted to external control device.

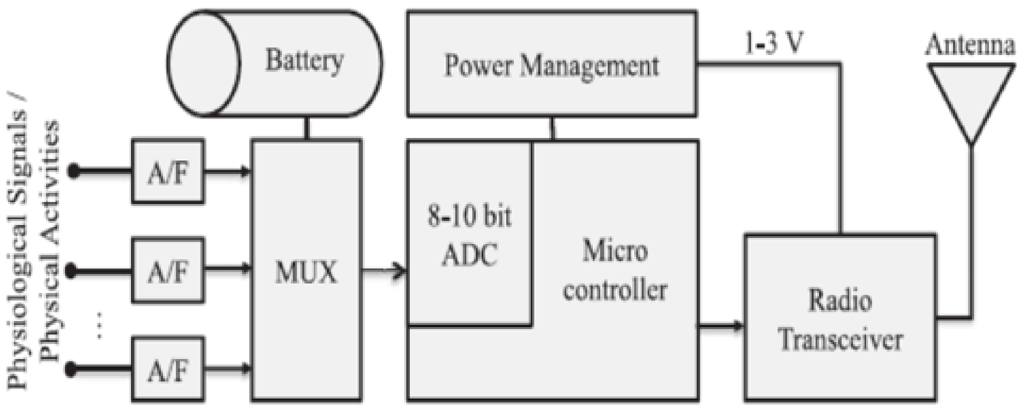

Fig. 2.1 Block diagram of Wireless Sensor Module [54]

WBAN systems consist of medical sensors, microcontrollers, battery, transceiver and base station with antenna. A multiplexer is then used to provide switching between each sensor node if more than one sensor signal is required. An analog to digital convertor (ADC) is required in a sensor module to convert the signal in digital format for signal processing. The microcontroller is required to code the data before transmitting to a radio transceiver [177]. Signals obtained from the human body are usually very weak and noisy. It is required to amplify and filter (A/F) these signals before transmission.

In bio-telemetry applications, antenna is integrated with sensor node. Sensor nodes are placed on or implanted in different organs of human body. It is very difficult for antenna to maintain its robustness in heterogenous bio environment. Thus, different design issues arise with the location of operation. Based on the location, bio-telemetry antennas can be classified as wearable and implantable antenna, and endoscopy capsule antenna.

2.2.1 Survey of Antennas for On-Body and Off-Body Communication Modes

Tak *et al.* [36] had proposed a circular patch, textile antenna. Two shorting pins were added to generate higher-order resonance mode. The conductive thread was embroidered on the felt substrate to design shorting pins. 2/3 muscle equivalent phantom model was fabricated for experiment. The antenna showed null below the antenna, which reduced the SAR value of antenna. Low gain and radiation efficiency had been observed due to conductive textile and fir substrate.

Bai *et al.* [37] had investigated the performance of the textile patch antenna for crumpling and bending. A partially grounded PIFA was first designed using Zelt as conducting material and Felt as substrate material. The separation gap between the microstrip feed line and the shorting stub was adjusted to achieve 50-ohm impedance matching at 2.45 GHz. Results under flat and crumpled state were studied for resonance frequency, gain, and efficiency. Maximum 130 MHz shifts of center resonance, 2 dB gain improvement, and 12% radiation efficiency enhancement were observed against crumpling.

Abbasi *et al.* [40] had proposed a monopole antenna at ISM band for BAN devices. The antenna was designed by printing a monopole radiator on one side of the substrate and a 2×1 EBG structure and partial ground plane on the opposite side. A conducting metal plate was placed under the antenna as a reflector for gain enhancement. The unit cell reflection coefficient was also evaluated. Antenna showed stable and robust performance when tested on different human body positions and subjected to structural deformation. Antenna was characterized for gain, efficiency, radiation pattern, and return loss for both free space and on body tissue operation.

Yan *et al.* [43] had designed a SIW technology-based dual-band textile antenna for on-body MIMO application. The fundamental cavity was used to excite TM_{110} mode for lower 2.45 GHz resonance. Two perpendicular arms of the rectangular cavity were shorted, and with the help of a via TM_{210} and TM_{120} modes were combined to achieve wide bandwidth for covering WLAN band. Six orientations of 2×1 array radiator was analyzed, and the least mutual coupling was obtained when two radiating elements were rotated over 180 degrees with respect to each other.

Kwak *et al.* [55] had proposed an antenna system in which slotted metamaterial was embedded in the planar inverted-F antenna. Antenna covered a wide band-code division-multiple-access band at the center resonance of 1.7 GHz. Metamaterial structure was used to reduce the SAR value. 43.2% of SAR reduction was achieved with 5 dB gain value. SAR was measured experimentally on a flat artificial phantom in the ETRI chamber with an MR900W test kit. The measurement probe measured the electric field, and the SAR value was calculated using a computer system.

Gil *et al.* [56] had designed a PIFA structure on the Jeans substrate. The antenna ground plane was sandwiched between two different dielectric materials to improve the on-body performance. The placing of two substrates had contributed to the improvement of radiation efficiency (23.1 to 29.1%) and gain (0.70 dBi to 1.98 dBi). The biocompatibility of antenna was also enhanced as it avoided the direct contact of metal and the human body. Pure silver-plated nylon yarn was used to stitch the radiator using an embroidery machine, and the adhesive copper tape was used for the ground plane.

Soh and Vandenbosch [57] had presented a rectangular slot etched textile PIFA structure. The simulation-based on-body performance was analyzed on the torso of HUGO model. Three prototypes on different materials, copper tape (CT), ShieldIt (SH), and PCPTF, were fabricated. The maximum stability of resonance frequency was achieved at PCPTF when tested on different human body locations.

Liu *et al.* [58] had worked on a PBG backed PIFA structure. Antenna radiator and PBG structure consist of circular metallic patches that were etched on the two sides of the Teflon substrate. The height of the shorting plate was optimized at 7 mm to achieve impedance matching. A large air gap between the ground plane and PBG structure effectively suppressed surface waves and enhanced radiation performance. A 40% improvement in impedance bandwidth was achieved with the purposed structure. The effect of body tissue on antenna characteristics was not analyzed.

Liu *et al.* [59] had compared the performance of a rectangular quarter-wave (QW) patch with a half-mode (HM) cavity in terms of resonance frequency and bandwidth. The electric field of the quarter-wave patch suffered more from the close vicinity of the human body, environmental and parasitic effects as compared to the half-mode cavity. In contrast, the quarter-wave patch required a smaller size to resonate at the same frequency as required by the half-mode cavity. Although a smaller size of the quarter-wave patch was advantageous in wearable applications.

Alves *et al*. [60] had designed two different antenna topologies (PIFA and monopole) on a common substrate, both operating at the same frequency of 2.45 GHz. CPW-fed with meandered line patch was used for the PIFA antenna, and a separate ground plane on the lower side of the substrate was designed for the monopole antenna. A circular disc was loaded at the height of 9.6mm. The matching network was designed at the strip line to obtain a 50-ohm impedance of monopole structure. PIFA showed broadside radiation pattern and dominated for on-off body communication while monopole antenna supported the creeping wave on the body surface and was suitable for on-on body transmission mode. Diversity performance was measured by signal to noise ratio. 7 dB diversity gain was obtained with the small antenna geometry. However, antenna was rigid and occupied a large vertical height that could create discomfort to the user.

Lin *et al.* [61] had explained the designed process of the PIFA antenna for on-body communication. Initially, PIFA was designed with two shorting pins (feeding and shorting); It resulted in poor impedance matching. Then, a shorting plate was added at the corner of patch; impedance matching improved but resonance frequency also increased. Finally, the folded ground plane's length was tuned to attain the desired band with a good matching condition. Three different phantom types were used during simulation, and the two-third muscle-equivalent phantom was used during measurement. Antenna showed stable performance for varying body tissue.

Casula *et al.* [62] had analyzed the magnetic and electric field distribution at the border of the PIFA antenna designed in [60]. The ground plane was extended in the direction of maximum electric or magnetic field density, and the product of efficiency and power transmission coefficient was analyzed. For the H-field extended ground, efficiency increased, and the power transmission coefficient decreased with the extended length. For the E-field extended ground, both factors increased with extended length. Hence, the ground plane's extension with electric field density could effectively reduce power absorption in body tissue.

Zhang *et al.* [63] adopted a multi-layered PIFA antenna to reduce planar antenna geometry at a low frequency of 433 MHz and to adhere easily with limited space inside the capsule. The three-layered structure lengthened the effective current length. An additional superstrate layer protected the antenna from the parasitic effects of other electronic components. An MCU of the capsule system was designed, which included a PCB board, 7-12bit ADC, temperature sensor, two-coin type batteries, and designed antenna. It was designed to analyze antenna compatibility with the electronic circuit of the capsule.

Gao *et al.* [64] had investigated a dual-band CPW fed PIFA antenna for wearable devices. A vertical slot line was used to connect the left corner of radiator with ground that generated resonance at the lower band. Another horizontal line was printed from the radiator to feed line that produced the second resonance band at 5.8 GHz. The designed antenna was backed by a 3×4 rectangular ring-shape dual-band EBG structure—that enhanced antenna robustness against structural deformation. EBG structure caused a unidirectional power pattern, which reduced power absorption in body tissue and maintained SAR under safety regulations.

Soh *et al.* [65] had incorporated a triangular-shaped Sierpinski fractal radiator with a PIFA antenna to achieve dual-band resonance. The antenna was designed using a textile substrate; however, on-body effects on antenna performance were not analyzed. The shorting plate's width was tuned to achieve resonance at 2.45GHz, and fractal dimensions were tuned for 5.2 GHz. Wideband performance of 570 MHz and 615 MHz at lower and upper bands made antenna suitable for on-body communication.

Yan *et al.* [66] had proposed a dual-band PIFA textile antenna operating at MICS and the ISM band. An L-shaped slotted PIFA was designed to tune the antenna at 433 MHz. Four parallel slots were cut on the ground to tune the resonance at ISM band. Three different types of phantom models were designed to measure antenna performance at different locations. The antenna was also tested for bending effect, and impedance matching was degraded significantly at the lower band. The efficiency of antenna reduced to 6% when it was placed near the human body.

Gao *et al.* [67] had worked on a PIFA structure for designing a wearable antenna covering a wide bandwidth of 940 MHz (5.02–5.96 GHz). A high permittivity metasurface was added above the antenna to get better gain and efficiency of antenna. A mathematical analysis of a square-shaped unit cell was presented. The stable on-body performance was obtained when antenna was operated on different body tissues and deformed along the x-axis.

Shang *et al.* [68] had designed a meandered PIFA for dual-band resonance at MICS and ISM band for in-body to on-body communication. Quarter-guided-wavelength at the lower band was achieved due to the shorting pins, and dual bands were excited due to meandered structure. This structure suffered from the narrow bandwidth; thus, five open-end slits were etched in the ground that contributed to wideband performance. The effect of each slot was explained with the surface current distribution and reflection coefficient plot. Antenna performance was measured in skin mimicking gel and on pork tissue as well.

Wu *et al.* [69] had designed a PIFA radiator with multiple rectangular slots. A shorting metallic surface was added to connect the radiator with ground to keep antenna size compact for implantable devices. Antenna was placed inside the leg tissue at a depth of 48 mm. Stable bandwidth and resonance frequency were observed with the varying depth of the implant. Shorting metallic surface also contributed to the null generation towards body tissue. Antenna had a high gain of -4.5 dB inside a pork tissue, which was much higher than other implantable antennas.

Al-Ghamdi *et al.* [70] had designed a layered dipole antenna on a polymer composite surface named Nitrile butadiene rubber (NBR). This substrate material provided good flexibility and mechanical strength to the antenna. To isolate the antenna electromagnetic radiations from the tissue, front to bank ratio was improved by locating a full ground beneath the dipole antenna. Still, low efficiency of 15.7% was observed in this work.

Sarestoniemi *et al.* [71] had evaluated the channel characteristic between an ingestible antenna and the on-body antenna over the wide frequency range of 0-5 GHz. The On-body antenna was located on the navel point, and the capsule was moved in the middle, and sides of the small intestine of the voxel body. A ring-shaped high directivity antenna enclosed with a cavity was considered an on-body receiver, and an encapsulated omnidirectional dipole antenna was considered an in-body transmitter. Power coupling was strongest in the sides as compared to the middle position even from the maximum depth of the intestine. The capsule was rotated at different angles, and a reduction in coupling was observed due to linear polarization.

Yan *et al.* [72] had proposed a magneto-electrical dipole antenna. Two u-shaped slots were added to tune the dual-band operation. Antenna performance had been analyzed on a tissue model under structural deformation. SAR value was also measured. Antenna performance was characterized for return loss, FBR, radiation efficiency, and radiation pattern on the body environment. Good radiation efficiency had been obtained for both the on and off-body communication.

Li *et al.* [73] worked on a meandered dipole antenna for capsule endoscopy. The ingestible antenna could miss its transmission reliability while traveling through the digestive tract. To resolve this issue, the dipole antenna was bent to achieve three orthogonal currents. Different orientations of three currents resulted in polarization diversity. Simulation was performed in a homogeneous tissue model, and measurement was done in the minced pork. Better orientation insensitivity performance was obtained as compared to the linear and circular polarized capsule antennas.

Moradi *et al.* [74] had designed a textile meander semi-circular ring-shaped dipole antenna for wearable applications. Antenna geometry was miniaturized to resonate at 325 MHz. Two parallel short-circuited transmission lines were designed with both magnetic and electric coupling, which in turn enhanced the radiation characteristics. The proposed structure was fabricated by using embroidered conductive thread on a felt substrate. Stable performance was achieved while structural deformation. However, the on-body effect on antenna performance was not investigated.

Azeez *et al.* [75] had proposed an E-shaped dipole antenna backed with a coupled L-slotted patch. Antenna showed tri-band resonance with omnidirectional radiation pattern. Denim substrate was used to fabricate the flexible structure. The on-body performance was validated on leg, arm, and chest. Three subjects were used to evaluate antenna robustness against tissue variation and different bending radii. Stable frequency and impedance matching were observed for all the operating conditions.

Al-Ghamdi *et al*. [76] had reduced the size of a dipole antenna designed in his previous work [70]. Multiple layers of magneto-electric material of 1.5-mm-thick NBR-M30 were added with antenna that caused 24% of size reduction. Free space-efficiency also enhanced from 16.3% to 30.5%. A metallic reflector was used to isolate the antenna from body. That makes antenna have good on-body radiation efficiency of 23.97%. However, antenna had thick geometry of 4.6 mm.

Aldaoud *et al.* [77] had investigated a wide dipole antenna for wireless power transmission to a millimeter-wave dipole antenna (1 mm× 1 mm × 20 mm) implanted inside body tissue. The implanted antenna was experimentally powered by a wide-dipole antenna that, in turn, stimulated the retinal ganglion cells to justify the functionality of the designed system. Wide dipole antenna was analyzed for transferring power at varying depth from 5mm to 35mm at the step size of 5mm. A saline solution was used for measuring power transmission efficiency. Wide dipole could transmit 1.3 mW power with 11% efficiency at a depth of the 10mm implant antenna.

Balakrishnan *et al.* [78] had designed a T-shaped folded dipole antenna for wearable devices. Folded arm enhanced electric current length and reduced the physical geometry. The width of the dipole arm was tuned for impedance matching. The ground plane was integrated with a 1×2 array of balanced fractal EBG structure, which reduced backward radiations towards body tissue. A thin polyester sheet of 0.1mm was taken as the dielectric material as it had a high degree of flexibility and mechanical strength, which made the antenna robust against structural deformation. Arm mimicking pig tissue was used for measurement. The antenna had high on-body gain and front to back ratio.

Kang *et al.* [79] had worked on a low-profile dipole antenna. Two parasitic radiator elements were loaded with dipole to tune antenna resonance frequency and wider bandwidth. Impedance matching was attained by cutting a rectangular slot in the ground. Parasitic elements also enhanced surface waves and made the antenna less sensitive to the body tissue. Antenna gain was also enhanced by five dBi in yz-plane and 6 dBi in the xz -plane due to the designed topology. An equivalent phantom was used to measure antenna performance.

Mobashsher *et al.* [80] had designed a three-dimensional dipole antenna for microwave head imaging. The antenna consisted of two dielectric substrates, t-slotted CPW fed dipole radiators, two parasitic stubs, two vertical copper plates, which connected two substrates of an antenna and four furled copper plates. The initial dipole structure provided resonant at 1.6 GHz, and then two stubs were added that created capacitive coupling and enhanced impedance matching. Impedance bandwidth was extended by adding unfolded furled arms that excited resonant at 1.1 GHz. It suffered from omnidirectional radiation characteristics; the addition of two vertical copper plates produced directional power patter with high gain but at the cost of narrow bandwidth. Finally, copper plates and unfolded furled plates were folded to attain the desired wide bandwidth as well as high gain performance. The time-domain analysis revealed more than 80% impulse fidelity factor (low distortion). Anatomical head model was used for SAR analysis with an array of 16 dipole antennas.

Lin *et al.* [81] had investigated a narrow strip dipole antenna of width 0.1mm at UHF bands ranging from 0.951 GHz to 0.956 GHz. Antenna was folded in slender shape to miniaturize antenna dimension, and a narrow gap of folds was optimized for impedance matching. Glass coating was used to insulate antenna from human tissue. The antenna's link budget was evaluated; the maximum radiated power of the antenna was about -125.1 dBm, and the calculated required power was -155.9 dBm. Link margin of 30 dBm made antenna reliable for wireless biotelemetry.

Scarpello *et al.* [82] characterized a folded slot dipole for implantable devices. Folded Slot enhanced the input impedance of dipole. The designed structure was embedded in the biocompatible Polydimethylsiloxane (PDMS) material. Antenna sensitivity was measured for flat and bend state demonstrated the covering of the ISM band in human muscle tissue. With decreasing bending radii, impedance matching was degrading significantly. SAR value was also measured experimentally using EX3DV4 cable for two mW of input power.

Bernety *et al.* [83] had worked on a novel approach for focusing radiation from an on-body antenna to the in-body antenna for maximum power transfer. Two conducting lines were placed horizontally along the two sides of antenna. The gap between the tips of lines could be tuned to vary the intensity of the focused field. As compared to the no lines cases, eight times and sixteen times more power was focused on single and double lines, respectively. The proposed mechanism acted as a crossed V-dipole antenna when two lines were placed orthogonal to each other and contributed to achieving a circular polarization mechanism.

Hong *et al.* [84] had proposed a dual-band, semi-circular patch antenna. Antenna was designed for on and off-body communication. A-half ring patch with two shorting pins was added with a semi-circular patch for bandwidth enhancement. A slot was cut at the ground plane to get the upper resonance band. The Taconic substrate was used for antenna designing. Feed had been provided through shorting vias from the middle layer of antenna. The muscle equivalent phantom model was designed to measure the antenna performance.

Tak *et al.* [85] had proposed an EBG integrated circular-shaped textile antenna for wearable devices. EBG structure was added on the common surface with a patch that reduced the antenna height and generated surface waves for on-on body communication. Antenna was designed using a center-fed circular patch. Eight periodic EBG structures were added around the circular patch. Antenna performance and SAR values were evaluated on the duke phantom model. Leather was used as a substrate for antenna design.

Ali *et al.* [86] had proposed a microstrip UWB antenna for wearable devices. Antenna was designed using a circular patch with a u-shaped slot. A defected ground plane was added for the bandwidth enhancement. Different types of phantom models had been designed for the evaluation of antenna performance on human tissue. The antenna was fabricated on Rogers Ro3003 substrate. Antenna performance was analyzed on 5.5 GHz and 13 GHz. Stable gain and omnidirectional radiation patterns had been observed for both frequencies.

Roy *et al.* [87] had designed a circular patch antenna for dual mode communication. The silver fabric was used on the PDMS substrate to enhance the practicality of the wearable antenna. Two arcs were etched in the radiator to get lower band resonance. A shorting pin was impinged to excite upper resonance mode TM_{02}. Pattern diversity was achieved for dual mode operation. A shift in lower resonance was observed when the antenna was bent along the surface current direction. Upper resonance was stable for the bending configuration due to the radial current distribution.

Shakib *et al.* [88] had worked on a compact tri-band (WiMAX, WLAN, and upper UWB) antenna with CPW feed for WBAN. Result analysis was presented for both the flexible textile substrate and FR4 substrate to show the antenna's suitability for using on the chest. The antenna was designed by connecting two Landolt ring-shaped strips to a rectangular strip. The width and gap of two rings were optimized for tuning the frequency. The ground plane was extended symmetrically for impedance matching. Three-layered biological tissue structures had been modeled using HFSS to simulate the antenna.

Lee *et al*. [89] designed a wearable antenna for the positioning of military persons. GPS L1 band was used for outdoor positioning, and ISM band was used for outdoor positioning. The proposed antenna had been designed using a circular ring with four shorting pins for indoor positioning and a truncated square patch for outdoor positioning. Dual feed was used for indoor and outdoor operations. Circular polarization and directional patterns were attained with the proposed design. The designed antenna had been integrated into a military beret and tested on a human head.

Bhattacharjee *et al.* [90] had proposed a circular shaped dual-band flexible antenna for on-body communication. Four open-ended l-shaped slots were etched in the ground to excite quarter wave resonance mode for 2.45 GHz and its odd multiple harmonic mode at 5.8 GHz frequencies. Circular polarization was also attained with the combined effect of horizontal polarization caused by ground slot and vertical polarization caused by a radiating patch. A superstrate dielectric layer was added to broaden the 3-dB bandwidth. Degradation in impedance matching at the lower band and sifting of resonance at the upper band was observed when antenna was subjected to structural degradation.

Wang *et al.* [91] had proposed a circular-shaped antenna with omnidirectional radiation pattern at 2.45 GHz and 5.8 GHz frequencies. Miniaturization was performed by printing two complementary symmetrically folded Alford loops as a radiator. A high gain of 6.8 dBi was achieved at the lower band. Reduction in impedance bandwidth with increasing bending radii was observed.

Wolgast *et al.* [92] presented a complete BAN system to detect heart failure (ECG) using Bluetooth signal transmitted to a smartphone for data analysis. The antenna used for this BAN is a simple patch antenna with a shorting plate at the sidewall. The shorting plate is used to raise the bandwidth. The insulating tape was used to cover the antenna that avoided shortening the antenna from the body. As the number of electrodes increases, the quality and reliability of the signal had been improved.

Grilo *et al.* [93] had designed a proximity coupled, textile patch antenna. The quarter-wave impedance transformer was cascaded with the feed line for bandwidth enhancement. Antenna was fabricated using the denim substrate. Four prototypes were designed with the same patch dimensions, but the feed lines and transformer width were varied to optimize the antenna's bandwidth. The effect of biological tissue was also analyzed on the performance of antenna.

Tak *et al.* [94] had proposed a three-layered dual-band antenna for dual mode communication. A T-shaped radiating element and a circular radiator were designed on the antenna's top and bottom layers. Two horizontal parasitic patches were added on the top layer of antenna for bandwidth enhancement. Shorting pins were used to provide feed to both layers. Antenna showed patch and monopole like pattern. Four shorting pins from top to bottom layer had been added for higher-order resonance mode. 2/3 semisolid muscle equivalent phantom gel was fabricated. The antenna was tested on this phantom gel at a gap of 10 mm using Styrofoam.

Zhang *et al*. [95] had worked on an aperture coupled antenna. Rectangular shaped coupling aperture was modified in meandered-shaped to reduce the antenna surface area. A T-shaped microstrip line was used for impedance matching. A high gain of 5.6 dBi and low cross-polarization were achieved with the help of a modified feeding network. The surface current was parallel to the y-axis, the surface current path reduced while bending along the y-axis, and frequency shifted slightly upwards with reducing bending radii. Along x-axis, effective patch width increased, which reduced the characteristics admittance and lowered the frequency.

Ferreira *et al.* [96] had designed a rectangular patch antenna at the ISM band. Double layered denim was used as a substrate material. The conductivity of denim was also calculated using the thickness and resistivity of the material. Antenna performance was characterized on different body positions like arm, chest, and wrist. Bending deformation caused degradation of antenna performance. Antenna gain and front to back ratio was also affected by the structural deformation.

Arif *et al.* [97] had proposed an antenna topology with Koch fractal structure in which meandered slots were etched to reduce the size of antenna. Antenna was tuned at 2.45 GHz and bandwidth was achieved by defected ground. Corner of ground plane were truncated and narrow slots were designed to improve the impedance bandwidth. Antenna parameters were characterized on various body tissues like leg, thigh, arm and back. Structure deformation effect was evaluated along x-axis and avoided for y-axis as antenna surface current is also oriented towards this axis.

Ashyap *et al.* [98] had designed a microstrip patch antenna with E-shaped radiator. Further to improve the performance of designed structure, an electronic band gap structure was integrated in the antenna. As the adverse effect of EBG structure, antenna 10-dB bandwidth reduced. Thus, to overcome this affect, multiple slots were designed in the ground plane of EBG array structure. Etching of slots reduced antenna quality factor, which in turns enhanced the bandwidth. It also contributed to alleviated the impedance mismatch effect while bending the antenna. Still, deviation of frequency was found when radiator was rotated at π/4 and bent along y-axis due to alteration of surface current between multiple slots.

Gao *et al.* [99] had designed a slotted patch antenna integrated with a compact-planar EBG structure for on-body communication. Mathematical analysis of the metallic PBG structure is performed on the basics of FDTD analysis as explained in [100]. 50% size reduction was achieved with the proposed unit cell geometry. Antenna showed stable performance when the array size was varied. Broadside type radiation characteristics were achieved after the adding of UC-EBG. Impedance matching degraded significantly with the increasing bending radii of antenna. It was found that the impedance matching diminished when antenna was located on arm and leg, and resonance frequency shifted downwards on chest and stomach position.

Gareth *et al.* [101] had proposed a higher mode (TM_{z21}) microstrip patch antenna for on-body surface wave transmission. Two shorting pins offset to the feed line were used to excite higher-order modes and generated nulls between patch and ground plane. Antenna performance was compared with three different antenna configurations, including the full ground patch, shorted wall patch, monopole antenna. It was analyzed that antennas with the full ground plane had minimum radiation efficiency and maximum gain tangential to the body surface, supporting surface wave propagation. 11 dB and 7 dB improvement in on-body path gain were obtained with the help of shorting pins and walls, respectively, even with $\lambda/20$ antenna height.

Elfergani *et al.* [102] had designed a 2×2 array MIMO antenna for on-body communication. The proposed design had occupied overall volume of 26 mm×26 mm×0.8 mm. P-shaped radiators with the partial ground plane were used to miniaturize antenna dimensions. 4-radiators were placed orthogonally to attain high diversity performance. Power absorbed on different parts of the body was evaluated, and maximum effective isotropic radiated power was limited to 100 mW (at chest), 239.2 mW (at arm), and 278.9 mW (at leg).

Ashyap *et al.* [103] had designed a u-shaped patch antenna operating at 2.45 GHz using jeans fabric. 2×2 array of metamaterial structure was added to enhance antenna performance and robustness in the biological environment. Significant improvement of bandwidth 14.5%, high gain (7.5 dBi), and front to back ratio (14.5 dB) was achieved after placing metamaterial structure. Tissue safety was also enhanced by 90%. As the textile fabric is much immune to structural deformation due to different body movements and postures, antenna was bent for different radii. Stable impedance matching and resonance frequency were obtained for all the bending conditions and varying gaps between body and antenna.

Anbalagan *et al.* [104] had proposed a textile on-body antenna. Zari and cotton cloth were used to design the structure. Ohm-shaped open-ended slot was etched in the radiator to minimize antenna dimension and to improve the radiation efficiency. The antenna was practically investigated for the moist environment and the crumpling conditions. Antenna shows wider bandwidth with a maximum of 14.28% detuning of central frequency for all the on-body measured conditions as compared to free space analysis. In addition to this, antenna was integrated with the Arduino UNO board and analyzed as an on-body transmitter for different body movements: slow walk, fast walk, and running. The maximum failure rate was 24.6% for the running state due to the average delay in transmission.

Liu and Ying [105] had worked on the miniaturization of a skin implantable antenna for blood glucose monitoring. A CSR resonator was imprinted at the center of a square patch radiator. Diameter and angle of the slits were varied to attain optimum impedance matching. To lengthen the electric current path, 'c-shaped' slits were designed on all sides of the radiator. Biocompatibility of antenna was improved by coating the antenna with thin layer of alumina. In addition, link margin was also evaluated for analyzing the transmission channel reliability.

Moro *et al.* [106] used cavity backing and surface integrated waveguide technology to enhance the antenna performance in biological environment. High efficiency of 73% and a compact geometry was achieved. Folded cavity and an annular ring were used to excite TM_{120} and TM_{210} degenerated modes. Two orthogonal modes lead to the generation of circular polarization as well as wide 10-dB impedance bandwidth of 337 MHz.

Divya Chaturvedi and S. Raghavan [107] had evaluated a quarter mode SIW cavity-backed antenna. The antenna's size was reduced by dividing the radiator into four equal quadrants (along magnetic wall) to attain the resonance, and a 35^0 rotated slot was etched to achieve wider bandwidth. Antenna showed good on-body radiation characteristics with 5.4 dB gain and 88.5% radiation efficiency.

Chaturvedi *et al.* [108] had designed a quasi-mode SIW antenna for dual-band resonance. The rectangular SIW cavity was bisected along the magnetic walls and converted into a triangular-shaped radiator. 70% of size reduction was achieved with QMSIW topology. After bisecting both the resonating modes, TE_{110} (dominating mode) and TE_{220} (third-order mode) were preserved due to symmetrical field distribution along the magnetic walls. At higher mode, two orthogonal modes were generated that contributed to a wider bandwidth of 225 MHz. Antenna had stable resonance on body tissue due to the full ground. Slanted arms of the triangular radiator were optimized; a slight difference in the length of two arms helped to generate circular polarization at the upper band. Although unidirectional radiation pattern, moderate gain, and good radiation efficiency made antenna suitable for WBAN applications, narrow bandwidth at lower band had restricted its practical utilization.

Mandal *et al.* [109] had designed a tri-band wearable radiator on the leather surface. The proposed structure was modelled to resonate at 2.4 GHz, 3.51 GHz, and 4.69 GHz frequency bands. Leather substrate made antenna suitable to integrate with wearable devices like belts, shoes, and gloves. An array of metallic vias were etched along the two slant sides of the radiator. The gap between the two vias was optimized to achieve three resonating modes. Two slits were etched on the magnetic wall to achieve good impedance matching. However, on-body and bending performance were not evaluated.

Hong *et al.* [110] had designed a cavity-backed, circular ring slot SIW antenna for on-off body communication. The proposed structure was mathematically evaluated through an equivalent rectangular cavity at fundamental TM_{110} mode. The initial SIW cavity feed structure provided the resonance at 4.96 GHz. A C-shaped slot was etched in the cavity, and the distance between feed and slot was optimized by the parametric sweep. The increasing gap reduced resonance frequency and vice-versa. The gap was tuned at 37 mm for center resonance at 5.76 GHz but with narrow bandwidth. Therefore, a C-shaped slot was modified into a circular ring slot, which excited another resonant frequency at 5.8 GHz (5.725 GHz-5.875 GHz), the radius of the ring was optimized, that merged the two bands and contributed in a wide bandwidth performance of 354 MHz. The stable on-body performance was obtained on muscle equivalent phantom.

Agneessnes [111] had demonstrated an eighth-mode couple cavity antenna. The Rectangular closed cavity was bisected into the eighth mode cavity by using a magnetic field profile. The open boundary cavity had five electric walls, and a magnetic wall. The resonating mode and frequency remained identical to the initially closed cavity. In the modified structure radiations leaked from the open boundaries, and acted as a half-mode structure. Another cavity resonating at slightly different frequencies was integrated on the common ground plane to widen the impedance bandwidth. Power from the first cavity was coupled to the second cavity due to their close vicinity and resulted in the wide bandwidth. Space between the driven and parasitic cavity was optimized for maximum field coupling. The electric field of parasitic was leading by 90◦, and this relationship could be used to achieve circular polarization at the expense of impedance bandwidth. LHCP (bottom cavity) and RHCP (upper cavity) could be decided by choosing the driver cavity. The on-body performance was evaluated on the human body's chest and leg, the capacitive coupling of body tissue was neglected by a full ground plane, and stable performance was achieved.

Lee *et al.* [112] had described an all textile, H-plane SIW horn antenna operating at 28 GHz for millimeter-wave BAN communication. Horn antenna with conducting threads was designed to attain resonance at the required frequency. The corrugated ground plane was extended towards the front side of the horn, which suppressed the back radiations (towards the body), resolved the beam tilting issue due to it waveguiding phenomenon. It acted like an inductive surface and created a radiation pattern parallel to the body surface. However, the on-body effect on antenna performance was not evaluated.

Chaturvedi *et al.* [113] had explained the working of a semi-hexagonal slotted half mode SIW antenna for WBAN applications. Semi hexagonal slot worked as a resonating slot, excited dominating mode (TE_{110}) at the desired band and suppress the second-order mode (TE_{210}). The dominating mode was even mode and in phase with electric field distribution and caused maximum radiation, whereas the second mode was odd and opposite to field distribution and get canceled. Besides this, the slot radius was taken slightly smaller than the half of the guided wavelength to avoid the excitation of higher modes. Antenna sides were shielded with an array of shorting vias, which avoided leakage of radiations and reduced surrounding body tissue's effect on antenna behavior.

Chaturvedi *et al.* [114] had described a semi-hexagonal shaped half mode SIW (HMSIW) cavity for dual-band operation. The proposed cavity did not support TM_{110} mode due to unsymmetrical E-field distribution along the magnetic wall. The cavity preserved three modes TM_{010}, TM_{210}, TM_{020}. A semi-hexagonal slot was etched in the cavity, that suppressed TM_{010} mode and preserved another two modes. Two open-ended slits were etched on the radiator's broader side, which enhanced the effective current length and helped to tune antenna at desired operating frequencies.

Jawad *et al.* [115] had worked on rectangular-shaped SIW antenna; Makowski-Sierpinski fractal geometry was etched on the patch to attain resonance at 60 GHz. The wide bandwidth of 3.5 GHz, radiation efficiency of 91%, and a high gain value of 7.9 dB, made antenna suitable for WBAN communication for millimeter-wave application.

Abirami *et al.* [116] had proposed a Yagi-Uda antenna for body area network applications. The antenna was integrated into an EBG structure. Antenna performance was evaluated on four locations. Substantial improvement in gain and the reduction of SAR value had been observed. However, the bandwidth of the antenna had been reduced to 30 MHz.

Aruna *et al.* [117] had investigated a Quasi-Yagi antenna. The proposed antenna showed 52.83% of size reduction as compared to the conventional Yagi antenna. The substrate's front side had two driver dipoles, and four parasitic strips worked as reflector; the bottom side was designed with the microstrip feed line. Coplanar strip (CPS) line had connected the ground plane and driver dipoles. The stepped slot line and CPS line together contributed to achieving 50-ohm characteristics impedance for an ultra-wideband spectrum. A metallic reflector was added that provided robustness again bending and isolated the antenna from body tissue. Antenna showed high gain, narrow beam, and stable performance on different parts of the human body (arm, chest, and abdomen). In addition, communication reliability was enhanced by designing a two-element array with beam steering capability. Out of phase feed provided in-phase beam with high gain performance.

Wu *et al.* [118] worked on a printed Yagi antenna structure, working at 60 GHz for on-body communication. The proposed structure consisted of a driven dipole, two reflectors, and 18 directors. A pair of dipole and reflectors were printed on two sides of a thin substrate (0.127 mm). A tapered microstrip line transition was used for impedance matching. The length of directors and the gap between them was decreasing from dipole to the other end; it reduced the sidelobe levels and enhanced gain. Further, an array of 4-similar Yagi antennas was designed with a distance of 3mm from the center to center. Symmetrical parallel lines with a 4-way power divider were used to feed the structures. Feed lines were designed on both sides of the substrate; phase difference on the feed lines of upper and lower sides degraded the side lobe radiations. The on-body performance was analyzed on the animal phantom.

Chahat *et al.* [119] had designed an end-fire wearable Yagi antenna for on-body communication at 60 GHz. The proposed textile antenna was made of a microstrip-fed, driven dipole and ten directors. The antenna had very high gain of 11.9 dBi and 48% efficiency on skin phantom. A similar antenna configuration was further investigated by **Guraliuc** *et al.* [120] for bending effects, and path gain was also evaluated experimentally by using a waveguide antenna. It was observed that the reflection coefficient remained under -10 dB value for the bent state, and the radiation pattern was affected in H-plane. A tilt of 10^0 on the H-plane power pattern was noticed. The antenna could support high-data-rate for wearable devices.

Agarwal *et al.* [121] had proposed a planar Yagi antenna structure on the latex substrate. Electrical properties of latex were experimentally measured through T-resonator and quality factor analysis at 2.45 GHz. Meandered slots were used for the design of reflectors. Balun was used to transit the unbalanced impedance into balanced load of the driven dipole. AMC surface was used to modify the bidirectional pattern into off-axis end fire type power pattern. It helped to achieve high radiation efficiency (79%) and reduce the SAR value (0.714 W/Kg.)

Kamardin *et al.* [122] had presented a coplanar waveguide (CPW) fed, circular patch wearable monopole antenna. A textile artificial magnetic conductor (AMC) jacket and the sheet had been designed and fabricated. Waterproof textile material Fleece had been used to avoid performance degradation under wet conditions. The transmission performance of antenna was improved with the use of the AMC sheet. Antenna performance was evaluated near the human body, and in free space with AMC jacket.

Tsai *et al.* [123] had worked on the miniaturization of an antenna and tuned at 433 MHz. Sigmoid shape monopole type radiator was designed to increase the current length. Coplanar ground plane was modified into asymmetrical C-shape ground from one side. It caused excitation of higher order resonance modes and contributed to wide band performance. Dupont Pyralux AP 9121R is a flexible di-electrical material which was used as protecting layer and substrate of the antenna. Antenna curvature was deformed as cylinder to implant in the tooth.

Bahrami *et al.* [124] had investigated and compared the behaviour of dual-polarized and single-polarized antenna structures for neural implants. Spiral shaped, and monopole radiators with defected ground coplanar waveguide fed topology was used to achieve the resonance at ultra-wideband spectrum. Combined effect of staircase type ground plane and truncated feed line contributed to achieve impedance matching in compact antenna. Flexible material Kapton Polyimide was used as substrate and superstrate layer. Experimental validation was performed in the brain of a fish and a sheep.

Jiang *et al.* [125] had designed a circularly polarized antenna for WBAN applications. A monopole antenna had been designed and fabricated using a low loss composite of PDMS and silver nanowires (AgNws). Antenna had been placed on a 2×2 EBG structure to obtain circular polarization. The unit cell of EBG structure had been designed by truncating anisotropic artificial ground (AAG) plane. Antenna showed stable performance when tested for structural deformation on the human body.

Sukhija and Sarin [126] had proposed four microstrip patch antennas. Rectangular slots of different sizes were truncated on the patch's left and right side to obtain resonance at ISM, WiMax, and WLAN band for biomedical applications. The liquid phantom gel was fabricated to evaluate the performance of antenna on the biological environment. All antennas showed good impedance matching and radiation patterns. However, the SAR was not considered for the biosafety.

Mendos and Peixeiro [127] had designed a single band, dual-mode antenna for on and off-body communication at 2.45 GHz. Coaxial dual-feed had been used for dual-mode operations. A meandered patch was designed in the center for off-body communication. A ring was placed outside the patch for on-body communication. 2/3 phantom muscle gel for the torso was fabricated for experimental performance. The performance of antenna had been degraded when analyzed for X and Y axis bending.

Hu *et al.* [128] presented a textile antenna by using fir as the dielectric material. The radiator was designed with two types of conducting material copper foil tape (CFT) and shieldex (SH). The antenna consisted of two F –shaped patches that were connected to the ground plane via two shorting pins. These shorting pins reduced the size of antenna, and reflection coefficient was also improved. On comparing the two types of conducting material, it was found that bandwidth was smaller on CFT but reflection coefficient was better than SH. The effect of bending of arms with or without clothes was also analyzed for both the material.

Alemaryeen and Noghanian [129] had worked on a CPW fed textile antenna loaded with an artificial magnetic conductor (AMC). Antenna is designed to operate at 5.8 GHz; significant improvement in gain and reduction in specific absorption rate was achieved with the use of AMC structure. Antenna robustness was measured for both the bending and crumpling conditions. A slight reduction in gain and rightward shifting of resonance frequency was observed.

Alornainy *et al.* [130] investigated the performance of six different planar antenna topologies on different body locations. Dipole, monopole, loop, inverted-l, parasitic-L, and wiggle type antennas were designed, and path loss was evaluated experimentally over the frequency range from 2.4 GHz to 2.525 GHz. Maximum gain and efficiency were observed with monopole structure, and the worst performance was observed in the wiggle type structure due to the high loss of radiated power. Antenna, with the full ground plane, was least sensitive with the varying distance with body-tissue.

Alrawashdeh *et al.* [131] had presented a flexible implantable loop antenna with CSRRs. Improvement in impedance matching, gain, radiation efficiency, and transmission coefficient had been observed by loading the antenna with CSRR. SAR was reduced due to the negative refraction coefficient of CSRR. The path loss link equation had been used to measure the communication link characteristics.

Qu *et al.* [132] had worked on ground radiator-based MIMO antenna for wearable devices. Lumped elements were used to excite the ground plane as a radiator. Two antennas were positioned in a way that they could generate both horizontal and vertical polarization simultaneously. An inductive metal plate was added at the lower edge of the ground plane to achieve a phase difference of 90^0 between horizontal modes. In this way, circular polarization and diversity between the two radiators were achieved. On-body high gain was achieved by using this single-layer structure.

Ruaro *et al.* [133] had tuned an antenna at ISM band for the hearing aid devices. Antenna was fabricated by 3-D printing technology and modelled on selective heat synthering (SHS) material. Shape of antenna was designed as a hemisphere so that it could match with the shape of human ear canal. A slot on the edge of hemisphere was etched to match the impedance. Antenna parameters like power pattern, |S11| parameter, efficiency and impedance were characterized in free space and ear tissue.

Mantash *et al.* [134] had proposed a finger worn, end-fire antenna for body area network applications. The antenna was designed to operate in mm-wave frequency bands from 25 GHz to 33 GHz. The antenna was designed in an axial-mode helical shape. Return loss, radiation pattern, gain, and axial ration had been measured using HFSS. The antenna was mounted on a plastic ring for wearing in finger and could also be used for other smart devices.

Hu *et al.* [135] presented a wearable button antenna with dual-band operation. The antenna was designed using a conductive textile ground plane and Rogers 5880 substrate using a shorting pin. A radiating patch was fabricated on both sides of the substrate using capacitive coupling to balance the shorting pin's inductive effect. Return loss had been measured under various humidity levels and bending angles to study real-life situations.

Kaim *et al.* [136] had designed an extremely compact square patch antenna with side 3 mm to implant with retinal prosthetics. Numerical simulation was performed in a spherical phantom model consisted of vitreous fluid with conductivity of 4.5 S/m and dielectric constant of 67 to characterize antenna with eye tissue. Antenna had broad operating frequency range that occupied both the ISM and UWB for down and uplink channels. Square loop radiator was bounded with meander line slots, and ground plane was loaded with annular ring to get the impedance bandwidth of 6 GHz.

Sambandam in [137] presented a circular ring slotted button type patch antenna. Multiple sots were etched to enhance the surface current path, and multiple strips were added to achieve triband resonance at 0.867, 2.38, and 5.85 GHz frequencies. Antenna showed unidirectional and broadside radiation characteristics that made it suitable for on-off body communication and compatible with multiple network standards.

2.2.2 Survey of Antenna Structures for In-body communication mode

Antenna structures which are characterized to deploy inside the different organs of body are termed as implantable antennas and for the surface of the body are considered as wearable antenna structures. These antennas are integrated with the sensor nodes used for neuron signal reading [138], ocular/retinal and cochlear prosthesis devices [139,140]. Design requirements for implantable antennas are quite stringent, and imposes challenges for real-world applications. Similar to the wearable antennas, implantable antennas should be biocompatible with different tissue properties. Some design issues for implantable antennas in accumulation with wearable antenna issues are briefed here.

Power requirement: To operate the antenna and other components of implanted sensor, battery is integrated. Battery power is consumed continuously and lifetime of the device reduced. Power consumption can be reduced by using the wake-up call method. Antenna can be activated by transmitting a signal. A dual band antenna for wake-up transmission was designed in [141]. In another work [142], spiral inductive coil was designed to couple electromagnetic power to the implantable device.

Insulating the antenna radiator from body tissue: Direct contact of antenna radiator with body tissue, may create short circuit effect. Thus, superstrate layer was used to cover the antenna’s metallic ground and radiator [143]. It improved the compatibility of antenna in biological environment. In another approach, antenna was coated with low loss materials. Some materials used for coating were Zirconia ($\boldsymbol{\varepsilon}_r$= 29, and tan $\delta \approx 0$) [144] and Silastik MDX-4210 Elastomer ($\boldsymbol{\varepsilon}_r$= 3.3, and tan $\delta \approx 0$) [145]. Adding of superstrate layer also affected the resonance frequency, thus essential to be considered in design stage.

Circular polarization: In order to maintain the communication link reliability of implantable antenna, circular polarization (CP) is the prominent feature. It also contributes to reduce multipath scattering of low power signals and improves transmission efficiency. Linear polarized antenna requires additional computation to enhance transmission quality [146]. To achieve circular polarization, two orthogonal modes should be generated in the antenna. Different techniques like adding diagonal slots [147], inserting shorting pins [148], and modifying the ground plane to couple multiple resonance mode in the radiator [143] are presented in literature.

2.2.3 Ingestible or endoscopy capsule Antennas

Capsule antenna is a well-known application of in-body to off-body data transmission mode. In endoscopy a capsule is swallowed by the patient for the examination of digestive and Gastro-Intestinal (GI) tracts. It supports detection of many diseases such as celiac, Crohn's, and bleeding in gastrointestinal. Endoscopy capsule is loaded with an antenna, a camera, a light source and battery for power supply [149]. The components embedded in capsule are shown in Fig. 2.2(a).

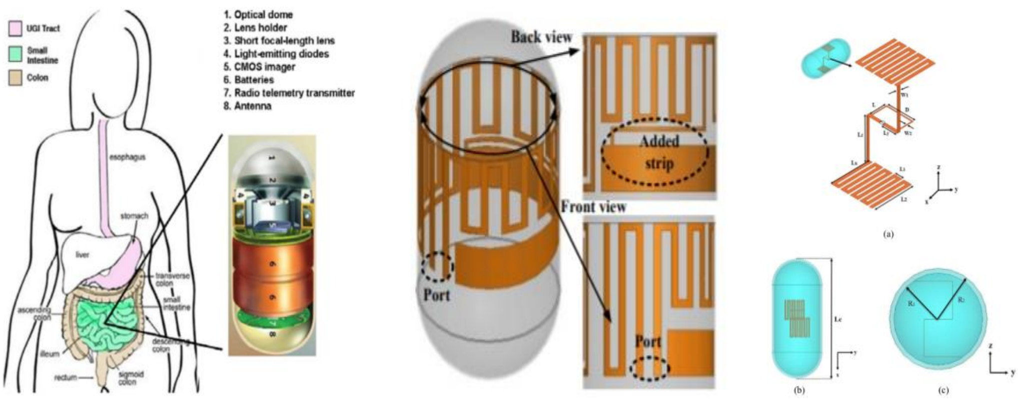

(a) (b) (c)

Fig. 2.2 (a) Schematic view of endoscopy [149] (b) antenna with bandwidth enhancement [156] and (c) polarization diversity [73] characteristics

Camera placed in the capsule gathers bio-statistical information as images and videos from the digestive system. Antenna transmits the real time data which is diagnosed by the medical representative. As compared to wired capsule endoscopy, wireless endoscopy is highly capable to track the hidden locations, providing better and high-resolution visualization of the intricated path, and help to maintain the comfort level of the user. Thus, antenna is the critical section of endoscopy to establish a reliable wireless transmission link for real-time signal transmission in endoscopy system. Some design necessities for endoscopy antenna are as follows:

Wide impedance bandwidth: Human digestive tract is a complex structure that is surrounded by different tissues like muscle, small intestine, stomach, and colon. All tissue layers have variations in their electrical properties. Relative permittivity (ε_r) of stomach, colon, and small intestine is 62.158, 53.879, and 54.125 respectively [150,151].

Antenna resonance frequency and impedance matching is the function of the tissue property also. Conducting nature of body tissue interferes with the antenna near field radiations and alters the antenna performance. Thus, for continuous functioning of capsule endoscopy, antenna with broad bandwidth and high impedance matching is required [152,153].

Orientation matching: While inspecting the digestive system organs, capsule travels in different directions, it varies the orientation of antenna radiator in random manner. It causes the mismatching of polarization orientation of transmitter and receiver antenna [154].

It may lose the communication link in this situation. Hence, antenna with circular polarization characteristics or polarization diversity is the suitable choice for endoscopy application [155-157]. In [73], a dipole antenna was twisted in such a way that it generated 3-orthogonal current modes as shown in Fig. 2.2(c). Three planes were covered by three current modes and provided polarization diversity.

In [158,159], circular polarized antenna structures were designed to reduce the problem of orientation mismatching between the receiver and transmitter antenna. A helical radiator was designed and three open loops consisting of multiple layers were connected to achieve axial ratio value below 3-dB. However, it lost the circular polarization characteristics while passing through the digestive tract.

2.3 Antennas for Diagnosis Applications

Various life-threatening ailments like cancer, occurrence of unhealthy cells, and tumour can be diagnosed by studying the variation of antenna parameters. Even curing of the paralyzed person can be monitored by detecting the muscle movements through variation in antenna performance. Some common applications of antenna in diagnosis applications are explained here.

In MRI technique, antenna is used to stimulate, transmit and receive the magnetic power. Electromagnetic pulses are transmitted in body at UHF band [160,161]. Variation in magnetic field is received by antenna coil and interpreted by signal processing algorithms. Magnetic field variation is converted into high resolution images and examined. Transmitter and receiver antenna of MRI system should consider the following requirements:

Enhancing B0 and reducing power deposition in body tissue: Electromagnetic energy generates strong magnetic field (B0) in the body. A part of this magnetic power is deposited in the tissues and increases specific absorption field. Absorbed power rises in square proportion of the magnetic field [162,163]. Thus, magnetic field to SAR value ratio should be enhanced.

Shimming of magnetic field to remove inhomogeneities of magnetic field: Similar to the electrical permittivity, susceptibility (χ) of each tissue layers is also differed. It leads to generation of inhomogeneities in the magnetic field. Static field gets distorted at the interference of two mediums or tissues. Susceptibility of air (χ =0.36 ppm) is approximately nine time lesser than body tissue (χ =-9.05 ppm) [164,165]. Bone and soft tissue with high water contents have minimum susceptibility difference of 2 ppm. This variation originates ghosting effect, blurring, and may cause loss of signal.

In [166], antenna for high power MRI system (7T) was designed. To maintain the SAR value segmented dipole antenna was designed. Inductance was introduced between the segments to enhance magnetic field. Fig. 2.3 shows the segmented and dipole antenna array. In Fig. 2.4, SAR value for the dipole and segmented dipole array on Duke model is represented. It is clear that SAR had been reduced to 2.8 W/kg from 7.6 W/kg due to the proposed structure.

A cylindrical antenna with flared patch was designed by **Emran and Elvi** in [167] to operate over the frequency spectrum from 7.8 GHz-15 GHz for MRI application. Slot was etched in the triangular radiator to get wide bandwidth. FSS (frequency selective surface) was designed on the inner surface of the antenna for the improvement of front to back ratio and gain. Electromagnetic information received from the body tissue was taken out from the reflection coefficient parameter.
In [168], **Hoffman** *et al*. had worked on an array of 24-patch antennas for brain MRI. S-parameters from 24 antennas were received simultaneously and image of whole brain was reconstructed. While simulation, Duke and Ella models were used for investigating the

magnetic field gradient. Antenna had less shimming in magnetic field but high value of SAR. Some more antennas are studied for diagnosis and presented in Table 2.1.

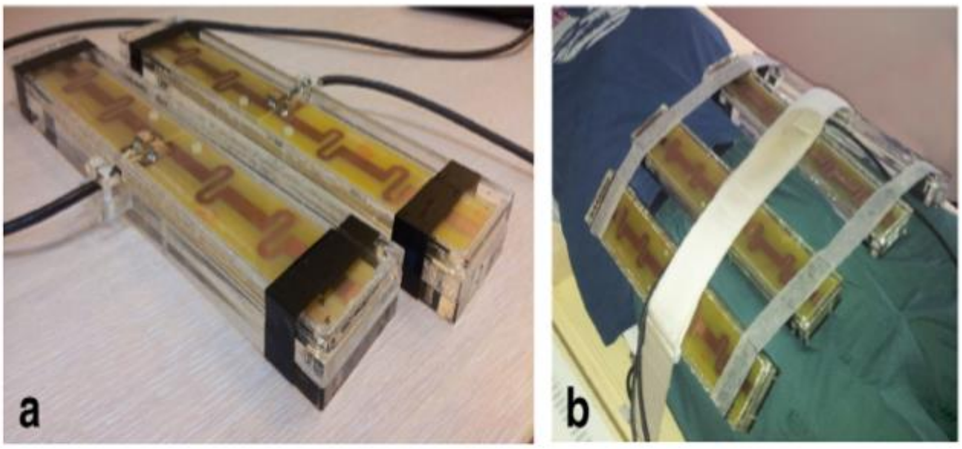

Fig. 2.3 (a) Structure of segmented dipole (b) antenna array located on body [166]

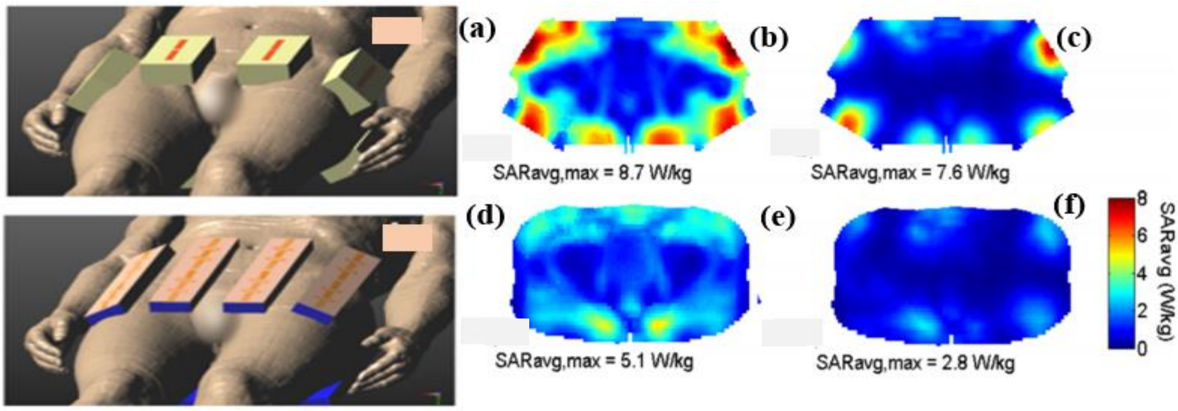

Fig. 2.4 Simulated SAR distributions (a–c) for the simple dipole array and (d–f) the segmented dipole array [166]

Table 2.1 Antennas for diagnosis applications

Ref.	Antenna design technique	Frequency	Application	Parameter used for diagnosis
[169]	Two-folded helix antenna	890 MHz, 2.4 GHz	Finger's muscle movement detection	Reflection coefficient and dynamic time wrapping algorithm
[170]	Monopole	433 MHz	Movement and posture detection of arm	Input impedance, S11 and dynamic time wrapping algorithm
[171]	Microstrip Patch	370 MHz	To sense heart beat and respiration rate	Phase of reflection coefficient, Fourier transform and Savitzky-Golay filtering
[172]	Defected ground patch antenna	2.45 GHz	Breast cancer detection	E-field, H-field and surface current variation
[173]	Slotted patch antenna	3.1-10.6 GHz	Breast tumour detection using microwave imaging	Back scattered signal, Figure of Merit and group delay
[174]	loop antenna	128 MHz	Magnetic resonance imaging (MRI)	Near field magnetic static field (B0)
[175]	Slotted patch with non- resonance surface coil	300 MHz	MRI for deep tissue imaging	Static magnetic field
[176]	Self-grounded Bowtie antenna	300,400, 500 MHz	Thermal MR at 7T for thigh	B1+field, SAR and temperature
[177]	Transverse slot antenna	300 MHz	High field MRI at 7T for hips	Reflection coefficient, B1+field and SAR
[178]	Corrugated tapered slot patch	1-4 GHz	Microwave head imaging	S21 back scattered parameter and conformal algorithm for imaging

2.4 Antenna Structures for Treatment Applications

Image guided thermal ablation techniques (Radio frequency and Microwave ablations) are fetching the attraction for the curing of tumor, cancer and hepatocellular carcinoma [179]. These are low cost, and less painful techniques that improve the effectiveness and success rate (up to 90%) of radiotherapy for completely removing the cancerous cell and tumours of very small diameter (below 1.5 inches) [180].

Variance in the heat sensitivity of healthy and malignant tissue is the principle of thermal and radio frequency ablation. Electromagnetic radiations are induced in tissue to raise the surrounding tissue temperature by 100^0 C. It has been opted as the standard technique to treat hepatocellular carcinoma for patients who cannot undertake surgery (0-A) patients [181,182]. Microwave thermal ablation (performed at 0.3 GHz – 300 GHz) is much preferrable than radio frequency ablation (performed at 460 KHz – 550 KHz). Microwave ablation is advantageous in terms of providing bigger and spherical ablation area, and high temperature in less time period. It does not create heat sinking and avoids reducing the blood circulation [183,184]. Experimental setup of ablation therapy [185] is displayed in Fig. 2.5. Basic design conditions for antenna in ablation therapy are explained further.

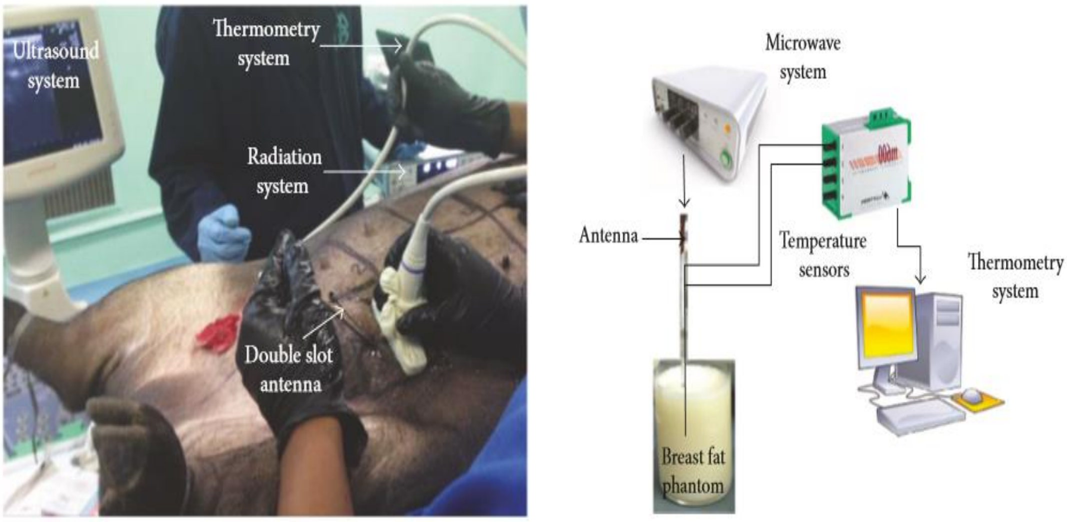

(a) (b)

Fig. 2.5 Experimental setup for ablation therapy (a) in mammary gland of swine (b) in phantom gel [185]

Needle shape geometry: Long and thin, coaxial antennas are needed to insert in the body. Different design approaches are incorporated to reduce the thickness of antenna and reflection coefficient. Using monopole and dipole antenna topology [186,187], adding asymmetrical slots [188,189] and choke coils are some methods to design the needle type antenna structures.

Change in tissue characteristics while ablation: Strong electromagnetic radiations interact with the tissue and alters its electric, mechanical and thermal properties [190,191]. Size of ablation zone depends on the tissue properties and may vary during therapy [192]. Thus, variation in the near field zone of antenna should be examined.

Reducing radiation along the antenna axis: Interstitial antennas deposit energy near the aperture of the tip, but the surface current flows along the coaxial conductor's length. It overheats the healthy tissue; therefore, proper techniques should be used to eliminate the backward heating [193,194].

Shape of the ablation zone and high SAR value: Unlike the other medical applications, ablation therapy requires high power deposition in the body tissue to destroy the unhealthy cells. High SAR value corresponds to more power absorption. In addition to this, spherical shaped power absorption zone is required. Less power should be dissipated along the antenna coaxial probe. Rise in tissue temperature is evaluated by bio-heat transfer formula [195,196].

To rectify the above said issues of ablation therapy antenna structures, different design techniques have been opted by the researchers. Ito in [197] had investigated a long and thin antenna for intercavitary ablation and presented experimental results for the treatment of tumour cell in the neck tissue. Further he modified his design by adding slots to define the shape of heating zone for ablation [198].

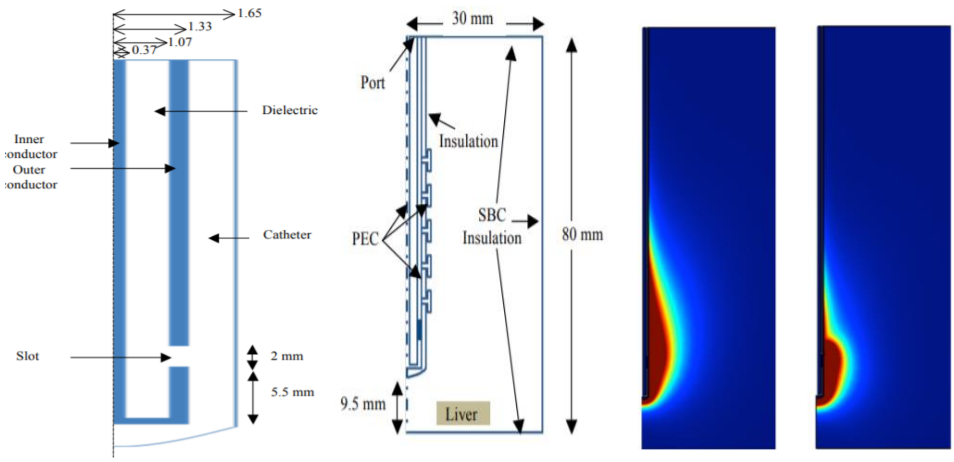

(a) (b) (c) (d)

Fig. 2.6 (a) Topology of single slot structure (b) topology of T-slot (c & d) power distribution of single slot and T-slot antenna structures [199]

In [199], multiple T-shaped slots were designed on a coaxial antenna to make power absorption zone spherical. In Fig. 2.6, SAR value of slotted and unslotted structure is represented. Dispersion of filed toward antenna probe is reduced, which confirms that much confined field is achieved with the designed slots. Summary of some antennas used for ablation therapy is given in Table 2.2.

Table 2.2 Summary of antenna used for treatment applications

Ref.	**Antenna design technique**	**Resonance Frequency**	**Feature**	**Application**
[187]	Interstitial sleeve dipole antenna	915 MHz	Uniform power distribution	Hyperthermia
[195]	Cap-choke antenna	915 MHz	Low backward current	MWA
[200]	Transmit-array lens antenna	915 MHz	Power concentration enhancement in deep tissue	Kidney cancer treatment
[201]	Capacitive antenna	2.45 GHz	water filled antenna to cool the healthy cells	MWA
[202]	Monopole and slot antenna	2.45 GHz	Uniform SAR pattern	MWA
[203]	Slot antenna with double choke	2.45 GHz	Low backward radiation	Cancer treatment
[204]	Cap-choke antenna	915 MHz	High radiation efficiency	MWA

In [205,206], to increase the heating effect of antenna for ablation therapy, a helical slot was added between two rectangular slots of a coaxial structure. This modification diminished the time required for the ablation process. Time taken by rectangular slot antenna to raise the temperature to 60^0 C was 120 seconds whereas after etching of helical slot it was reduced to 90 seconds.

From the study of different applications, it can be concluded that antenna has high potential to connect body area network wirelessly. Antennas are extremely sensitive for medical diagnosis and thermal ablations. Important parameters like circular polarization, reflection coefficient, impedance matching and SAR for corresponding application are listed out. From this research work; it can be concluded that, dipole structure with polarization diversity feature is the required feature for ingestible capsule. On-body antenna, demands conformality along with low interaction of radiation with body. Surface integrated wave guide technique and planar Yagi structures are promising candidates in this contest but have complex geometry and large surface area as compared to the microstrip patch antenna geometries. Future implantable devices need miniaturization along with better power options.

Electromagnetic power transfer mechanism can be the possible solution. Electromagnetically coupled antenna structures are appropriate option for in-body power transfer. MRI techniques demands antenna array configuration with low SAR value and high magnetic field to integrate with 7T systems for receiving high resolution pictures. Monopole antenna with co-axial probe is a good choice for designing needle shape antennas for ablation therapy. Mitigating the back current flow towards the transmission probe and getting spherical ablation zone are the critical antenna design requirement in treatment application.

2.5 Research Gaps

From the study of different antenna structures, it can be concluded that different antenna configurations such as PIFA, monopole, dipole, SIW, Yagi-Uda, and microstrip patch antennas with different performance enhancement techniques are used for body-centric communication. PIFA structure provides wide bandwidth, and dipole antennas are more compatible with implantable and diagnosis applications. Planar Yagi structures are a good choice for high-frequency on-body antennas. SIW technology provides a good solution to reduce radiation coupling from the body tissue. SIW structures have complex geometry and requires high fabrication accuracy. Microstrip patch antennas are widely used for wireless body area network applications due to their high degree of design and shape flexibility, low profile, and manufacturing ease. Different technologies have been opted by researchers to enhance bandwidth, conformality, gain, and efficiency of patch antennas to make them compatible with the biological environment.

From the literature review, following gaps are identified:

1. Most of the existing antenna designed for on and off body communication devices have very large dimensions. It makes the antenna difficult to integrate with the sensor module and also creates discomfort to the user. So, there is a scope to miniaturize the size of antenna [84,86,95,100,132].
2. In the previous designed antenna, most of the antennas are designed on textile substrates. Performance of antenna degrades due to environmental effects, wrinkling and crumpling. It is required to use a flexible material with good mechanical strength [87,112,122].
3. Due to common human activities and body postures, it is virtually impossible to maintain a fixed position. Most of the antenna studied, undergoes a frequency shift when tested for bending. It is required to design a wideband antenna to maintain the reliable communication link under the structural deformation [104,121,128,129].

4. Human body is a multi-layered complex and lossy medium for the transmission of EM waves. Antenna efficiency decreases when placed on heterogeneous tissue model. Antennas reported in literature has poor radiation efficiency and low gain. There is a scope to improve on-body efficiency and gain [35,110,124,126].
5. Some antennas have very high specific absorption rate or not measured for the bio safety level. It is required to evaluate the SAR value for ensuring the safety of user [85, 88, 93,98,134].

2.6 Research Objectives

Based on the initial studies and understanding, the following research objectives have been proposed:

1. To study existing antenna designs for wireless body area network medical applications.
2. To simulate, design and fabricate conformal antenna structures for on body communication at ISM band and test the performance on equivalent phantom.
3. To simulate, design and fabricate antenna structures for on and off body communication and test the performance on equivalent phantom.

2.7 Research Methodology

After studying the literature, an idea is modelled and design parameters are calculated to find the outcomes. The design is simulated using EM solver tool CST Microwave Studio. If the simulated results match well with the desired goals, then a prototype of the simulated design is fabricated otherwise move back to the design step. Prototype is measured in laboratory using Vector Network Analyzer. Process of research methodology is represented through the flowchart in Fig. 2.7.

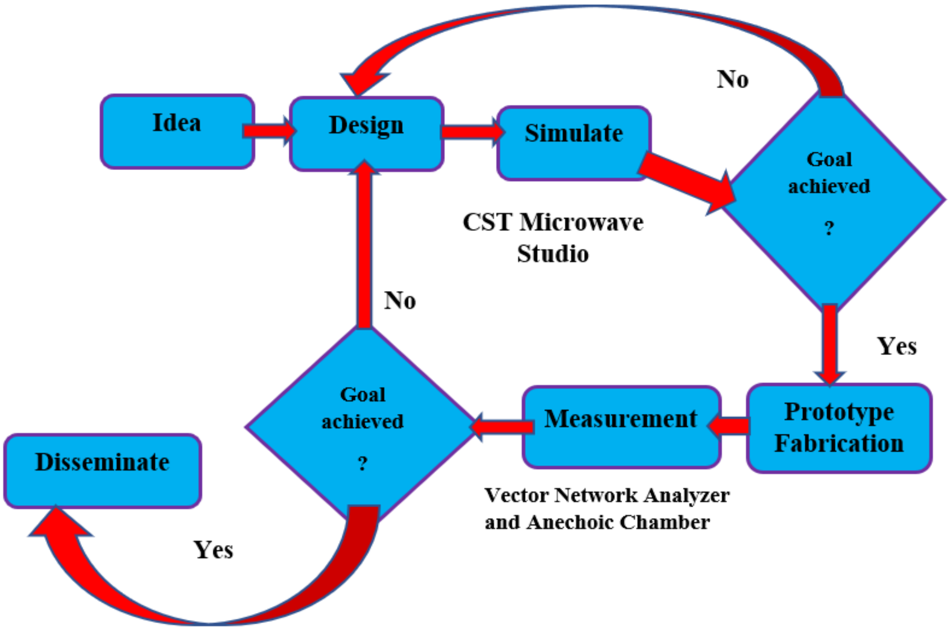

Fig. 2.7 Flowchart of research methodology

If the measured results are not satisfactory then switch back to the design. Small differences in simulated and measured results are obviously due to manufacturing tolerances, cable and connector loss. Major discrepancies are removed by redesigning and modifying the structure.

Chapter-3

Compact Wearable MIMO Antenna for Reduction of Mutual Coupling

3.1 Introduction

Wearable devices are getting more attention to the integration of health care sensor nodes. It accelerated the demand for low profile, compact and conformal on-body antennas. It is always challenging to enhance the antenna performance of a compact and thin structure. Moreover, the proximity of human tissue and body movements interferes with impedance matching. Thus, researchers have opted different methods to improve the impedance bandwidth and miniaturization of wearable antennas, which includes partial slotted ground [35], coupled-cavity [111], PIFA with shorting pins [207], the slotted patch with parasitic strips [208], and L-shaped symmetric CPW feed with narrow slits in patch [25]. The ongoing growth of MIMO technology has also stimulated the research interest in wearable technology. Low efficiency and gain of on-body antennas lead to multipath fading of the transmitted signal. MIMO technology provides an excellent solution to improve transmission quality [209-212]. Additional decoupling structure [211] or large physical distance [209,212] is maintained between the radiators to enhance diversity performance but it increases the size of antenna.

This chapter aims to present a conformal on-body MIMO antenna suitable for Industrial Scientific and Medical band (ISM). Section 3.2-3.4 describes the details of antenna design process. Section 3.5 and 3.6 explains the stability of the antenna on body-tissue and validation through experimental analysis. In section 3.7, the SPLSR value is evaluated. Section 3.8 covers the structural deformation effects. Finally, in section 3.9, MIMO performance is evaluated.

3.2 Single Radiator Antenna Geometry

Semi flexible Rogers 5880 substrate with a thickness (t) of 0.51 mm, relative electric permittivity ($\boldsymbol{\varepsilon}_r$) of 2.2, and tan δ of 0.0009 is used to design the antenna. Antenna dimensions are minimized to 14 mm × 25 mm (0.114 × 0.204 λ_0^2). Four open-end slots are etched in the radiator along the x-axis, and the optimum length is selected to achieve the maximum impedance matching and to miniaturize the antenna. A rectangular three-layered tissue model of size 40 × 60 mm^2 is designed to characterize the antenna performance with the human body. Electrical properties of skin (2 mm), fat (5 mm) and muscle (10 mm) layers are taken as given in Table 1.2.

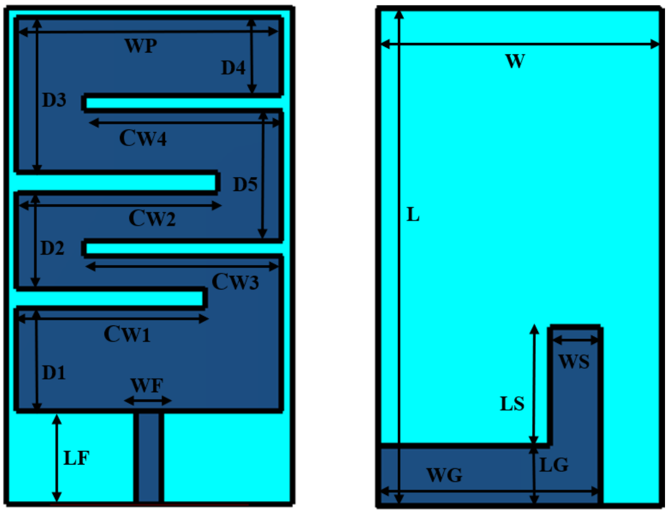

(a) (b)

Fig. 3.1 Single element antenna configuration (a) front side (b) back side

The partial ground is modified by adding a short vertical arm with it for bandwidth enhancement. Fig. 3.1 shows geometry of a single radiator antenna. All the simulations and optimizations of the antenna are performed on the phantom model.

3.3 Antenna Design Evaluation

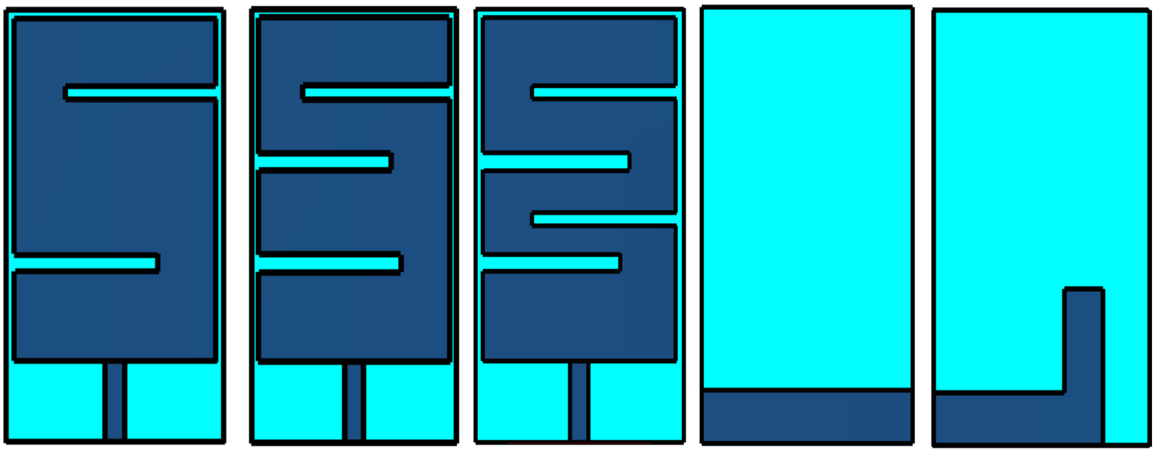

(a) (b) (c) (d) (e)

Fig. 3.2 Step wise configuration of single radiating element (a and b) front side of step 1 and step 2 (c) front side of step 3 and step 4, (d) back side of step 1 to step 3 and (e) back side of step 4

To begin with antenna design, a partial grounded commercial patch antenna is considered and modified as an open-end slotted structure to tune the resonance. The stepwise configuration of designing process is represented in Fig. 3.2. The reflection coefficient of each step is drawn in Fig. 3.3.

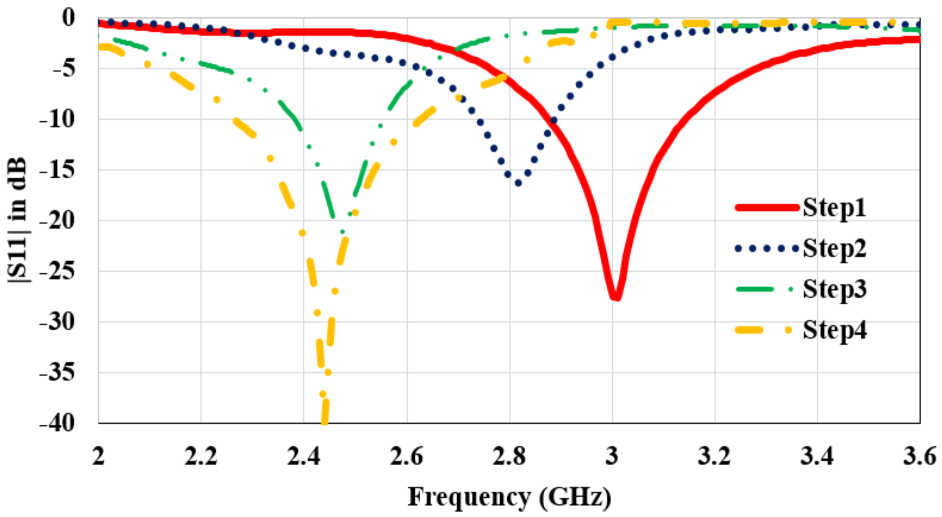

Fig. 3.3 Reflection coefficient for each design step of single element antenna

Step 1: In step 1, two horizontal slots are etched at the parallel sides of the radiator. A slot of length (*CW1*) 8 mm is printed at the lower left side of the patch, which provides wide impedance bandwidth from 3.8 GHz to 6.0 GHz. Then, slot length is optimized from 8 mm to 11 mm through the parametric sweep. From the reflection coefficient plot (Fig. 3.4(a)) of *CW1* variation, it can be found that the resonance frequency can be lowered by increasing the slot length but it degraded the impedance matching.

Thus, *CW1 =9 mm*, providing resonance at 3.9 GHz is taken for the further design process. The second slot is designed on the patch's upper right side, which added an inductive effect in antenna. Adding of this slot resulted in shifting of resonance at 3.0 GHz.

Length *CW4* of the second slot is also varied from 7 mm to 10 mm. Fig. 3.4(b) shows that reflection coefficient is not varying with slot length *CW4* variation. In this way, impedance bandwidth of 200 MHz (2.9 GHz - 3.1 GHz) is achieved in step 1 (Fig. 3.3).

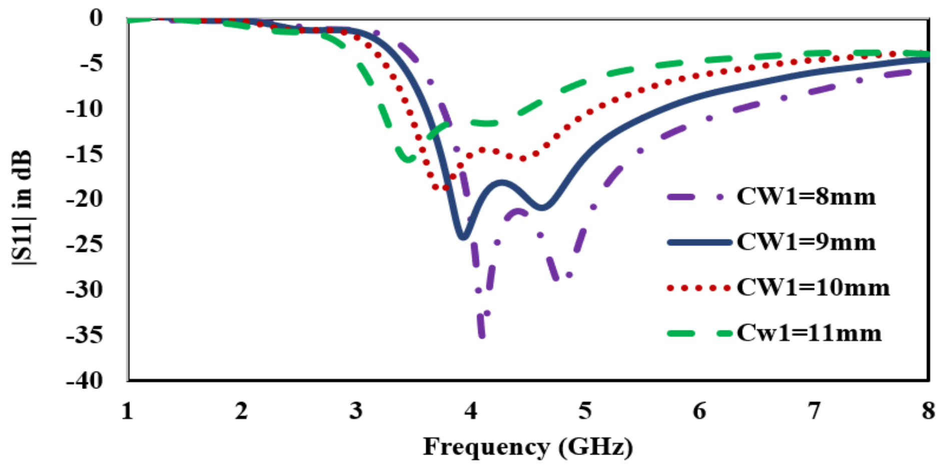

(a)

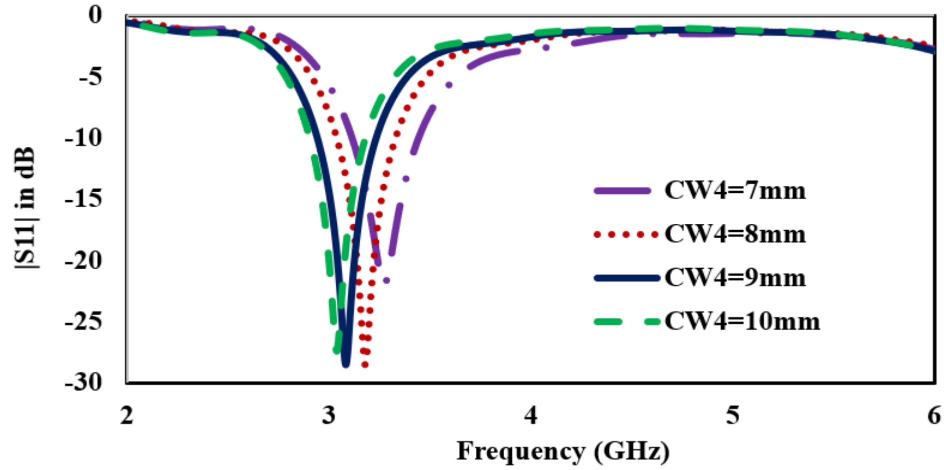

(b)

Fig.3.4 Reflection coefficient (a) for lower slot length *CW1* variation (b) for upper slot length *CW4* variation

Step 2: In this step, a new slot is etched corresponding to the lower slot. It raises the inductance and retune the frequency at 2.8 GHz. The effect of slotting, on the antenna impedance is displayed in Fig. 3.5. Imaginary impedance curve is showing the upward shifting of the reactance curve, which depicts high inductive reactance in the antenna ($xl = \omega l$).

Step 3: In step 3, the desired resonance at 2.45 GHz is achieved. To attain this, fourth slot is designed corresponding to the uppermost slot. Impedance plot representing the downward shifting of the impedance curve, making reactance capacitive. In step 3, desired resonance with 120 MHz bandwidth is achieved. It has effectively covered the required ISM band from 2.4 GHz to 2.48 GHz. Still, on-body antenna requires wider bandwidth to withstand frequency detuning and impedance degradation effect in real-time applications. It is studied from the literature that antenna impedance and frequency vary with changing body tissue. Therefore, additional modification is done in step 4 to make antenna more robust and reliable.

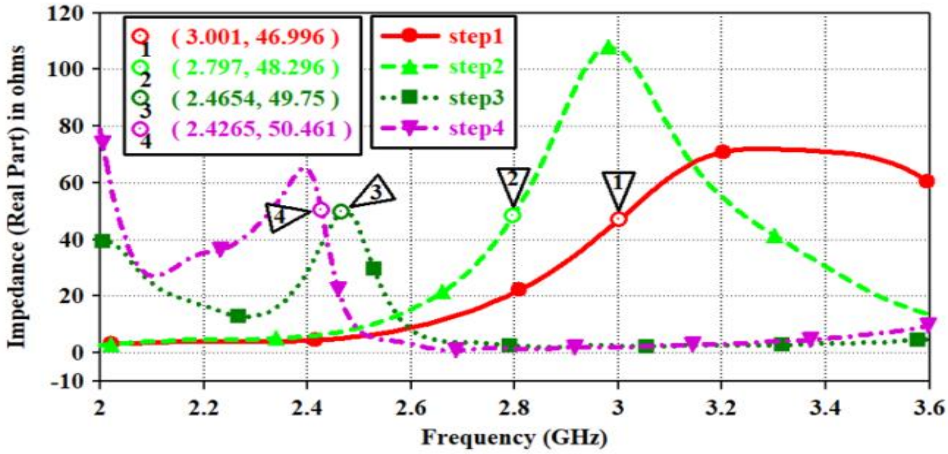

(a)

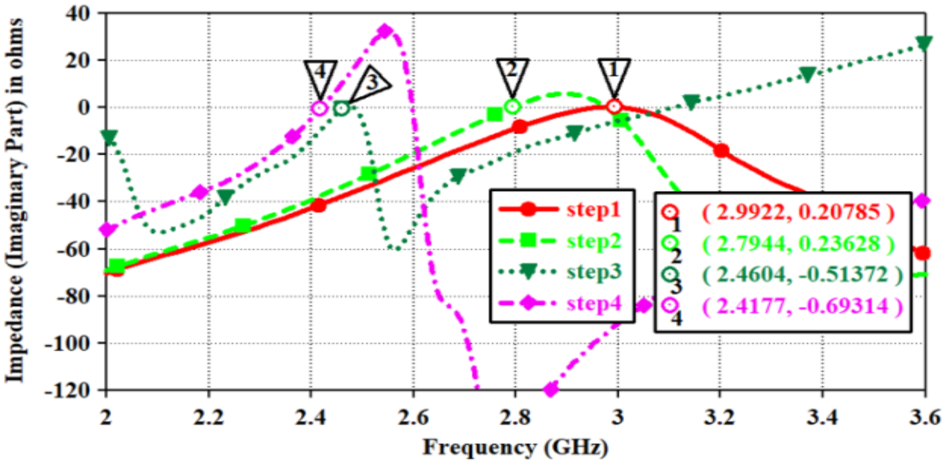

(b)

Fig. 3.5 (a) Real impedance (b) imaginary impedance plot

Step 4: In this step, the partial rectangular ground is changed as inverted-*L*. It causes the improvement in impedance bandwidth. The impedance graph is representing the upward shift of the reactance curve, depicting high inductance and low Q-factor value. At 2.42 GHz, 50-ohm resistance and zero reactance justify the impedance matching of antenna. Return loss improved by 20 dB and bandwidth is upgraded by 180 MHz.

To calculate the electric current length at 2.45 GHz, surface current is analyzed and relation between frequency and antenna geometrical parameters is found.

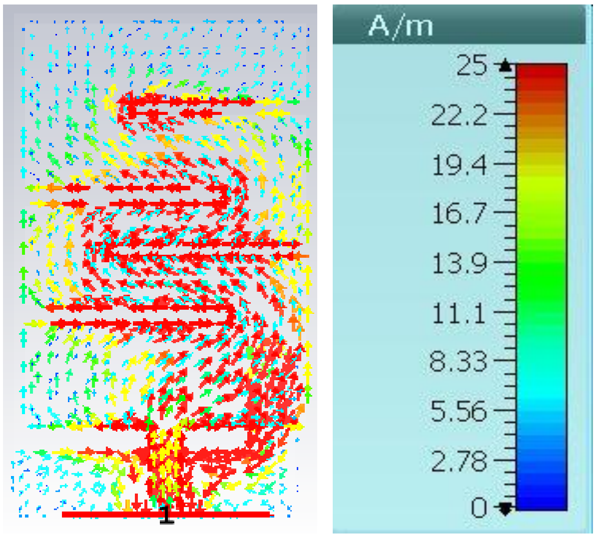

Fig. 3.6 Plot for electric current distribution

Fig. 3.6 represents the electric current path followed at 2.45 GHz. Hence, Current path length *(LR)* contributing the resonance can be evaluated by using equation (3.1).

$$LR = D1 + \frac{(WP - WF)}{2} + (2 \times CW1) + (2 \times CW2) + D2 + D3 \tag{3.1}$$

Based on the antenna dimensions, *LR* is calculated as 47.3 mm. Resonance frequency f_{r1} at the length *LR* is calculated at half wavelength with the equations (3.2 and 3.3). Here, the value of effective dielectric constant (ε_{reff}) is 1.645 which is calculated from the equation (3.3).

$$f_{r1} = \frac{c}{2 \times LR \times \sqrt{\varepsilon_{reff}}} \approx 2.477\text{GHz} \tag{3.2}$$

$$\varepsilon_{reff} = \frac{\varepsilon_r + 1}{2} + \frac{\epsilon_r - 1}{2}\left[1 + 12\frac{t}{WP}\right]^{\frac{-1}{2}} \tag{3.3}$$

Where, *t* is the height of antenna substrate and *WP* is the width of the radiator. Theoretically evaluated resonance frequency is in close approximation with numerically simulated frequency and justifies the antenna geometry.

3.4 Design of Dual Radiator MIMO Structure with Inverted U-Shaped Ground Stub

Antenna designed in previous section is arranged as 1×2 array MIMO structure. Two radiators are arranged as mirror image. To reduce the mutual coupling an inverted U- shaped stub is designed on the ground plane which behaves as a parasitic resonator. Its length is nearly equal to 47 mm ($Wc+2\times Lc$), and matches with the radiating current length *LR*. Design of the proposed MIMO antenna is shown in Fig. 3.7. Antenna dimensions are listed in Table 3.1.

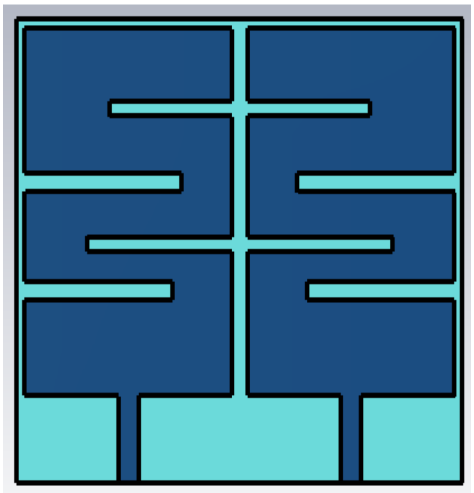

(a)

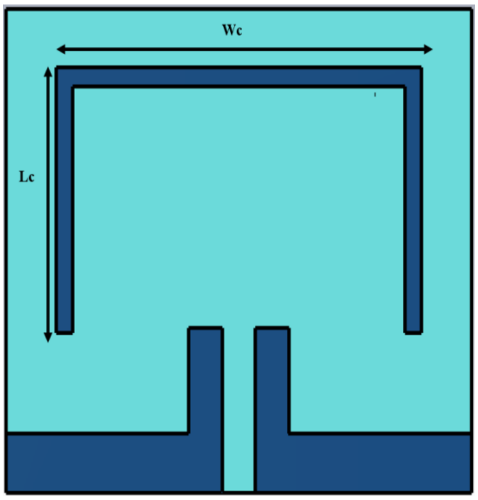

(b)

Fig. 3.7 (a) Front side (b) back side of MIMO antenna

Table 3.1 Dimensions of the designed antenna

Design Parameter	Size (mm)	Design Parameter	Size (mm)	Design Parameter	Size (mm)	Design Parameter	Size (mm)
W	14	L	25	D5	7.18	WP	13
D1	4.53	CW1	4.47	LF	4.8	WF	2
D2	4.41	CW2	7.34	LG	3.2	WG	13.0
D3	9.26	CW3	9.3	Lc	13.5	Wc	20.0
D4	3.9	CW4	8.85	WS	2.0	LS	4.4

S-parameter curves of antenna with the parasitic stub and without the stub are plotted in Fig. 3.8. |S21| curve shows that deploying of stub has reduced the mutual coupling from -11 dB to -32 dB.

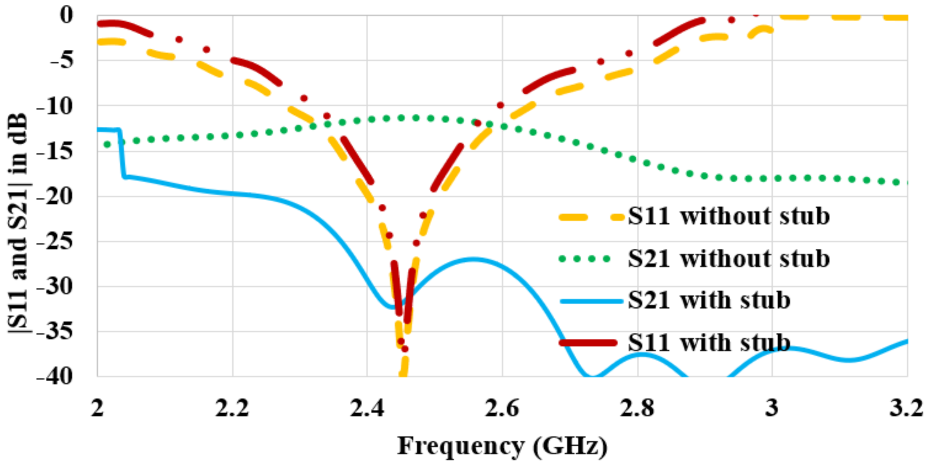

Fig. 3.8 Plot for S-parameters of MIMO antenna

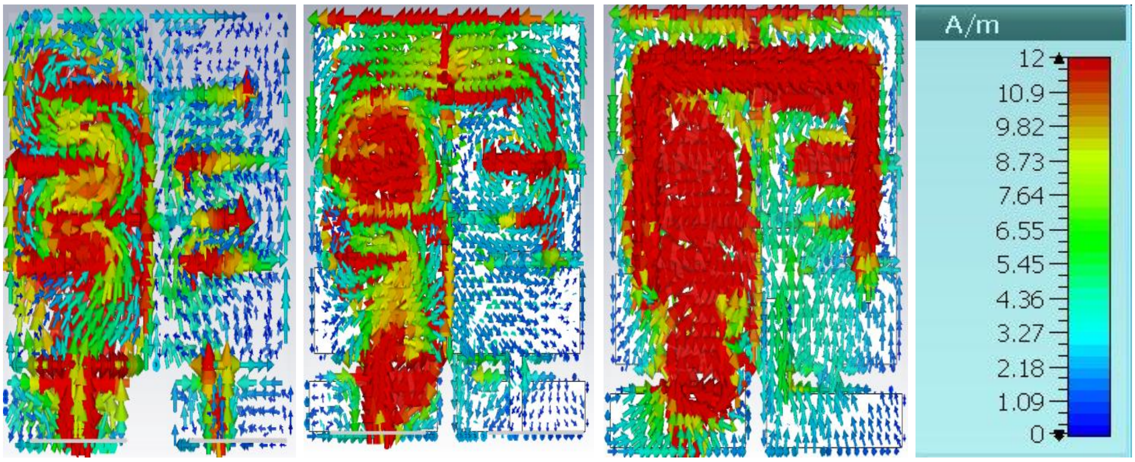

(a) (b) (c)

Fig. 3.9 Current distribution plot (a) before adding decoupling stub (b) front side with decoupling stub and (c) back side with decoupling stub

Effect of decoupling parasitic stub can be analyzed through surface current distribution which is displayed in Fig. 3.9. It can be examined that in each radiator, current is generating at the open end of the lowermost slot. Thus, parasitic stub is designed from the lowermost open edge of patch-1 to patch-2. It creates an additional current path between two radiators and offsets the current passing from port-1 to port-2. Hence, isolation between two radiators is improved successfully.

3.5 Effect of Varying Antenna-Tissue Gap on Antenna Performance

There is a massive difference in the dielectric constant of body tissue and the antenna substrate. Direct contact of body and antenna may alter the effective dielectric constant that can shift the resonance frequency. The space of '*s mm*' is kept between the antenna and tissue model to reduce this effect. Due to body movement, sustaining of stable separation distance is difficult. Hence, to report the boundaries of antenna performance in real time applications, value of '*s mm'* is varied at 2 mm, 4 mm and 6 mm. Effect of varying antenna tissue gap on return loss, gain and efficiency are plotted in Fig. 3.10.

From Fig. 3.10 (a), it can be seen that central resonance frequency is decreasing with an increasing gap. Still, required bandwidth from 2.4 GHz - 2.48 GHz is effectively covered for all values of '*s mm'*. The central resonance frequency of 2.45 GHz is obtained at *s = 4 mm*. However, all the simulations and measurements are performed with this value.

At the lowest separation gap of '*s = 2 mm'*, the minimum value of gain (-0.9 dB) and efficiency (38%) can be noticed. It keeps on increasing with the larger gap values. Power absorbed by tissue directly varies with tissue conductivity (σ), and electric field intensity (|E|) in near field zone [213] as given in equation 4.4. It is clear from the equation (4.5) that field intensity is inversely related to the distance from antenna [214]. Power absorption in body tissue is decreased with increasing value of *s mm*. Radiation efficiency improved by 8% and gain value increased by 1.2 dB when value of '*s mm*' is raised from 2 mm to 6 mm.

$$P_{abs} = \frac{1}{2}\int \sigma|E^2| \, dV \tag{3.4}$$

$$E = \frac{I_m \times LR \times \sin\theta}{4\pi\varepsilon}\left[\frac{-\omega \sin \omega t}{c^2 s} + \frac{\cos \omega t}{s^2 c} + \frac{-\omega \sin \omega t}{s^3 \omega}\right] \tag{3.5}$$

Where, I_m is the antenna maximum current, *c* is the speed of light, *E* is the electric field, and ε is the absolute permittivity.

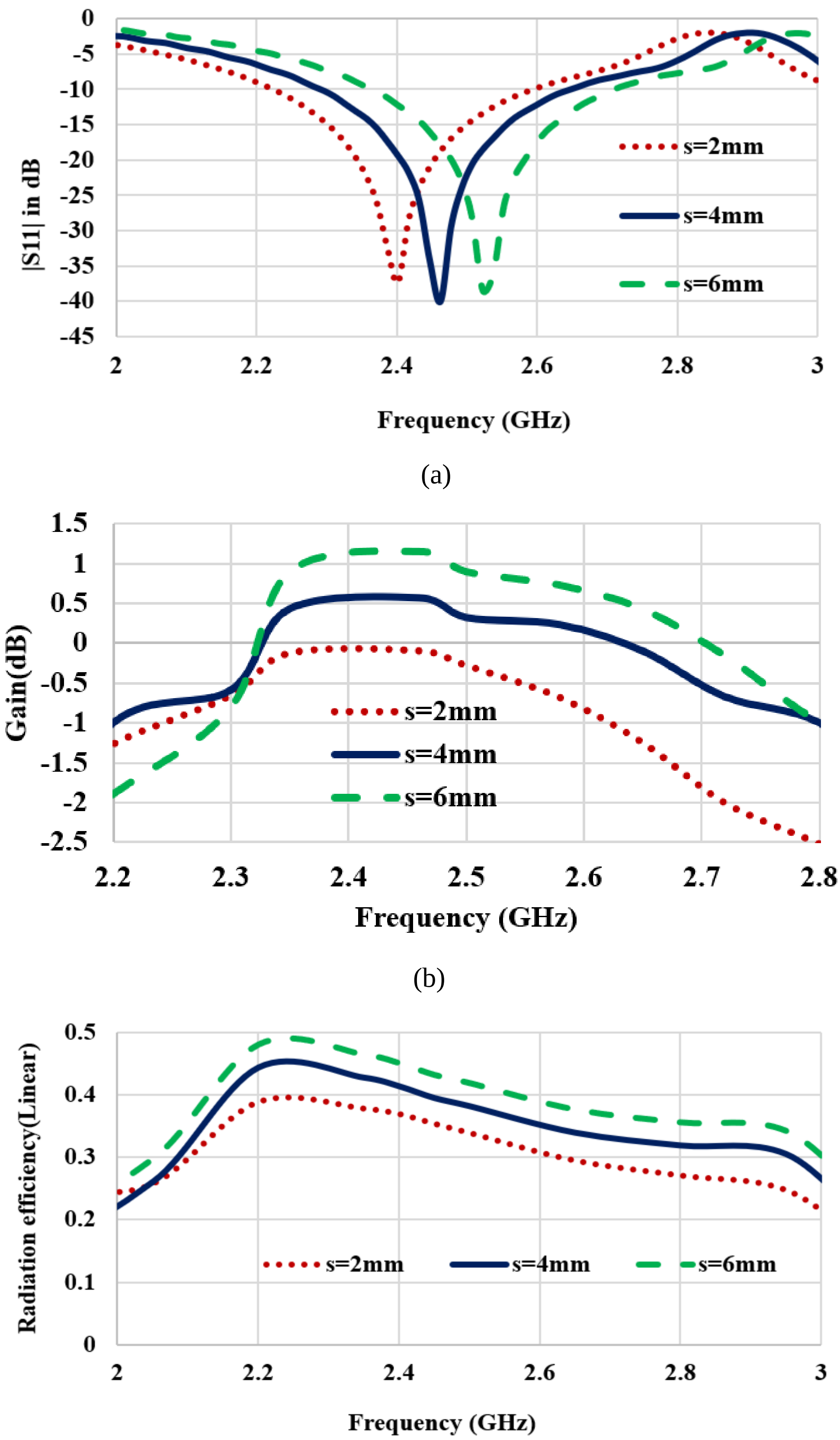

(a)

(b)

(c)

Fig. 3.10 (a) Reflection coefficient (b) gain, and (c) radiation efficiency plot for varying antenna tissue gap '*s mm*'

3.6 Measured Scattering Parameters

A prototype of the simulated MIMO structure is fabricated and simulated results are verified by measuring s-parameters on a programmable network analyzer. To measure the antenna performance on body tissue, pork tissue is placed below the antenna. Snapshots of the measurement system are displayed in Fig. 3.11.

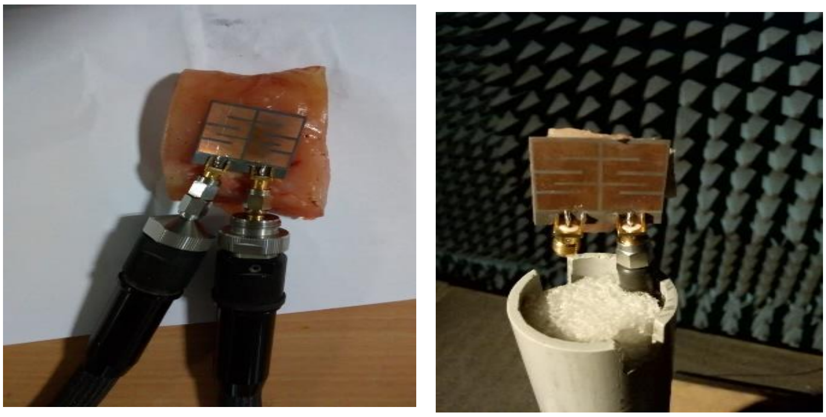

(a) (b)

Fig. 3.11 Snapshots of measurement setup (a) antenna on pork phantom (b) antenna in anechoic chamber

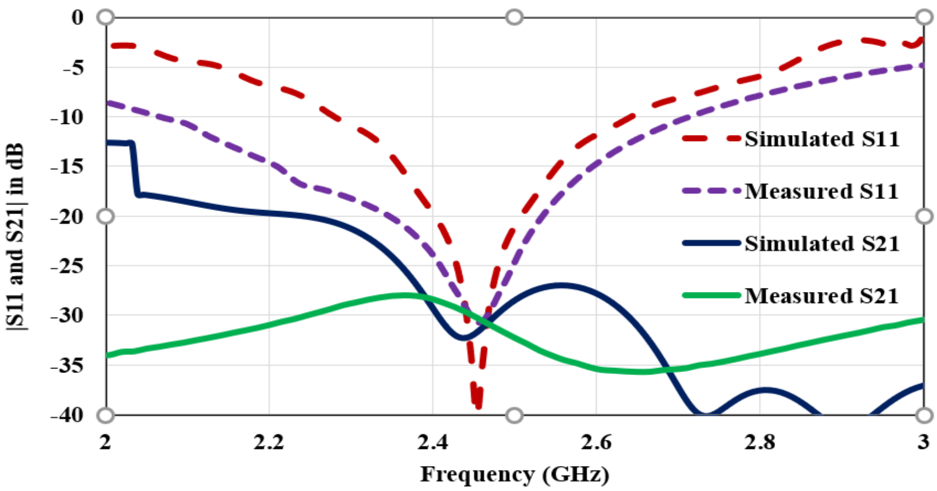

Fig. 3.12 Measured and simulated scattering parameters of MIMO antenna

Scattering parameters are the essential factors to examine the 10-dB impedance bandwidth and port isolation through reflection coefficient (|S11|) and transmission coefficients (|S21|). Measured and simulated S-parameters are compared in Fig. 3.12. Measured -10 dB bandwidth is 2.12 GHz to 2.6 GHz (480 MHz) whereas simulated -10 dB bandwidth is ranging from 2.3 GHz to 2.6 GHz (300 MHz). The measured value shows broader bandwidth as compared to the simulated value. This kind of variation in the bandwidth of measured and simulated results have been studied in the literature [128]. Both simulated and measured |S21| plots show that port isolation is more than 30 dB at ISM band.

3.7 Radiation Characteristics

H-plane (phi = 90^0) and E-plane (phi = 0^0) radiation pattern plots for port1 excitation are shown in Fig. 3.13. In both the planes, broadside radiation characteristics are presented by the proposed structure, which is the desired feature for on-off body data transmission. The simulated gain is compared with the measured values and plotted in Fig. 3.13(c). Positive gain value of about 0.5 dB is held over the operating bandwidth. 3-D, directivity at 2.45 GHz is represented in Fig. 3.13(d).

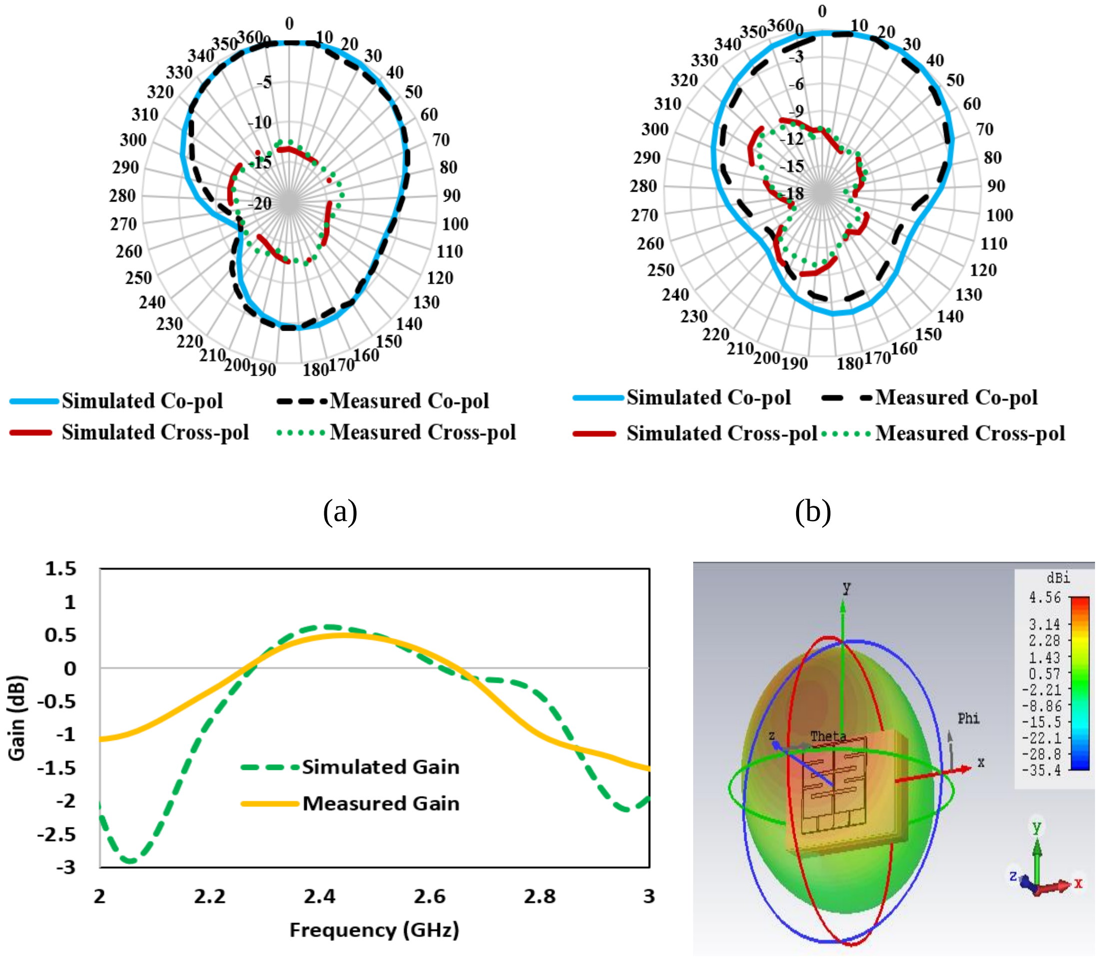

(a) (b)

(c) (d)

Fig. 3.13 (a) Far field pattern in E-plane (b) far field pattern in H-plane (c) simulated and measured plot for gain (d) simulated 3-D directivity pattern

Maximum directivity of 4.56 dBi is obtained. Directivity is much higher as compared to the gain. Internal reflection of EM waves is caused by the dissimilar thickness and permittivity of every tissue layer. That causes the superposition of reflected waves and antenna radiations and results in high directivity.

3.8 Specific Absorption Rate (SAR) to Peak Distance Location Ratio (SPLSR)

SPLSR is the parameter to evaluate the effect of closely placed, simultaneously excited radiators on SAR value. According to FCC regulations, it should be less than 0.4 W/Kg/cm when separation between two radiators is below 5 cm [215]. Mathematically SPLSR is defined as:

$$\mathrm{SPLSR} = \frac{\mathrm{SAR1} + \mathrm{SAR2}}{\mathrm{D}} \tag{3.6}$$

Where, SAR1 and SAR2 are the specific absorption rates for the two radiators respectively. D is the distance between the maximum SAR locations of the closely placed radiators.

Fig. 3.14, shows the simulated SAR value on 1 gram of body tissue for 20 mW of input power. Maximum power absorption intensity can be absorbed at the centre of each radiating element. According to the dimensions of the antenna distance *D* is 1.3 cm. Calculated SPLSR value for the designed MIMO antenna is 0.203 W/Kg/cm and satisfied the safety regulations.

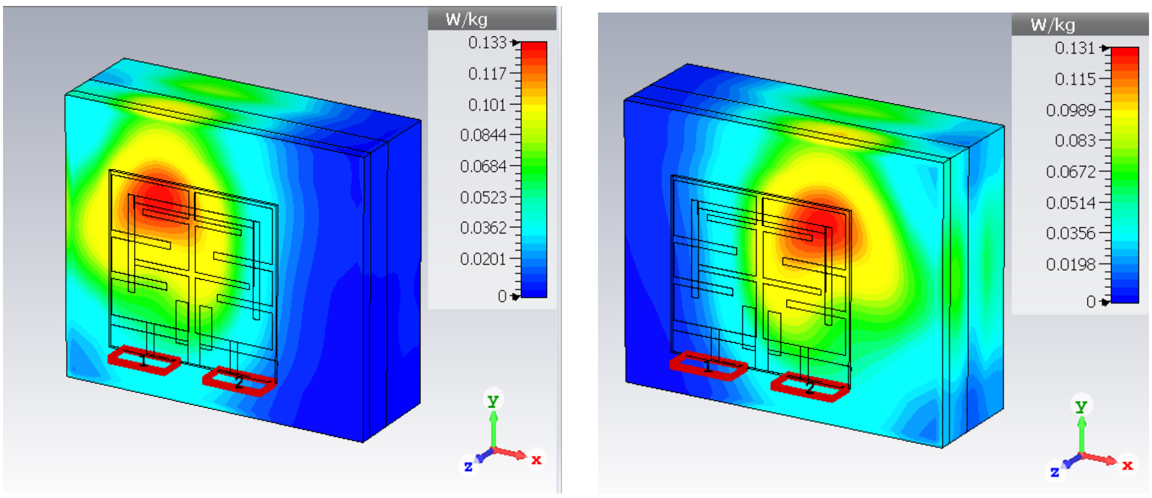

(a) (b)

Fig. 3.14 SAR value of proposed MIMO antenna at 2.45 GHz (a) radiator1 (b) radiator2

3.9 Effect of Bending on Antenna Performance

There is a possibility of structural deformation for a wearable antenna due to various body movements. According to this, antenna behavior is examined under the bent state. Antenna is bent for two radii values (20 mm and 25 mm) around a circular phantom. The compact size of antenna makes it self-conformal for the larger radii. The minimum radius is taken as the average size of an adult's wrist.

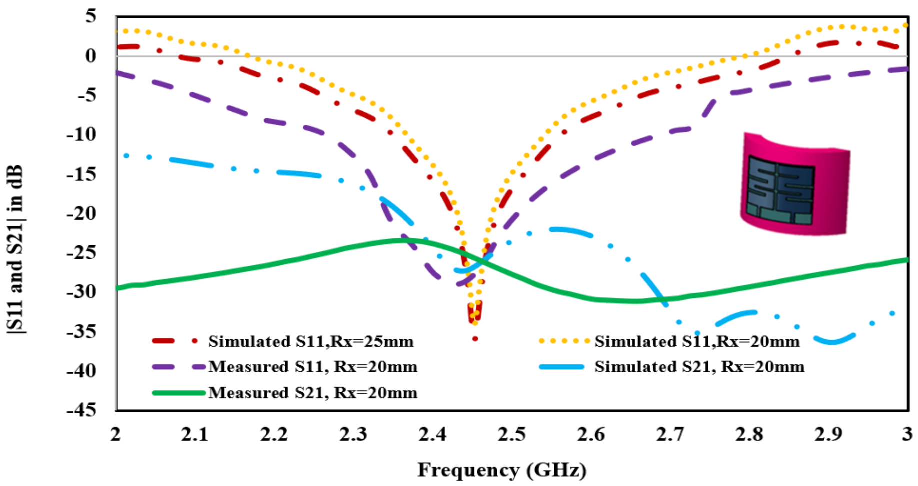

Fig. 3.15 Measured and simulated S-parameters for x-axis bending

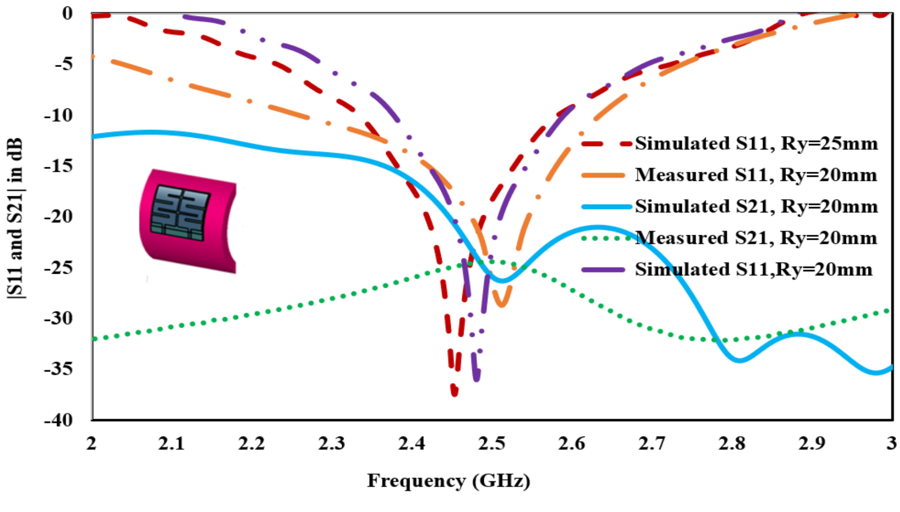

Fig. 3.16 Measured and simulated S-parameters y-axis bending

Variable '*Rx*' is the bending radii for x-axis and '*Ry*' for the y-axis. S-parameters for both the curvature deformation are drawn in Fig. 3.15, and Fig. 3.16. Bending across the x-axis has insignificant effect on resonance and impedance matching for all radii. Even at minimum bending radius (at 20 mm), simulated return loss has slightly shifted by 6 dB as compared to flat geometry. Measured return loss has shown almost stable response to bending. X-axis structural deformation has no impact on the mutual coupling.

Slight rightward shifting of resonance frequency can be observed with decreasing radii along the y-axis. In comparison with the flat structure, simulated return loss is changed to 35 dB from 40 dB with extreme banding at 20 mm. This is because of the variation in the widths and gap of the open-ended slots between them. The measured return loss plot shows that the central resonance frequency is detuned by 0.06 GHz. Still, the antenna is capable of retaining its resonance for the desired band due to wideband impedance matching. Slight degradation in port isolation can be noticed for deformation along y-axis. It has varied the length of vertical arms of the parasitic stub. This possibly led to the increase in mutual coupling. Proposed structure is reliable for structural deformation and can successfully retain the reflection coefficient well below -10 dB for the ISM band.

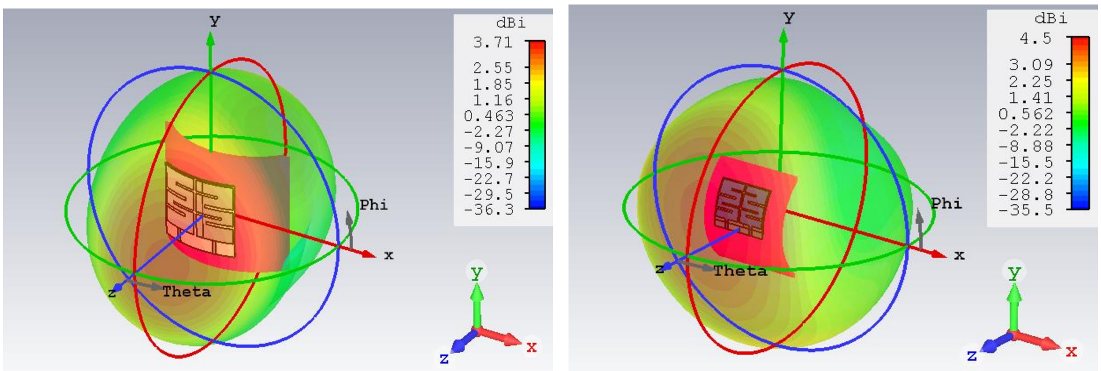

(a) (b)

Fig. 3.17 3-D directivity plot (a) bending along x-axis (b) bending along y-axis

Fig. 3.17 shows the 3-D radiation pattern during structural deformation conditions. Under both the bending condition, maximum radiations are oriented opposite to the body. Slight reduction in directivity from 4.56 dBi (flat state) to 3.71 dBi is found for x-axis structural deformation. For y-axis bending, there is a negligible reduction in the directivity of 0.06 dBi.

3.10 Diversity Performance

Important diversity functions like diversity gain (DG), channel capacity loss (CCL), and envelope correlation coefficient (ECC) are examined to support the MIMO ability of antenna. ECC signifies the correlation between the radiation of two closely placed radiators. Low value of ECC is desired for MIMO applications. From 3-D radiation pattern ECC value is calculated using the equation 3.7 [216].

$$\rho_e = \frac{|\oiint_\Omega [\vec{E}_1(\theta,\phi) \cdot \vec{E}_2^*(\theta,\phi)] d\Omega|^2}{\oiint_\Omega |\vec{E}_1(\theta,\phi)|^2 d\Omega \, . \, \oiint_\Omega |\vec{E}_2(\theta,\phi)|^2 d\Omega} \tag{3.7}$$

Where, $\vec{E}_1(\theta,\phi)$ is the radiator-1 far field, and $\vec{E}_2^*(\theta,\phi)$ is the complex conjugate of the far field of radiator-2. Diversity can be calculated by using the equation 3.8.

$$DG = 10\sqrt{(1 - |\rho_e|)} \tag{3.8}$$

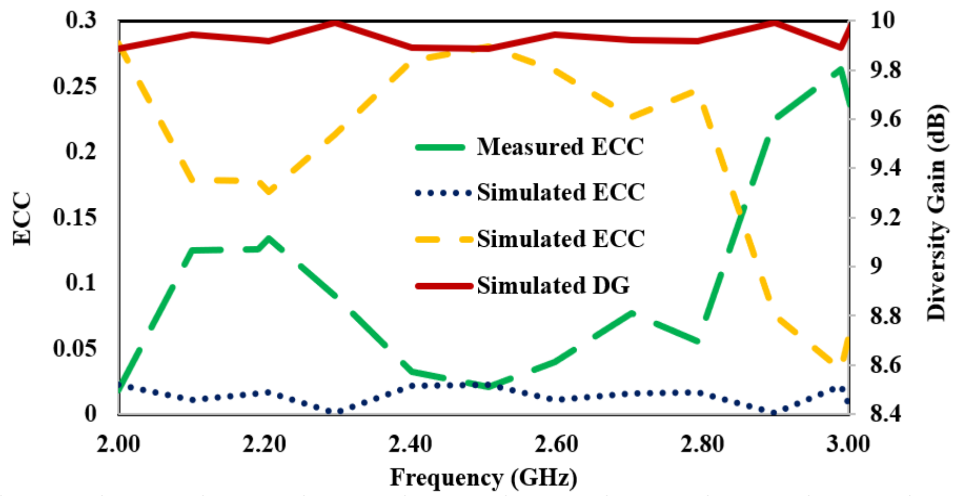

Fig. 3.18 Measured and simulated Plot for DG and ECC of the MIMO antenna

Fig. 3.18 shows the diversity gain and ECC plot of the designed antenna. ECC value is lower than 0.025 and DG value is higher than 9.8 dB over the ISM band. Small CCL value supports higher transmission rate. Lower than 0.4 bits/sec/Hz value of CCL is desired for a MIMO antenna, and it can be calculated by equation 3.9.

$$CCL = -\log_2 \det(a^R) \tag{3.9}$$

Where elements of 2×2 correlation matrix (a^R) are given as: $a_{ij} = 1 - (S_{ii}^* S_{ij} + S_{ji}^* S_{jj})$, and $a_{ii} = 1 - \left(|S_{ii}|^2 + |S_{ij}|^2\right)$. Plot in Fig. 3.19 shows CCLL value of less than 0.12 bits/sec/Hz at 2.45 GHz for the proposed antenna.

Beside this performance of antenna is compared with some of the on-body MIMO antennas and listed in Table 3.2.

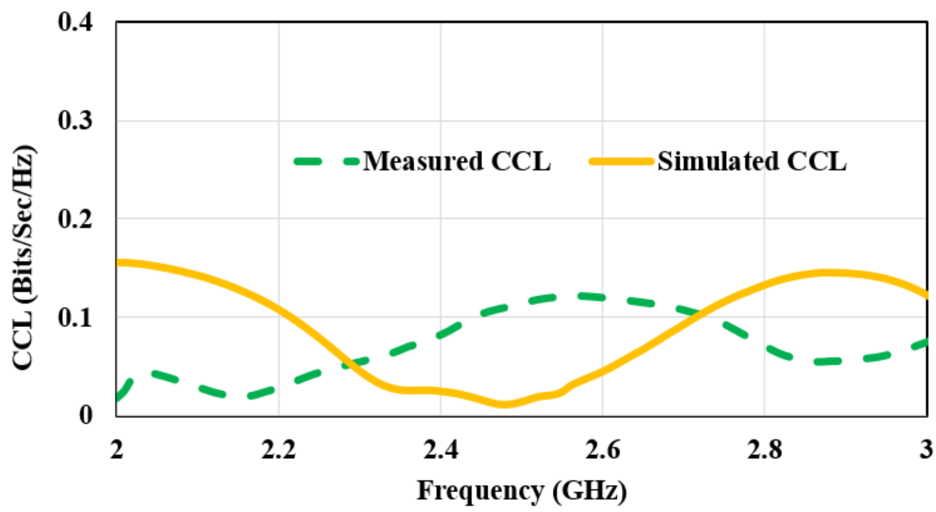

Fig. 3.19 Measured and simulated Plot for channel capacity loss (CCL)

Table 3.2 Comparison of on-body MIMO structure with reported work

Ref.	Frequency (GHz)	Size (mm^3)	Gain (dBi)	Bandwidth (MHz)	Efficiency (%)	|S21| (dB)
[43]	2.45, 5	101.9×92.3×3	NA	160,671	50,58	20
[132]	2.45	30×30×0.5	NA	140	40	20
[209]	UWB (2.74-12)	110×35×1.5	6.9 dB	9.26 GHz	NA	26
[210]	UWB (3.5-8)	30×50×1.5	NA	700	NA	32
[211]	2.45	54.98×76	2.83	1900	NA	12
[216]	2.45	height = 3.2 mm, Radius=22.9 mm	3.0	90	40	15
This Work	**2.45**	**28×25×0.5**	**0.5 dB**	**300**	**40**	**30**

Data in Table 3.2 shows that proposed structure is the smallest of all the antennas reported in the literature with excellent diversity and on-body performance. Designed MIMO antenna has maximum port isolation among the reported antennas operating at 2.45 GHz.

Research Contributions

In this chapter design process, numerical simulation, and characterization with bio-tissue environment of a MIMO antenna are described. Antenna is consisted of dual patch radiators, self –complementary pair of L-shaped ground and a port isolation enhancement stub. Major attainments of the proposed antenna are as follows:

- Designed slotted patch 1×2 array MIMO antenna with defected ground structure featured very small footprint with dimensions of 28×25×0.51 mm^3 and provided wide impedance bandwidth of 12% (2.3-2.6 GHz).
- Broadside radiation characteristics for on/off body transmission mode with directivity of 4.56 dBi is achieved.
- Robust impedance matching and steady radiation characteristics when bent for various radii along y-axis and x-axis.
- Excellent MIMO performance, low port coupling of -30 dB is achieved after adding the parasitic stub at the ground plane. Low ECC and CCL value with high diversity gain over the operating bandwidth is obtained.
- Satisfied safety regulation is attained for the MIMO configuration.
- In comparison to reported literature proposed antenna structure has maximum isolation and high robustness against structural deformation effect.

Published Paper Related to This Chapter:

1. Gupta, A. Kansal, P. Chawla “Design of A Wearable MIMO Antenna Deployed with An Inverted U-Shaped Ground Stub for diversity performance enhancement.” International Journal of Microwave and Wireless Technologies, vol.13, no.1, pp.76-86. 2020. https://doi.org/10.1017/S1769078720000471

Chapter-4

Flexible Antenna Structures for On Body Communication

4.1 Introduction

Preventing the interaction of antenna radiation with body tissue is one of the most potential factors that make designing wearable antenna very challenging. As more power is penetrated into the body, antenna efficiency, and gain reduce critically. Moreover, radiation absorbed by the body causes severe health hazards. Therefore, it is essential to design antenna structures that possess maximum power orientation normal to the surface of body along with small geometry. In [217] Left-Handed metamaterial had been used to miniaturize the patch antenna. Metamaterials had been also used prominently for providing isolation between antenna and body tissue. An array of EBG and AMC unit cells had been used as the back reflector to reduce the effect of radiations on tissue and for gain enhancement [215,218] of planar antennas. Large array configurations of metamaterial structure occupy the large surface area and difficult to assemble with compact sensor nodes. Adding of periodic stubs at the radiator edges is also the effective way to improve the efficiency as it confines the electric field penetration [219]. SIW technology-based wearable antenna is designed to enhance on-body radiation efficiency [107]. The array of shorting pins in SIW technology confine the electric field and reduces power leakage, but it enhances antenna fabrication complexity. Multiple substrate layers had been used in [220] for making antenna performance stable and robust on-body tissue. These structures are thick and not flexible. Recently, dielectric resonator antennas have been presented for the gain enhancement on-body antennas. The dielectric resonator has large vertical height which restricts antenna flexibility and creates uneasiness to the user [221,222].

In this chapter is two flexible antenna structures with high isolation of electromagnetic radiations from body tissue has been designed. Two different approaches are used to enhance antenna performance for WBAN applications. Metallic reflector and AMC surface are integrated with two patch antennas.

This chapter is prepared as: Section 4.2 covers the L-shaped ground and radiator antenna with a metallic reflector. Section 4.3 describes the defected ground patch antenna with AMC reflector

4.2 L-shaped Ground and Radiator Antenna with a Metallic Reflector

This designed structure consists of an L-shaped radiator, coplanar L-shaped ground and a metallic reflector. Further, metallic reflector plate is added for improving the radiation characteristics and avoiding the interference of electromagnetic waves with body tissues.

4.2.1 Antenna Configuration and Body-Tissue Design

Antenna is designed on thin flexible board of RO 3010 with $\boldsymbol{\varepsilon}_r$= 10.2, thickness = 0.5 mm, and tan δ = 0.0022. Antenna has planar dimensions of 30 mm × 31 mm which is equivalent to $0.245\lambda_o \times 0.253\lambda_o$. Only lower band (2.45 GHz) is excited due to the L-shaped radiator. Upper band (5.8 GHz) is excited by the L-shaped ground plane. Two bands are resonating together when metallic plate is integrated with the antenna at a distance of 's mm'. A 3-layered phantom model of 60 mm × 60 mm is designed to represent antenna operation on human tissue. Geometry of the on-body simulation setup and proposed antenna structure is shown in Fig. 4.1.

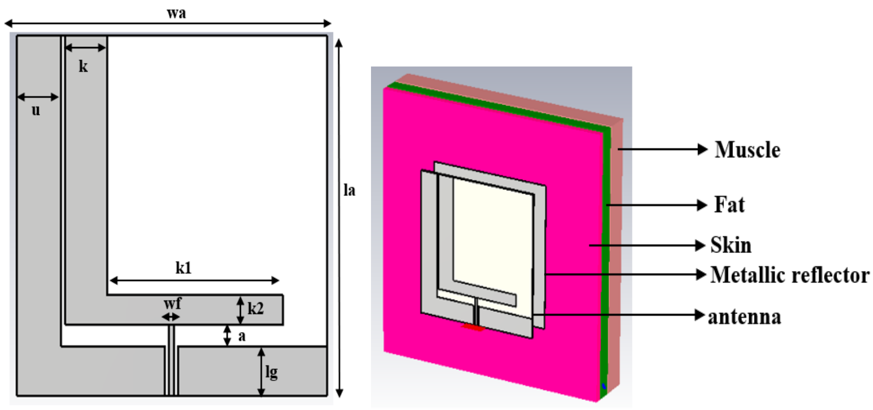

(a) (b)

Fig. 4.1 (a) Geometry, and (b) simulation setup of the proposed structure

4.2.2 Tuning Process of Dual Band Resonnace and Effect of Metallic Reflector on Antenna Performnace

Three antenna configurations are taken to explain the stepwise design procedure of the proposed antenna. Antenna topology for the three steps is shown in Fig. 4.2, and their reflection coefficient plots are drawn in Fig. 4.3. A distance of 6 mm is maintained to isolate the antenna and tissue model in step 1 and step 2. Antenna is directly placed on tissue after placing the metallic plate in step 3.

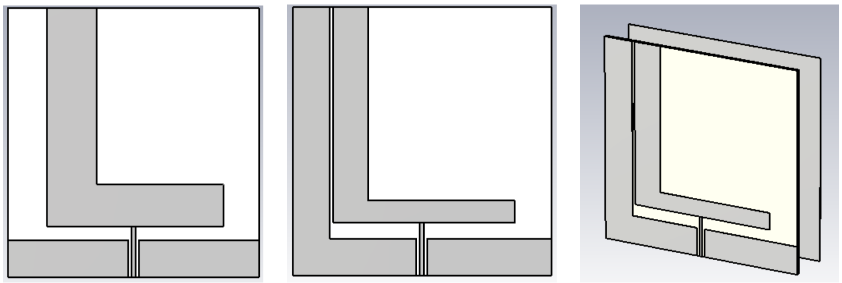

(a) (b) (c)

Fig. 4.2 Geometry of antenna for step wise design evaluation (a) step 1 (b) step 2 and (c) step 3 (proposed antenna)

Step 1: To begin with, a CPW structure with an L-shaped patch is designed in step 1 (Fig. 4.2(a)). It excites the antenna resonance at 2.45 GHz (Fig. 4.3). This structure is modified sequentially as a dual-band radiator that covers lower and upper ISM bands. The resonance frequency is significantly influenced by the vertical arm width 'k mm' of the radiator. To validate this, parametric analysis is performed by varying the value of 'k mm' from 4 mm to 7 mm. Effect of variation in vertical arm width on resonance is represented by the reflection coefficient plot, and shown in Fig. 4.4.

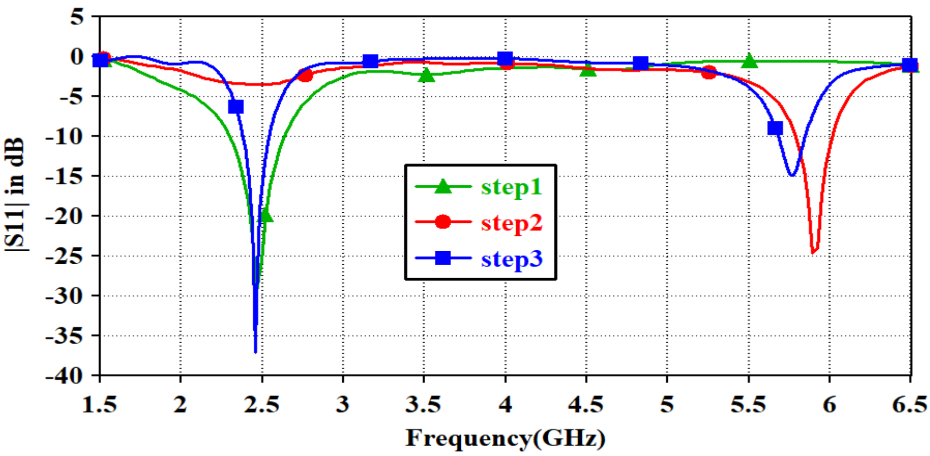

Fig. 4.3 Simulated input reflection coefficient plot for step wise evaluation of antenna

Fig. 4.4 shows that resonance is shifting leftward with reducing value of 'k mm'. When the value of 'k mm' is reduced after 5.5 mm, the reflection coefficient curve also starts shifting upward, and the increased value of |S11| shows the degradation of impedance matching. Thus, the optimum value of '$k = 4.75\ mm$' is fixed for tuning the resonance at desired frequency with good impedance matching.

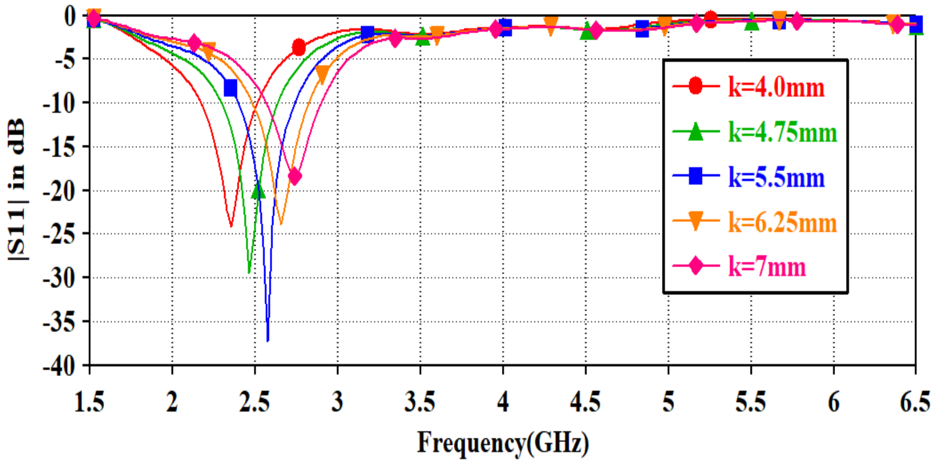

Fig. 4.4 Simulated input reflection coefficient plot for varying width '*k*' of vertical arm of radiator

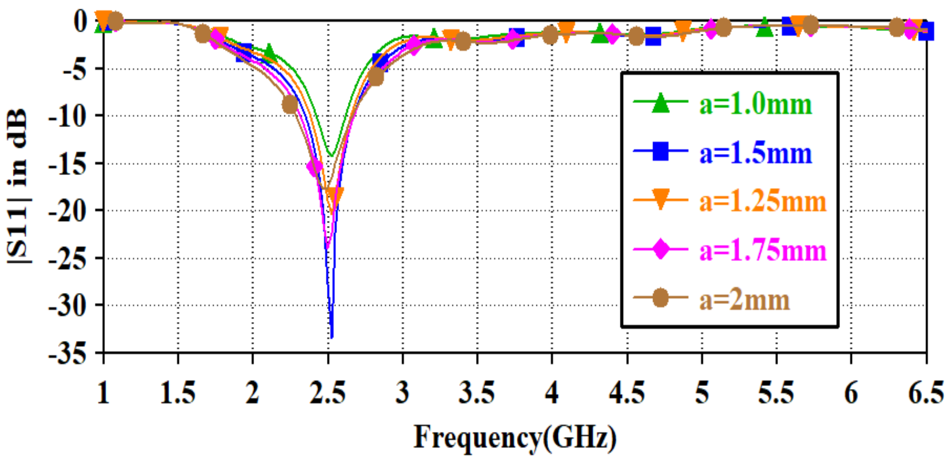

Fig. 4.5 Simulated input reflection coefficient plot for varying gap '*a mm*' between ground and radiator of antenna

Space between the ground plane and radiator of a coplanar structure is also a vital factor for preserving the impedance of antenna. Effect of varying this gap '$a\,mm$' on antenna impedance is also investigated through the parametric sweep. Fig. 4.5 represents the input reflection coefficient plot for varying 'a mm' gap. The value of 'a mm' is changed from 1 mm to 2 mm with a step size of 0.25 mm. Initially, reflection coefficient value decreases with the increasing value of '$a\,mm$' till 1.5 mm. On further increasing the value of '$a\,mm$' reflection coefficient starts increasing, resulting the reduction of impedance. Thereby, '$a = 1.5\,mm$' is considered for best coupling results between ground and radiator.

Step 2: At this step, antenna configuration is changed by modifying the ground plane into an L-shaped form. The vertical arm of ground plane is added parallelly to the vertical arm of the radiator, as shown in Fig. 4.2(b). This modification has extremely changed antenna resonance. Impedance matching at 2.45 GHz is lost, and antenna is tuned at 5.8 GHz (Fig. 4.3). To understand the physical significance of this effect, input impedance for the three designed configurations is investigated. Plot for input impedance is illustrated in Fig. 4.6.

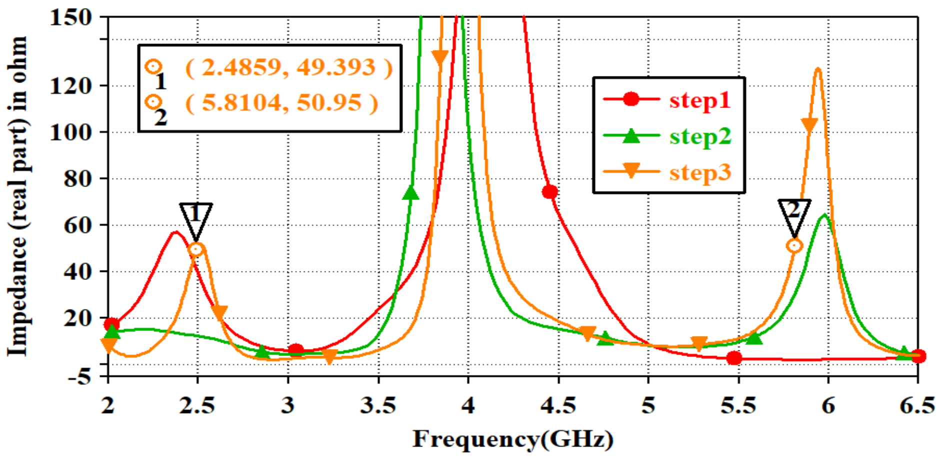

(a)

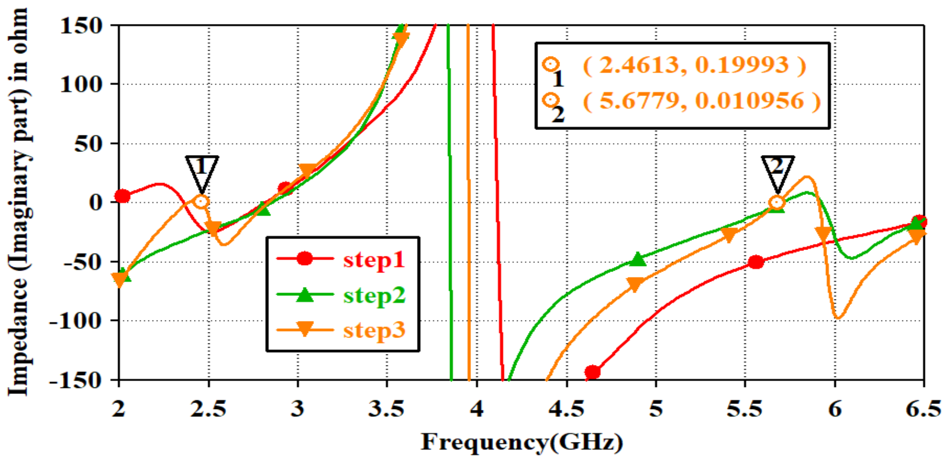

(b)

Fig. 4.6 Input impedance plot (a) real part, and (b) imaginary part

From the real impedance, it can be found that adding of the vertical arm with ground plane in step 2 has reduced the impedance from 50 ohms to 11 ohms at 2.45 GHz. Reactance becomes highly capacitive as the imaginary impedance curve shifts downward from 0 ohms to -25 ohm (2.45 GHz). At 5.8 GHz, the real value of impedance moves up from 5 ohms to 50 ohms, and the reactance value also moves upward from -40 ohm to 0 ohms, depicting only the resistive component in input impedance.

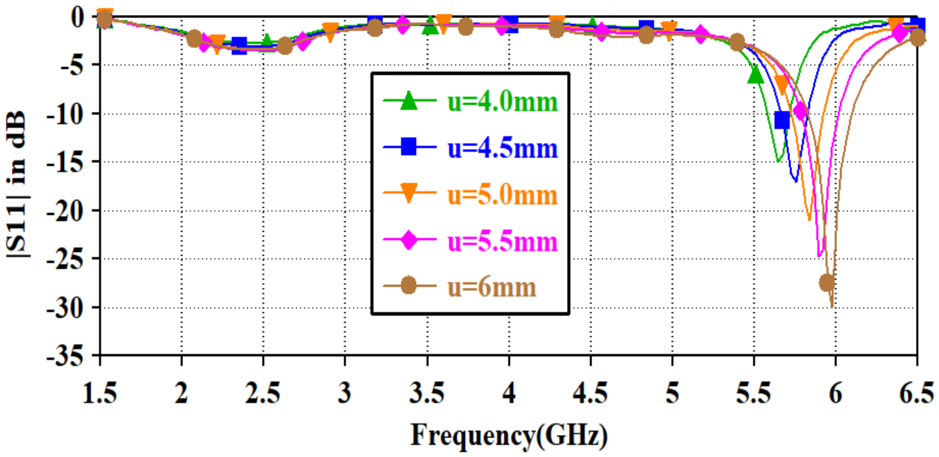

Fig. 4.7 Simulated input reflection coefficient plot for varying width 'u' of vertical arm of ground plane in step2

Upper resonance (5.8 GHz) is the function of capacitive reactance created by an L-shaped ground plane. Therefore, the width *'u mm'* of vertical arm of ground is varied to tune the operating frequency at 5.8 GHz. The input reflection coefficient for varying '*u mm'* is drawn in Fig. 4.7. Resonance frequency is increasing with increasing value of '*u mm'*. Desired band is achieved at '$u = 5.5\ mm$'. Thus, '$u = 5.5\ mm$' is considered for the next step.

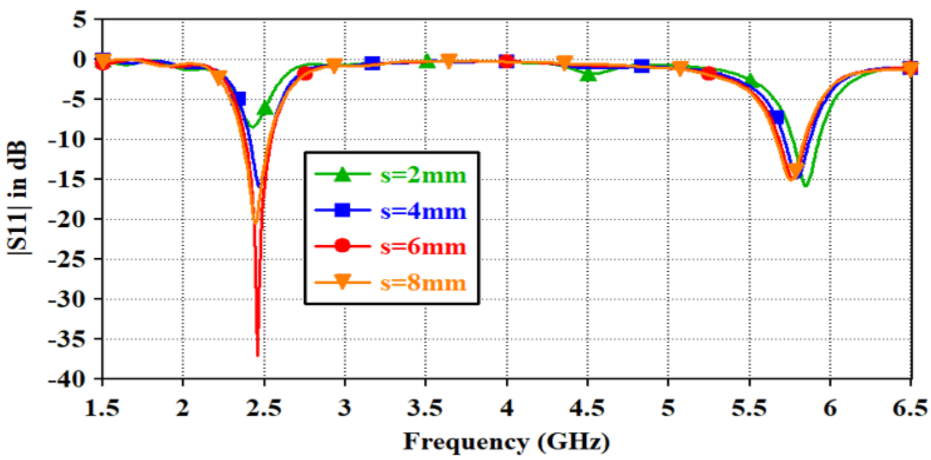

Fig. 4.8 Simulated input reflection coefficient plot for varying gap between antenna and reflector plate

Step 3: In this configuration, a metallic plate is placed beneath the antenna substrate at a gap of *'s = mm'* (Fig. 4.2(c)). This step is the most important part of antenna design process. Dual-band resonance and high isolation between antenna and body tissue are achieved after adding the reflector. This plate has added a parallel capacitance in antenna impedance. It is validated by the impedance plot shown in Fig. 4.6(b). The impedance curve also shows that capacitive reactance at 2.45 GHz is nullified due to an increase in capacitance *(xc = 1/jwc*). The reactance curve has shifted to zero value that makes antenna suitable to operate at the lower ISM band. At 5.8 GHz, metallic plate has a negligible impact on impedance value. Reactance has become slightly more inductive as the curve is shifted upward still approximate zero value of reactance, and 50 ohms value of resistance is sustained. In this way, antenna is tuned for dual-band resonance at required frequencies (Fig. 4.3).

Distance 's mm' of antenna and metallic reflector is optimized, and the return loss plot for the varying value of 's mm' is represented in Fig. 5.8. Impedance matching of antenna is improved with increasing value of *'s mm'*. No significant impact on resonance frequencies is observed. The value of *'s = 6 mm'* is maintained for attaining the optimum impedance matching at both the resonance frequency. Dimensions of the proposed structure are listed in Table 4.1.

Table 4.1 list of geometrical parameters

Design Parameter	Size in mm	Design Parameter	Size in mm
Wa	30	La	31
K	4.775	k1	3.54
k2	19.52	a	1.5
U	5.44	wf	0.5
Lg	5.23	-	-

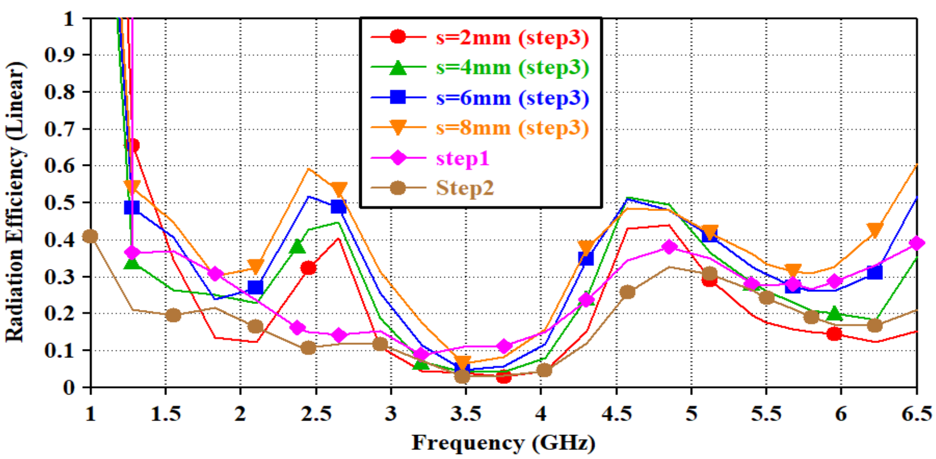

Fig. 4.9 Plot for radiation efficiency

Benefits of adding metallic plate are analyzed with the help of gain and radiation efficiency parameters. The metal plate behaves as a reflector for antenna back radiations. It reduces the back radiations by reflecting them towards the antenna. It helps to achieve directional radiation pattern, which is oriented away from the body tissue. Hence, penetration of EM radiation in lossy body tissue is protected, and improvement in radiation characteristics is achieved. The impact of this plate on antenna efficiency and gain is investigated with varying distances' and compared with the values achieved in step 1 and step 2 without the reflector plate.

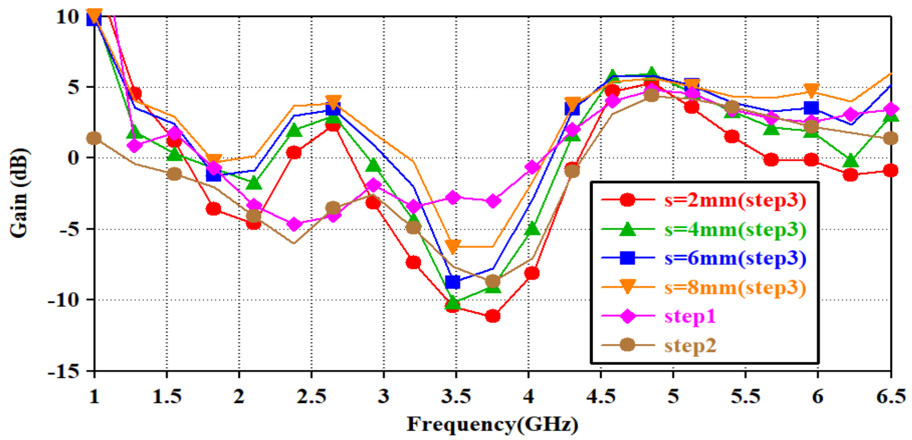

Fig. 4.10 Plot for Gain

Table 4.2 Comparison of the antennas designed in three steps

Parameters → **Antenna ↓**	**Frequency (GHz)**	**Reflection coefficient (dB)**	**Input Impedance in ohms (real, imaginary)**	**Efficiency (%)**	**Gain (dB)**
Step 1	2.45	-25	50,0	18	-5
	5.8 (not resonating)	0	5, -40	27	3
Step 2	2.45 (not resonating)	-3	11, -25	10	-6
	5.8	-25	50.0	20	3
Step 3	2.45	-35	49.39,0.19	50	3
	5.8	-15	50.95, 0.01	32	4

The plot for efficiency and gain parameters are represented in Figures 4.9 and 4.10, respectively. Adding of metal plate has demonstrated significant improvement in the performance at the lower band. At 2.45 GHz, the radiation efficiency is improved by 32%, and gain by 8 dB. Upper band is less influenced by the metallic plate.

Radiation efficiency is improved by 12%, and gain is improved by 1 dB at 5.8 GHz. The performance of the antenna can be enhanced further by increasing the value of space between antenna and reflector plate. It can be analyzed that with every 2 mm increase of '*s mm'* 6% improvement in efficiency and 1 dB improvement in gain can be achieved. Table 5.2 summarizes the performance of the antennas designed in three steps.

4.2.3 Return Loss Analysis in Flat and Bent State

Numerical simulation of the proposed antenna is validated by measuring the performance of a fabricated prototype of proposed antenna. Lab measure is performed on N5247A programmable network analyzer. To test antenna for on-body operation, pork tissue is used. Low loss foam spacer is placed between the antenna and back reflector to cover the space of 6 mm. Fig. 4.11 represents the photographs taken while measurement. To confirm the stability of the antenna, reflection coefficient is measured on both rectangular and cylindrical pork tissue.

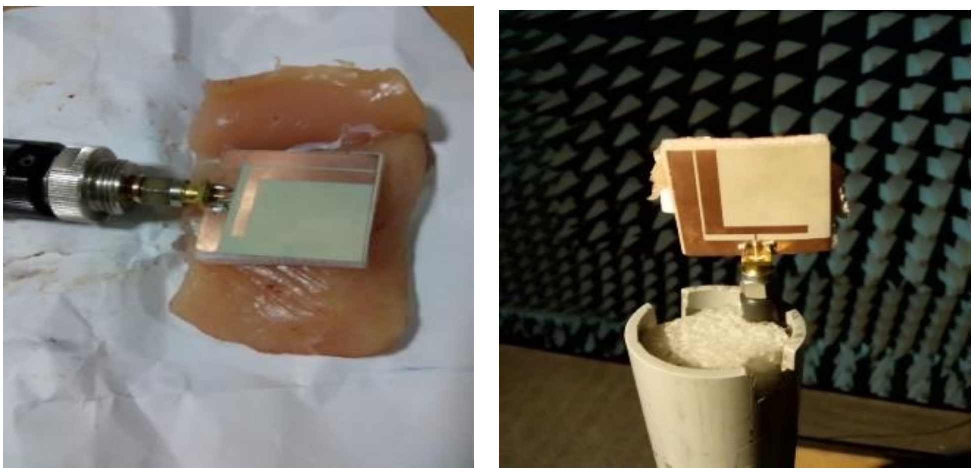

(a) (b)

Fig. 4.11 Photographs during measurement (a) antenna placed on rectangular pork loin (b) antenna in anechoic chamber

Measured results are compared with simulated results for both the flat and bent state of antenna. Fig.4.12 depicts the measured and simulated reflection coefficient curve for both the operating conditions. On the rectangular surface, the simulated antenna has covered the impedance bandwidth of 210 MHz (2.39 GHz to 2.6 GHz) and 220 MHz (5.70 GHz to 5.92 GHz) at the lower and upper band, respectively. The fabricated prototype has covered the bandwidth of 310 MHz (2.29 GHz to 2.6 GHz) and 330 MHz (5.59 GHz to 5.92 GHz) for lower and upper bands. This result reveals that measured bandwidth is more than the simulated for both the resonance frequencies. This variation is possibly the result of high cable loss and difference in the tissue properties used in simulation and measurement setup.

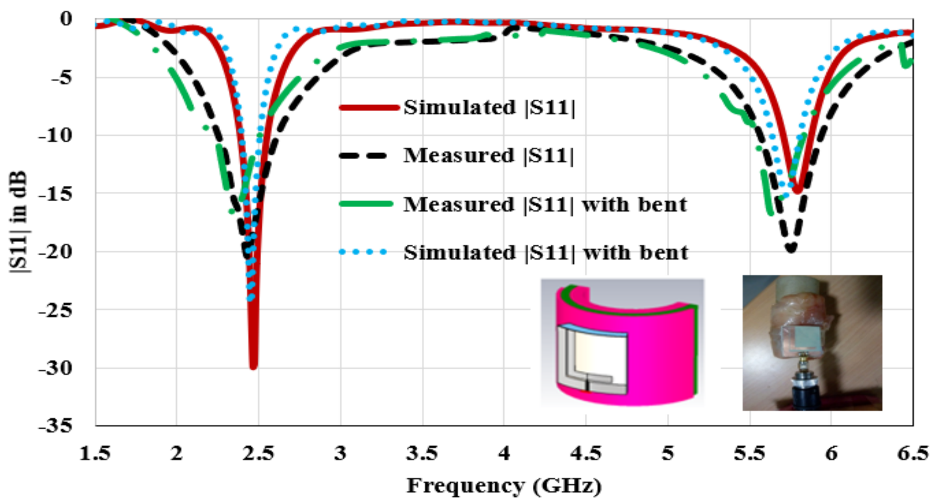

Fig. 4.12 Simulated and measured input reflection coefficient plot

Antenna is first numerically simulated on a cylindrical phantom. Three-layered cylindrical body-tissue of radius 25 mm is designed for the simulation. Compact size of antenna makes it self -conformal for the larger radius values. To test the antenna reliability on different body parts, antenna is bent around the cylindrical phantom and pork tissue for simulation and measurement purposes. While measurement transparent tape is pasted to grip the antenna in the bent state.

The return loss plot with bent conditions shows that at lower band (2.45 GHz), resonance frequency is stable, and the reflection coefficient value is increased slightly. At the upper band (5.8 GHz), center resonance frequency shifts leftward. Frequency detuning at upper band is probably due to the stretching of the coupling gap between the standing arm of the ground and radiator. Still, the designed antenna has sufficiently covered the required bandwidth in deformed state.

4.2.4 Radiation Characteristics of Proposed Antenna

Normalized radiation plots at 2.45 and 5.8 GHz frequencies are presented in Fig. 4.13 (a & b). 3-D simulated radiation plots for both the frequencies are also displayed in Fig. 4.13 (c & d). At 2.45 GHz, radiation plots are depicting broadside forward beam in both planes.

The 3-D plot is also confirming the high directivity of 6.31 dBi in positive *z* direction (normal to the body surface). At 5.8 GHz, unidirectional type of radiation pattern can be observed. Towards the surface of the body (at 180^0), null in radiation pattern can be observed. The 3-D plot shows directivity of 8.75 dBi, which is a noticeable achievement for an on-body compact size antenna. Broadside and unidirectional radiation patterns are highly demanded features of an antenna for using in close vicinity of the body. Relative study of the designed antenna with reported dual-band structures is given in Table 4.3.

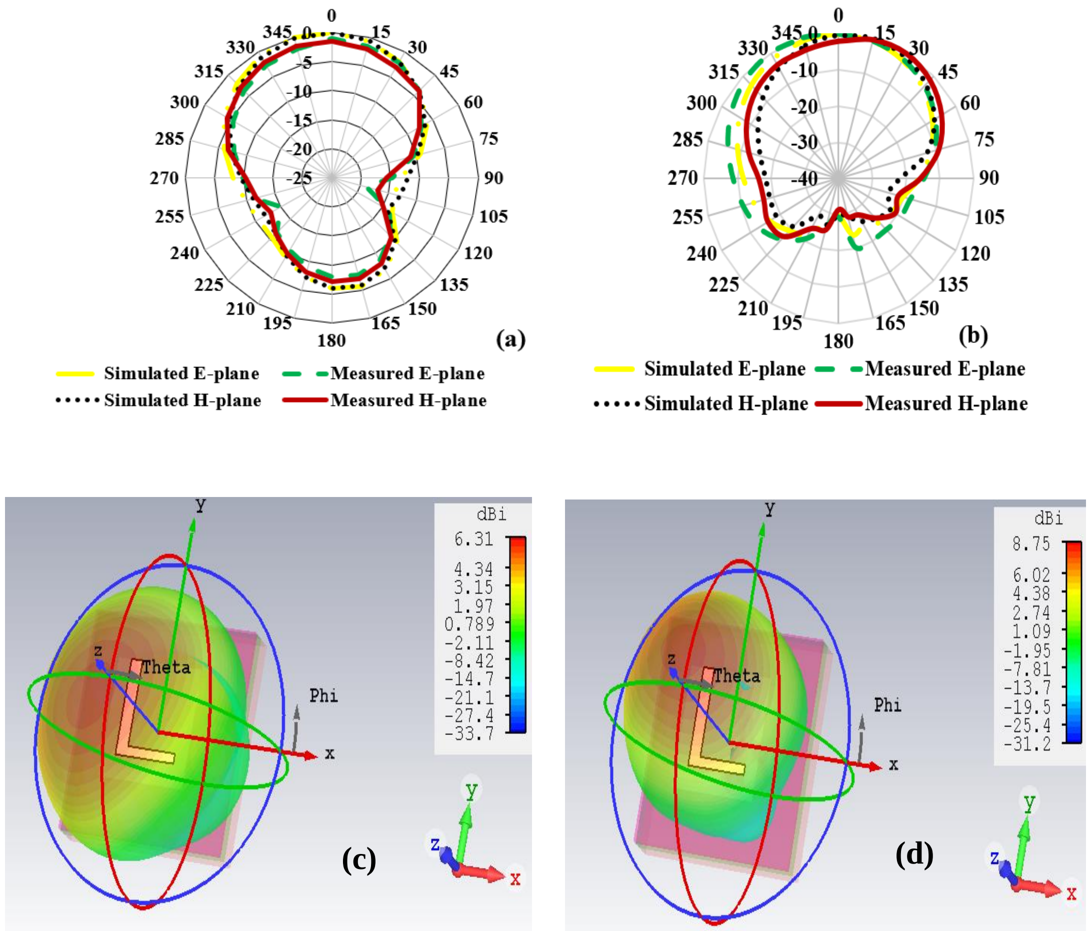

Fig. 4.13 Radiation plots (a) 2-D radiation plot at 2.45GHz (b) 2-D radiation plot at 5.8 GHz (c) 3-D directivity plot at 2.45 GHz (d) 3-D directivity plot at 5.8 GHz

Table 4.3 Antenna performance comparison with the existing literature

Ref.	Resonance Frequency (GHz)	Dimension (mm^3)	Substrate Material	Gain (dBi)	10-dB Impedance Bandwidth (MHz)	Radiation Efficiency (%)	Bent Effect
[43]	2.45/5	102×92.3×3	Felt	NA	160/671	50/58	Stable
[64]	2.45/5.8	60×30 mm	Noxa dell Cr fabric	4.5/5.6	NA	NA	Stable
[87]	2.45/5.8	π×35×35×3	PDMS	4.16/4.34	84/247	58.6/50	Lower band shifted leftward
[90]	2.45/5.8	π×25×25×5	Felt	-5.1,3.3	320/550	11.8/48	Higher band shifted leftward
[218]	2.45/5.8	72×72×6.5	Polyamide	5.2/7.7	400/260	61.3/67.3	Unstable
[223]	2.4/5.5	50×40×4.6	Rubber	1.5/2.5	500/1000	25/27	NA
[224]	2.45/5.8	42×63×8	Felt	5/7.3	NA	55/60	Stable
This Work	**2.45/5.8**	**31×30×6.48**	**RO 3010**	**6.31/8.75**	**310/330**	**50/32**	**Higher band shifted leftward**

From Table 4.3 it can be seen that the proposed antenna has high gain, wide bandwidth and compact geometry.

4.2.5 Specific Absorption Rate Evaluation for Confirming Tissue Safety

To confirm user's safety, SAR value is simulated for both resonance frequencies. Fig. 4.14 shows the SAR results of proposed antenna.

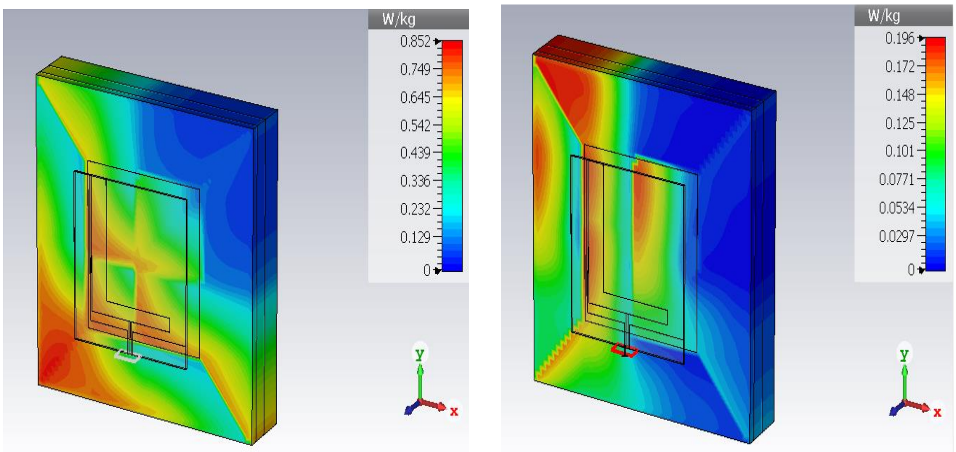

(a) (b)

Fig. 4.14 Specific absorption rate (a) at 2.45 GHz (b) at 5.8 GHz

Peak SAR value is 0.852 W/Kg. (at 2.45 GHz) and 0.196 W/Kg. (at 5.8 GHz). Input power is set at 0.1 W for SAR evaluation and averaged over 10 g of tissue mass. SAR value is under the safety limits for both frequencies.

4.3 Defected Ground Patch Antenna with AMC Reflector

This designed antenna is a conformal defected ground patch antenna with artificial magnetic conductor operating at 2.45 GHz frequency. Antenna is characterized for on-body communication with high directivity and wide impedance bandwidth.

4.3.1 Design and Configuration of on-body Patch antenna

A defected ground patch antenna occupying planar dimensions of 25 mm × 32 mm (0.204λo × 0.261λo) is designed on RT Duroid 5880 substrate with thickness of 0.5 mm. Reactive loading through a shorting pin and a rectangular ground strip is done to reduce antenna size. Square phantom with electrical properties of muscle tissue, side of 80 mm, and thickness of 15 mm is modelled to represent body.

To avoid direct contact of antenna and body tissue, gap '*s = 3 mm'* is maintained between antenna and muscle phantom. Simulation set up and antenna topology of proposed antenna is represented in Fig. 4.15. To explain the design process, four steps are considered and shown in Fig. 4.16. Return loss for all topologies is compared in Fig. 4.17.

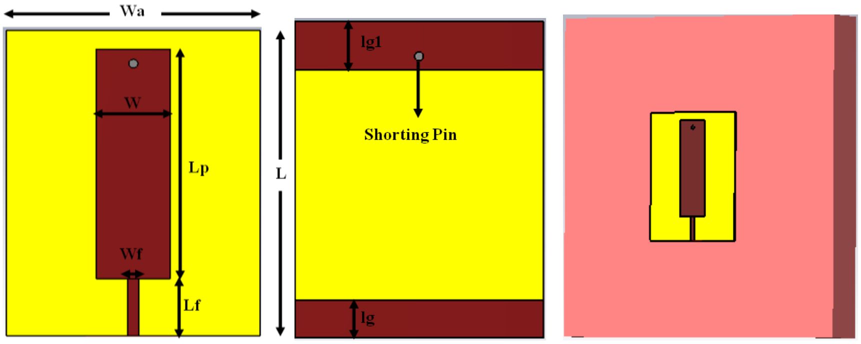

(a) (b) (c)

Fig. 4.15 Geometry of proposed antenna structure (a) front side (b) back side (c) simulation setup where antenna is placed on the muscle tissue

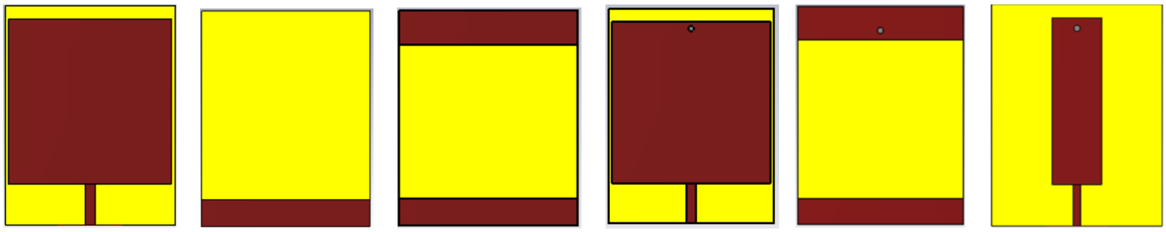

(a) (b) (c) (d) (e) (f)

Fig. 4.16 Topologies of stepwise antenna (a) front side of step 1 and step 2 (b and c) back side of step 1 and step 2 (d) front side of step 3 (e) back side of step 3 and step 4 (f) front side of step 4

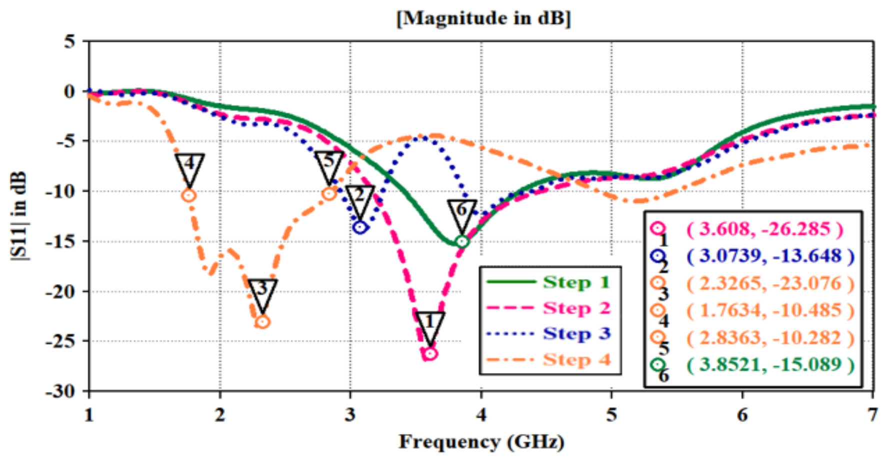

Fig. 4.17 Comparison of reflection coefficient |S11| for step wise design topologies

Antenna in step 1: It is a partial ground, quarter wavelength microstrip patch antenna which is tuned at 3.85 GHz with -10 dB bandwidth of 880 MHz ranging from 3.37 GHz to 4.25 GHz. Due to muscle tissue effect, resonance frequency is less than free space frequency at quarter wavelength. Length of the partial ground *(lg)* is optimized for impedance characteristics.

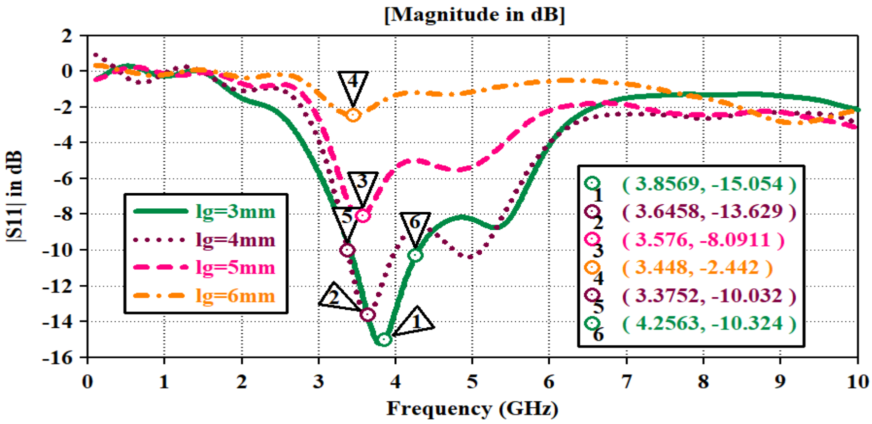

Fig. 4.18 Simulated reflection coefficient |S11| for varying ground length

Curves in Fig. 4.18 shows that, reflection coefficient and frequency is decreasing with reducing ground plane. |S11| plot is below -10 dB for less than 5 mm value of ground length. Minimum ground length of 3 mm is taken for the proposed antenna.

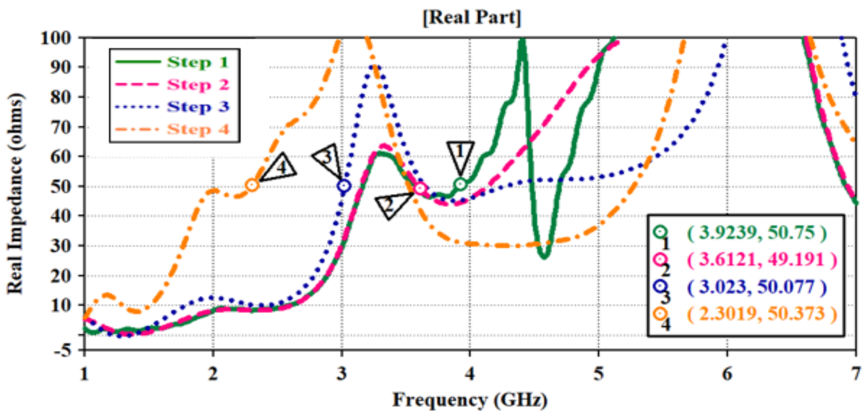

(a)

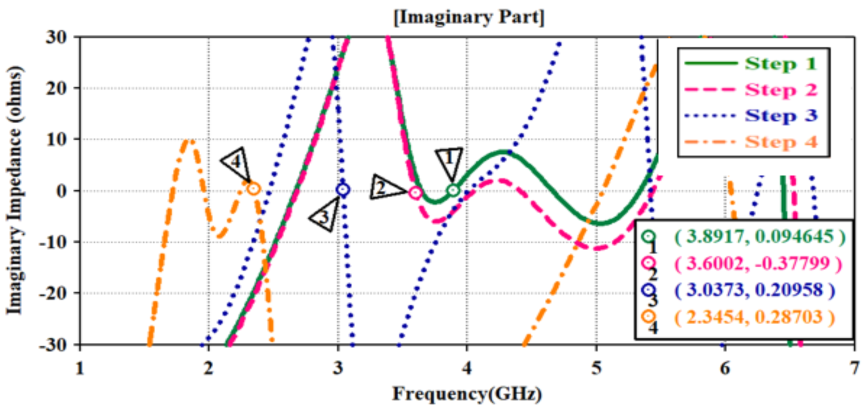

(b)

Fig. 4.19 Impedance plot for step wise antenna topologies (a) real impedance (b) imaginary impedance

Antenna in step 2: A parasitic strip is printed on the ground plane. Impedance plot in Fig. 4.19, shows that capacitance effect is increased in step 2. Imaginary impedance graph shifts downward depicting high capacitive reactance. It causes lowering of resonance frequency at 3.6 GHz with better impedance bandwidth. Reflection coefficient plot for varying strip length '$lg1$' in Fig. 4.20 depicts that resonance is not varied much with different strip length.

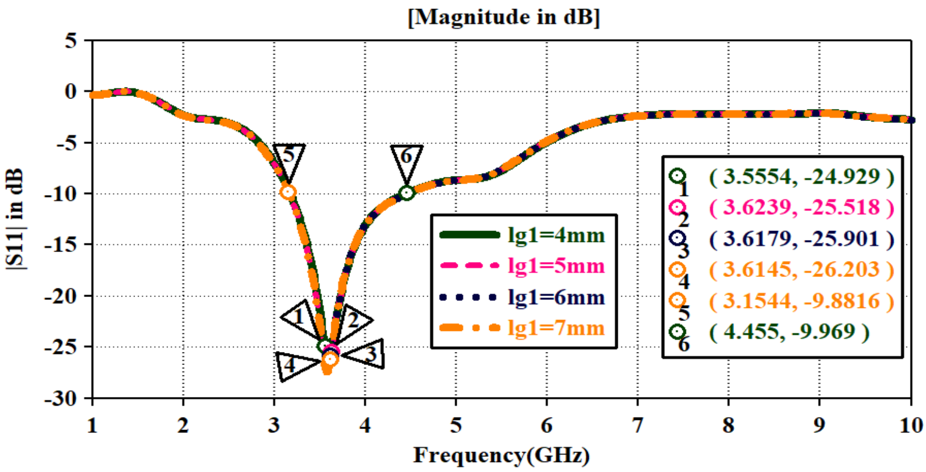

Fig. 4.20 Simulated reflection coefficient |S11| for varying ground strip length '$lg1$'

Antenna in step 3: In this topology, shorting pin is inserted between radiator and parasitic strip. It is an operative method to reduce the frequency of quarter wave radiators. It is clear from Fig. 4.17 that resonance frequency is shifted to 3.0 GHz but with narrow -10 dB bandwidth. Shorting pin location influence the antenna impedance. Large gap between feed point and shoring pin creates high impedance. Real impedance curve in Fig. 4.19 (a) shows that impedance of antenna reaches to 90 ohms. It expands the quality factor of antenna; therefore, antenna in step 3 has narrow impedance bandwidth. Imaginary impedance plot shifts more downward due to parallel inductance of shoring pin. In step 3, second resonance mode can be observed at 4.0 GHz.

Antenna in step 4: Multiple harmonic modes are generation is the inherit property of patch antenna. To avoid this effect, patch width is modified to unite the two resonance frequencies. This alteration shows significant improvement in antenna performance by tuning the frequency at 2.45 GHz and attaining broader bandwidth. Impedance plot of step 3 is showing zero reactance and 10 ohms resistance at 2.45 GHz. It is clear that antenna has excited the resonance at 2.45 GHz but has poor impedance matching. At 2.45 GHz, |S11| value of antenna in step 3 is also less than 0 dB. Thus, to improve the impedance, width is altered in step 4. Reducing patch width has increased the resistance and enabled the radiator to give resonance at desired band. Moreover, two bands merged and widen the bandwidth. Reflection coefficient plot and real impedance plot in Fig. 4.21 shows that required resonance frequency is achieved at '$W = 7\ mm$' with bandwidth of 1.07 GHz (1.76 GHz to 2.83 GHz).

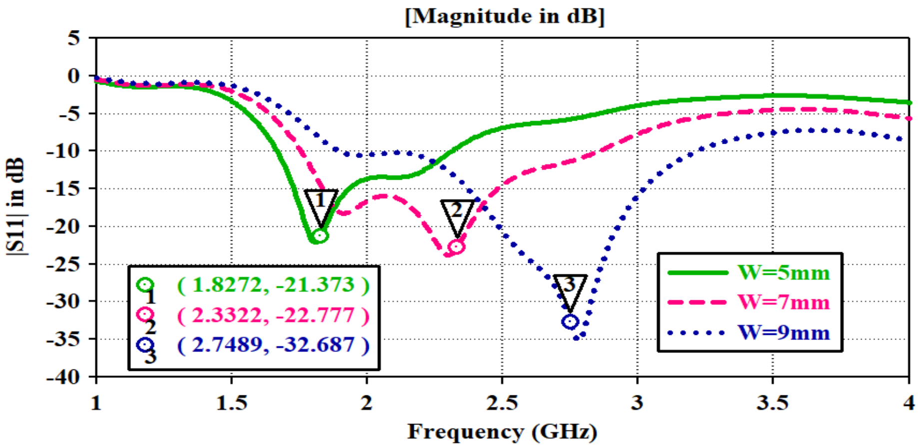

(a)

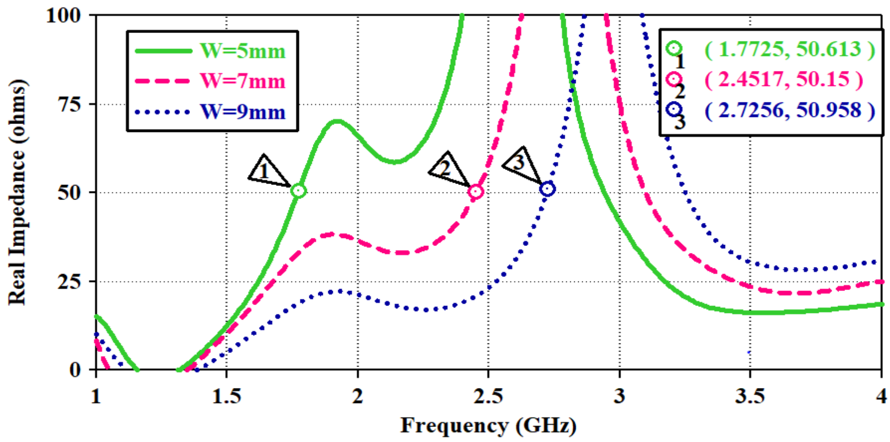

(b)

Fig. 4.21 (a) Reflection coefficient |S11| (b) real impedance plot for varying patch width

4.3.2 Design of AMC structure

To mitigate the conducting effect of body, an AMC surface is placed between the antenna and muscle tissue. Resonance frequency (f_u) of a square unit cell is evaluated from the equations (4.1-4.3) that has zero reflection phase at 3.1 GHz [225,226].

$$L = \mu_s \times h3 \tag{5.1}$$

$$C = \frac{W_{u1}}{\pi}(\varepsilon_0 + \varepsilon_s) Cosh^{-1}\left(\frac{W_u}{W_u - W_{u1}}\right) \tag{5.2}$$

$$f_u = \frac{1}{2\pi\sqrt{LC}} \tag{5.3}$$

$$BW = \frac{1}{120\pi}\sqrt{\frac{L}{C}} \tag{5.4}$$

Where, μ_s, ε_0, ε_s , h3, W_u, and W_{u1} represents substrate material permeability, vacuum permittivity, substrate permittivity, substrate thickness, unit cell width and square patch width respectively.

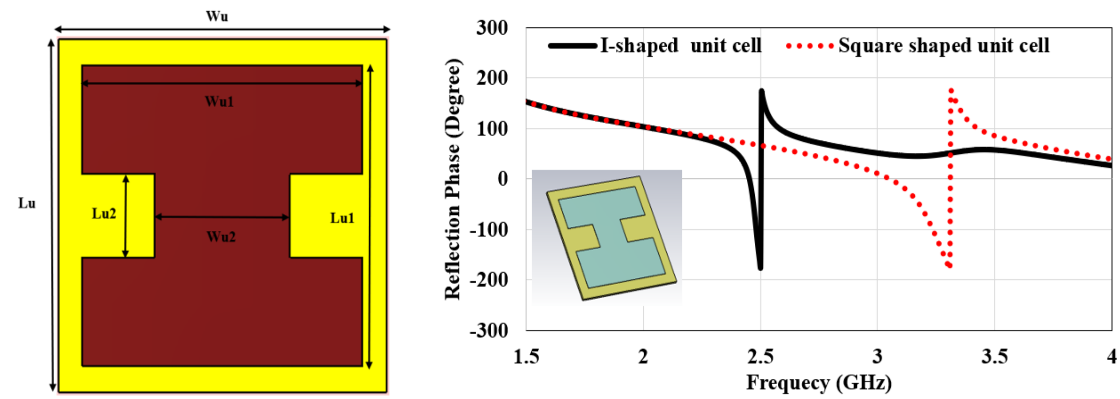

Fig. 4.22 Geometry and Reflection phase of I-shaped unit cell

Table 4.4 Geometrical parameters of antenna and unit cell structures

Geometrical Parameter	Value (mm)	Geometrical Parameter	Value (mm)	Geometrical Parameter	Value (mm)
Lu1	29	Lg	3.78	Lg1	4.9
Wu2	14	Wf	1.12	Lf	6.02
Wu1, Lu1	29	W	7.4	Lp	24
h3	1.235	h1	0.51	h2	3
Wu, Lu	34,34	Wa	25	L	32

Unit cell is improved as I-shaped cell to get zero reflection phase at 2.45 GHz. Fig. 4.22 shows the topology and reflection phase of the unit cell. Geometrical dimension of antenna structure and unit cell is listed in Table 4.4. Configuration of AMC surface designed with of 2×2 array of unit cells is located below the patch antenna is shown in Fig. 4.23. Low loss foam is used to fill the gap ‘$h2 = 3\ mm$’ between antenna and AMC surface. AMC surface follows the reflection phase theory [227,228]. Reflection range of I-shaped unit cell from -90^0 to $+90^0$ is covering the ISM band from 2.4 GHz to 2.48 GHz. Surface current plot in Fig. 4.23(c), shows that linearly polarized patch and AMC surface has resonance response only towards the y-axis

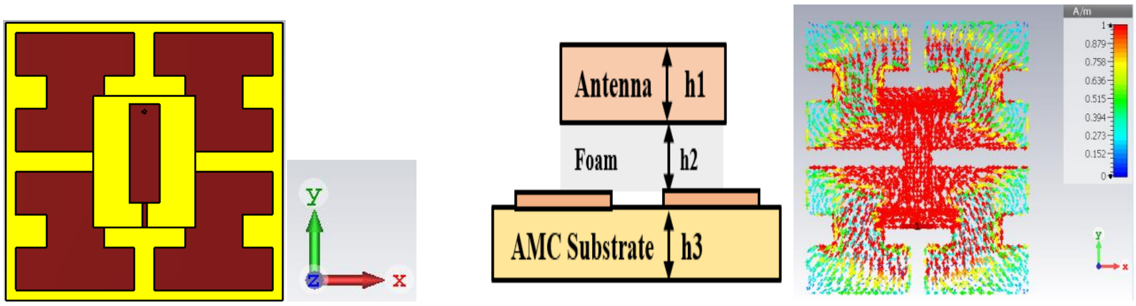

(a) (b) (c)

Fig. 4.23 (a) Front side of antenna with AMC (b) cross-sectional side (c) surface current distribution

4.3.3 Results and Discussion

PCB board etching method is used to fabricate the designed antenna configuration. Ingredients listed in Table 4.5 is used to prepare the muscle equivalent phantom gel for measurement. Fig. 4.24 displays the snapshots of antenna while measurement.

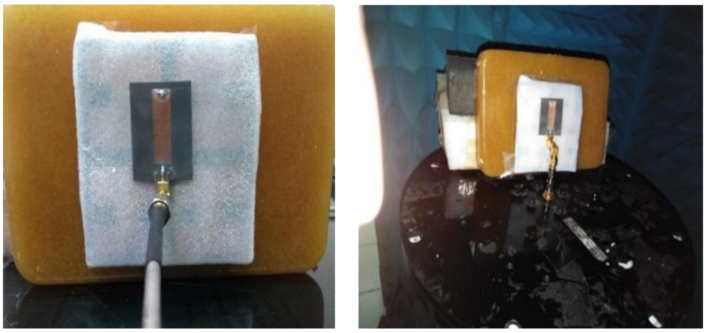

(a) (b)

Fig. 4.24 Antenna during measurement (a) antenna on phantom gel (b) antenna in anechoic chamber

Table 4.5 Preparation of phantom gel [87]

Constituents	Quantity (grams)	Constituents	Quantity (grams)
Deionized water	338	Polyethylene powder	126.5
Gelatine	10.46	Preservative	2.0
NaCl	1.5	TX-151	3.4

4.3.3.1 Reflection Coefficient

Measured data of antenna with AMC surface is compared with simulated data (antenna alone and with AMC surface). It can be studied that bandwidth of antenna with AMC surface is 700 MHz (1.9 GHz to 2.6 GHz) as compared to 1.07 GHz bandwidth of antenna alone. Measured and simulated overlapping impedance bandwidth is 600 MHz (2.0 GHz to 2.6 GHz). Both the configurations (with AMC surface and antenna alone) have covered the ISM band frequency range with enough margin of reliability.

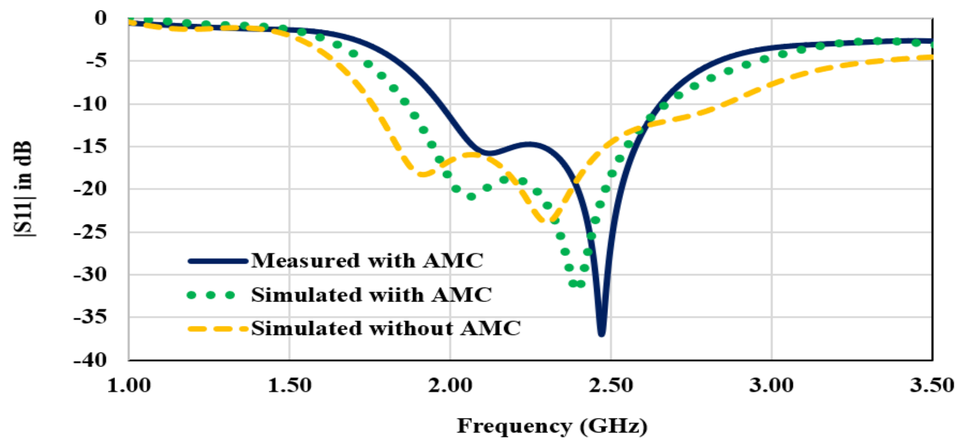

Fig. 4.25 Simulated and measured reflection coefficient of AMC patch antenna and patch antenna alone

4.3.3.2 Structural Deformation Effect

Cylindrical shaped phantom model with varying radii is used to investigate structural deformation effect on antenna performance reliability. Figures 4.26 and 4.27 show the comparison of simulated return loss for three bending radii with flat surface.

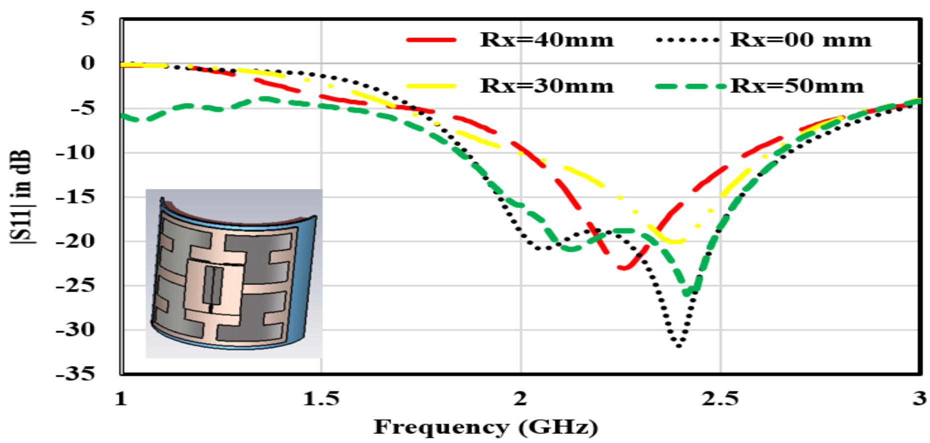

Fig. 4.26 Simulated reflection coefficient for deformation along x-axis

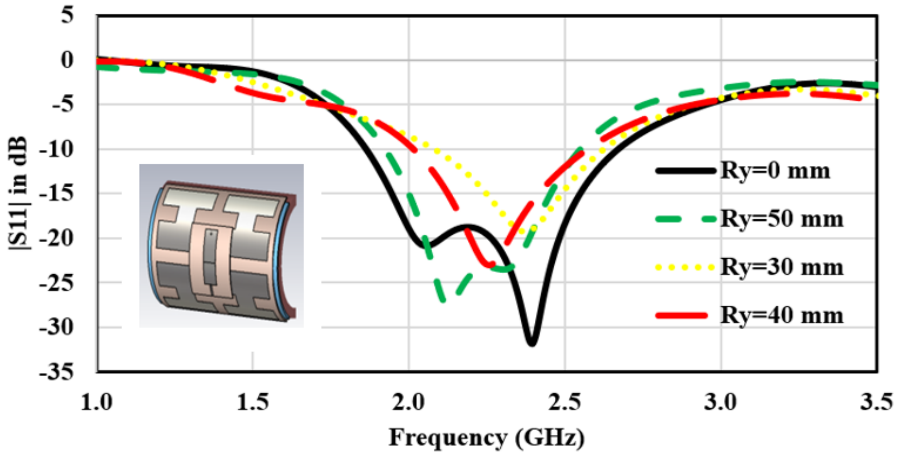

Fig. 4.27 Simulated reflection coefficient for deformation along y-axis

Bending along both the axis shows that resonance frequency is shifting rightward with reducing bending radii from 50 mm to 30 mm. Deterioration of impedance and reduction of impedance bandwidth can also be observed with smallest bending radii. The proposed antenna structure has covered the ISM band for all structural deformation condition.

4.3.3.3 Radiation Pattern

Normalized radiation pattern at $\phi = 0^0$ and simulated 3-D directivity is represented in Fig. 4.28. Bidirectional radiation pattern can be observed for the patch antenna alone. When integrated with AMC structure radiations are reduced towards the body tissue and broadside radiation pattern in positive *z* direction is obtained. Directivity of patch with AMC structure is also improved from 3.97 dBi to 7.3 dBi.

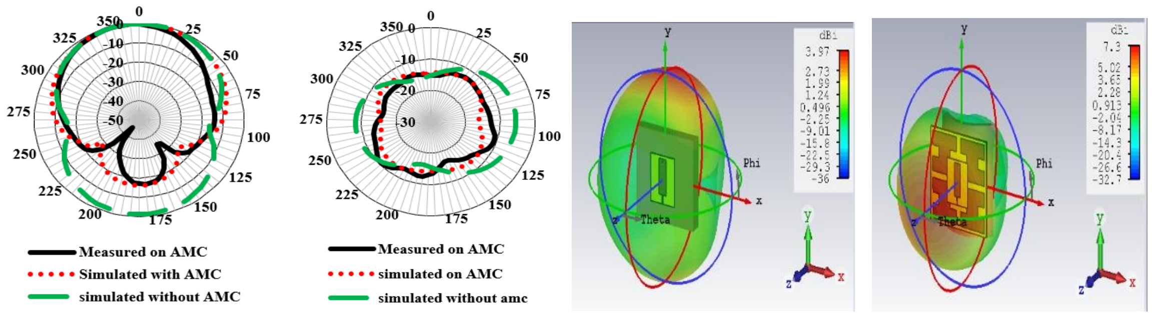

(a) (b) (c) (d)

Fig. 4.28 Radiation pattern (a) Co-polarized (b) Cross-polarized (c) 3-D radiation pattern without AMC (d) 3-D radiation pattern with AMC

4.3.3.4 Radiation Efficiency and Gain

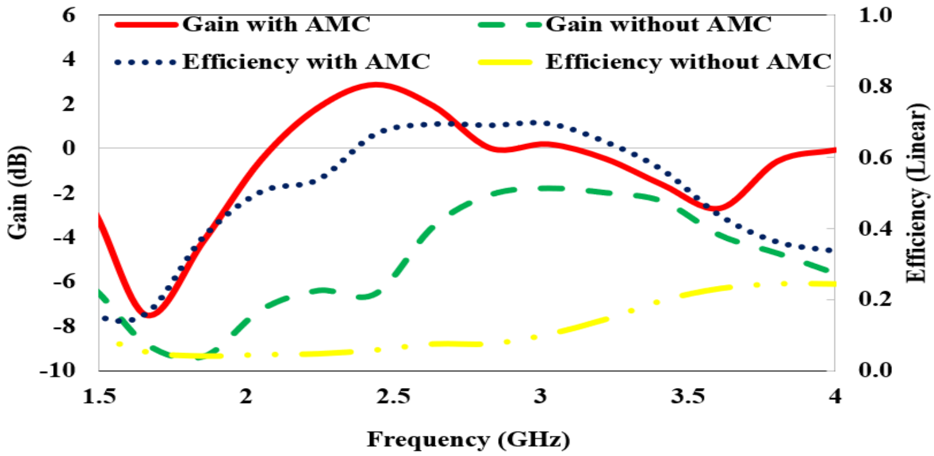

Fig. 4.29 Simulated plot for antenna gain and radiation efficiency

Improvemet in efficiency and gain with AMC integrated antenna can be observed from Fig. 4.29. Patch antenna alone has 10% efficiency while 65% efficiency is achieved after adding the AMC surface. Gain of patch antenna is -6.4 dB whereas peak gain value with AMC is 2.86 dB.

4.3.3.5 Specific Absorption Rate

SAR value of both antenna configurations is simulated for 0.1 W of input power and averaged over 10 grams of tissue which is represented in Fig. 4.30. SAR value of patch antenna alone is 7.73 W/Kg. After placing the AMC surface SAR is reduced to 1.43 W/Kg. Finally, the comparison of antenna performance with and without AMC structure is tabulated in Table 5.6.

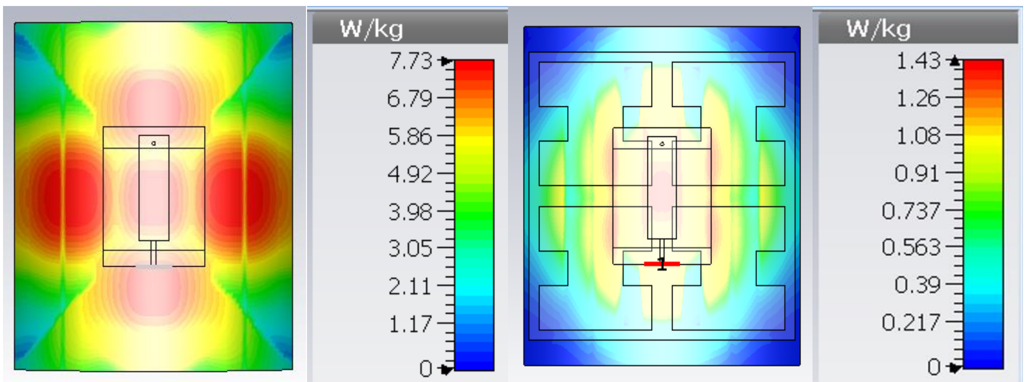

(a) (b)

Fig. 4.30 Specific absorption rate (a) without AMC (b) with AMC

Table 4.6 Antenna performance with and without AMC structure

Antenna2	Size(mm^3)	Gain (dB)	SAR(W/kg)	Bandwidth (MHz)	Efficiency (%)	Radiation pattern
Without AMC	25 × 32× 0.51	-6.4	7.73	1100	10	Bidirectional
With AMC	68×68×4.5	2.86	1.43	600	65	Broadside

From the data of Table 4.6, it is clear that the AMC structure has improved the antenna performance by 55% at the cost of size and bandwidth.

Research Contributions

L-shaped Ground and Radiator antenna with a Metallic Reflector

The proposed dual-band antenna has covered all design challenges of wearable antenna like miniaturization, immune to frequency detuning against structural deformation, high gain, and efficiency with unidirectional radiation characteristics. The research contribution of this structure are as follows:

- The antenna is designed on soft, flexible material RO 3010 with good mechanical strength, and its effectiveness is evaluated by bending the antenna.
- Antenna has covered dual-band resonance at 2.45 GHz and 5.8 GHz bands, featured independent tuning capability for each band. The vertical arm of the radiator and ground tuned the lower and upper band frequencies. Large bandwidth of 310 MHz and 330 MHz is achieved with this antenna.
- Dual-band resonance is achieved by adding a metallic reflector plate below the antenna.
- Radiation performance is enhanced successfully by adding the reflector plate. Broadside and unidirectional radiation pattern, high directivity of 6.31, and 8.75 dBi, the efficiency of 50% and 32% are attained at 2.45 GHz and 5.8 GHz by the proposed antenna.
- Simulated and measured results revealed that the proposed CPW antenna is robust and reliable against frequency detuning with minimum change in resonance and impedance while bending and loading of bio-tissue.
- SAR below safety regulation is achieved with 0.1W of input power.

Defected Ground Patch with AMC Reflector

This antenna consisted of a rectangular patch with the defected ground and a shorting pin and incorporated with an artificial magnetic conductor. The research contribution of this antenna are as follows:

- Defected ground antenna has covered 2.45 GHz ISM band with wide bandwidth of 1.07 GHz (1.76 GHz-2.83 GHz) but suffers from poor on-body radiation efficiency of 10% and gain of -6.4 dB.
- An array of (2×2) unit cells is designed and located below antenna, which improved antenna gain by 9 dB, and efficiency by 55% at the cost of reduced bandwidth 600 MHz (from 2 GHz to 2.6 GHz).
- Broadside radiation pattern and SAR value of 1.43 W/Kg is achieved with the proposed structure.
- Slight reduction in impedance bandwidth is observed with decreasing bending radii, but antenna wide band response helped to cover the desired ISM band.

Published paper related to this chaptetr:

1. A. Gupta, A. Kansal, P. Chawla "Design and performance analysis of L-shaped ground and radiator antenna with a metallic reflector for WBAN." International journal of Electronics, (2020). https://doi.org/10.1080/00207217.2020.1793408

Chapter-5

Dual Band Antenna Structures for On and Off Body Communication

5.1 Introduction

In WBAN, multiple sensor nodes are distributed on different body locations, and located inside the body. Various communication modes are required to interconnect these sensors. Three communication modes are classified based on sensor node position: in-on body, on- on body, and on-off body [10, 229]. The low transmitted power of in-body antenna limits the communication link range of implanted nodes up to a few centimeters. Therefore, data is first transmitted to the on-body antenna (in-on body mode). The On-body antenna operates in dual mode; receive data from the implantable device and other on-body nodes (placed on remote locations like foot) known as on-on body mode and retransmit the data to the external access point in on-off body mode [230]. To improve the commercial application, on-off body antenna can be designed to support heterogeneous wireless standards. It also enhances the data transmission rate [231].

On-body dual-mode antenna must satisfy the dual-band resonance with omnidirectional/ monopole like radiation for on-on body mode and broadside patch-like pattern for on-off body mode [232]. Single-band antenna with dual-feed mechanism [233], dual-band antenna with polarization diversity [234] are designed for dual-mode operation of WBAN.

The aim of this chapter is to design dual-band antenna structures for dual-mode operation. Two CPW fed antenna structures are presented in this chapter. First design is a compact slotted patch antenna with omnidirectional and patch like radiation characteristics at 2.45 and 5.0 GHz, respectively. Second antenna is designed with a ground-coupled truncated patch covering 2.45 GHz (ISM), 2.6 GHz (LTE), and 5.2 GHz (WLAN) bands. Both the antennas are analyzed for free space and on-body operation.

This chapter is ordered as: Section 5.2 covers the details of open-end slotted compact dual band antenna for on-/off body communication**.** In the subsections, antenna design process is explained and the equivalent dielectric constant is calculated. Section 5.3 covers the details of wide band truncated patch antenna with ring-shaped ground. In subsections, ground coupling mechanism is explained and followed by antenna performance analysis.

5.2 Open-end Slotted Compact Dual Band Antenna for On-/Off Body Communication

It is a dual band, dual mode antenna structure which is designed for on-body and off body communication modes. Antenna is miniaturized by etching slots and possess wide bandwidth.

5.2.1 Antenna Configuration

RT/Duroid 5880 substrate of thickness = 1.57 mm, is taken to design the antenna. Antenna has occupied the planar dimensions of 15 mm × 28 mm, which is equivalent to 0.120 λ_o × 0.224 λ_o, and λ_o specifies the wavelength in free space at the lower resonance frequency (2.45 GHz). Dual-band resonance is generated by etching two asymmetrical slots on the rectangular patch of a CPW fed antenna. Two open-ended slots perturbated the surface current and helped to excite dual bands. Fig. 5.1 represents the topology of the designed antenna. Table 5.1 lists the optimized values of antenna dimensions.

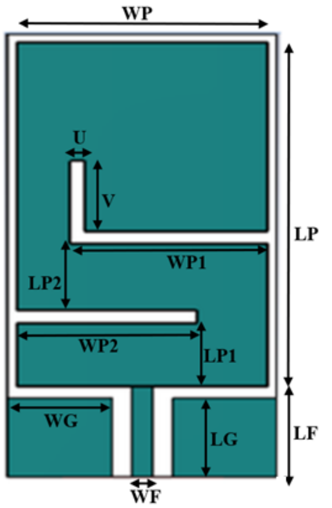

Fig. 5.1 Configuration of the designed antenna

Table 5.1 List of the geometrical parameters

Design Parameter	Size (mm)	Design Parameter	Size (mm)	Design Parameter	Size (mm)
WP1	10.5	LP2	4.2	WG	5.82
WP2	9.5	LG	4.95	V	7
WP	14	LF	5.7	LP	21
WF	1.1	U	0.8	LP1	4
W	4	-	-	-	-

The detailed design process of antenna is explained with the help of three design steps. Result of antenna design steps are taken on tissue phantom. Structure of each design step and respective reflection coefficient plot is represented in Fig. 5.2 and Fig. 5.3. Initially, a conventional coplanar waveguide fed rectangular patch is considered in step (a). This structure shows the single band resonance at 4.5 GHz. Next in step (b), the first open-ended horizontal slot is cut near the feed line at the left side of the radiator. The integration of this slot adds on the electric current path length that shifts the center resonance leftward at 3.5 GHz.

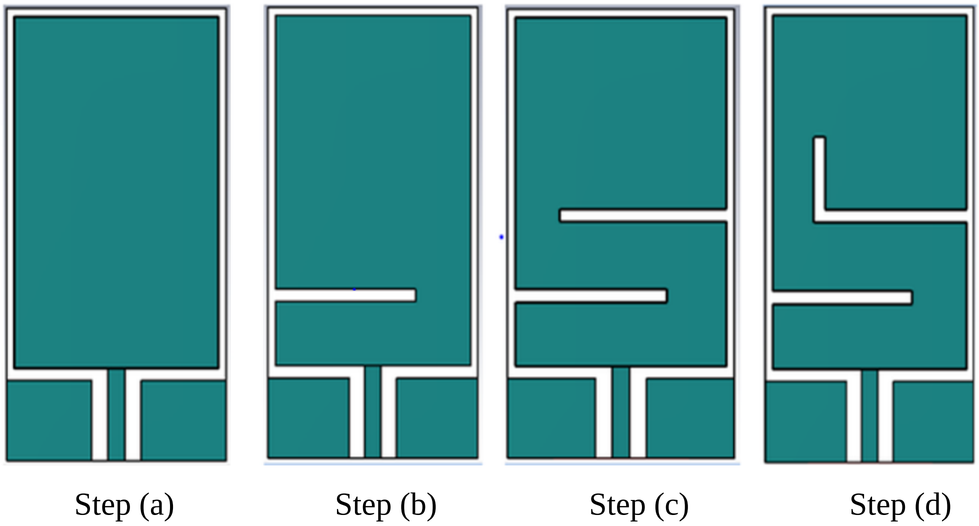

Fig. 5.2 Design evaluation configurations of proposed antenna

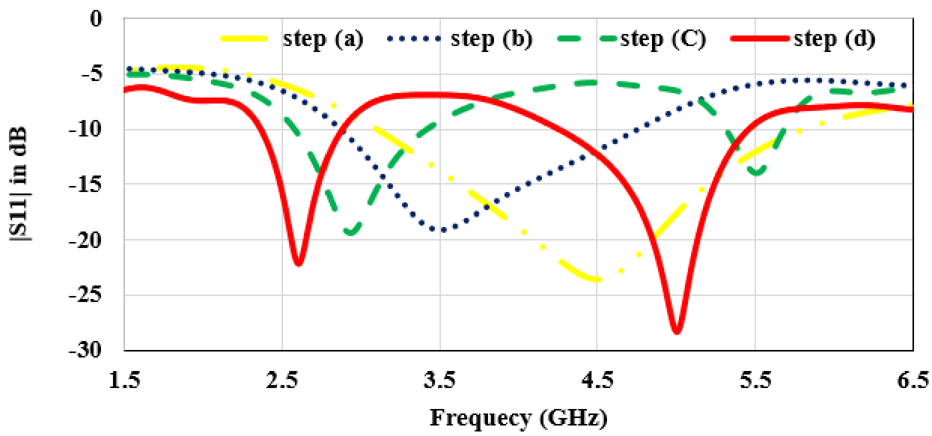

Fig. 5.3 Simulated reflection coefficient plot of four design steps

Further, in step (C), the second slot is added parallel to the first slot but at the opposite side of the radiator. It generated two resonance frequencies at 2.7 GHz and 5.5 GHz. The return loss plot also shifted upwards, showing reduction of impedance matching. Finally, to tune the antenna resonance at desired bands, the second horizontal slot is converted into an L-shaped slot in step (d). It shifts both the bands leftward at 2.5 GHz and 5.0 GHz. The vertical arm length *'v'* of the L-shaped slot is optimized through parametric sweep to tune the frequencies. |S11| plot for the varying value of *'v'* is shown in Fig. 5.4. The result shows that length *'v'* has a significant impact on both frequencies. Both frequencies are reducing with increasing length but with slight degradation of impedance matching at higher band.

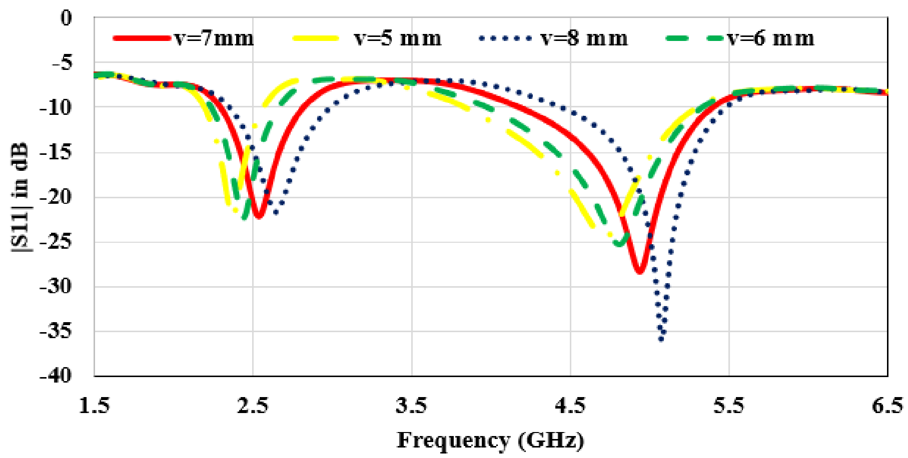

Fig. 5.4 Effect of varying length *'v'* on desired frequencies

5.2.2 Equivalent Dielectric Constant of body Tissue Model

As antenna is designed to work on bio-tissue, a three-layered tissue model is designed for on-body simulation. The tissue model has a planar dimension of 80 mm × 80 mm and shown in Fig. 5.5. The thickness of muscle, fat and skin layers is considered as 8 mm, 4 mm and 2 mm, respectively. Based on the literature, the separation gap of 3 mm is maintained between body and antenna to lessen the conductive effect of body on radiator.

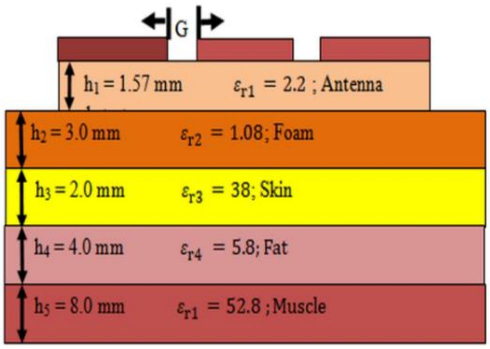

Fig. 5.5 Tissue layer with thickness and dielectric constant

The effective dielectric constant of an on-body antenna is also influenced by the high relative permittivity of body tissue. Therefore, an equivalent dielectric constant is calculated by using equations (5.1 to 5.4) [235,236].

$$\varepsilon_{eq} = \frac{d1+d2+d3+d4+d5}{\frac{d_1}{\varepsilon_{r1}} + \frac{d_2}{\varepsilon_{r2}} + \frac{d_3}{\varepsilon_{r3}} + \frac{d_4}{\varepsilon_{r4}} + \frac{d_5}{\varepsilon_{r5}}} \tag{5.1}$$

Where ε_{r1}, ε_{r2}, ε_{r3}, ε_{r4} and ε_{r5} represents the relative permittivity of antenna substrate and tissue layers below the antenna substrate. d_1, d_2, d_3, d_4, and d_5 parameters represent the distance between the boundaries of each layer that can be calculated as [235,236]:

$$d_n = \left\{ \begin{array}{ll} \frac{K(k_n)}{K'(k_n)} = \frac{\pi}{\ln\left[\frac{2\left(1+\sqrt{k'_n}\right)}{\left(1-\sqrt{k'_n}\right)}\right]} & ;\ 0 \le k_n \le 0.707 \\ \frac{\ln\left[\frac{2\left(1+\sqrt{k'_n}\right)}{\left(1-\sqrt{k'_n}\right)}\right]}{\pi} & ;\ 0.707 \le k_n \le 1 \end{array} \right\} \tag{5.2}$$

$$K'_n = \sqrt{1} - {k_n}^2 \tag{5.3}$$

Where n = 1, 2…5 representing number of substrate layers; $K(k_n)$ and $K'(k_n)$ are the first kind elliptical integral and its complement. Value of k_n for the CPW fed antenna can be found using the equation 6.4.

$$k_n = \frac{\mathrm{Sinh}\left(\frac{\pi WF}{2h_n}\right)}{\mathrm{Sinh}\left(\frac{\pi(WF+2G)}{2h_n}\right)} \sqrt{\frac{1 - \frac{\sinh^2\left(\frac{\pi(WF+2G)}{2h_n}\right)}{\sinh^2\left(\frac{\pi W}{2h_n}\right)}}{1 - \frac{\sinh^2\left(\frac{\pi WF}{2h_n}\right)}{\sinh^2\left(\frac{\pi W}{2h_n}\right)}}} \tag{5.4}$$

Where $G = 1.13\,mm$, defines the space between feed line and antenna ground; $WF = 1.1\,mm$, specifies the feed line width and $W = 15\ mm$ is the antenna width. Putting the geometrical dimensions and tissue properties from Table 5.1 and Fig. 5.5 in equation (5.1) calculated value for equivalent dielectric constant ε_{eq} is 4.8.

5.2.3 Electric Current Distribution

Fig. 5.6 indicates that maximum current is focused near the edges of slots. Working mechanism of the two slots for the generation of dual band resonance and the relation of slot dimensions with resonance frequency is explained.

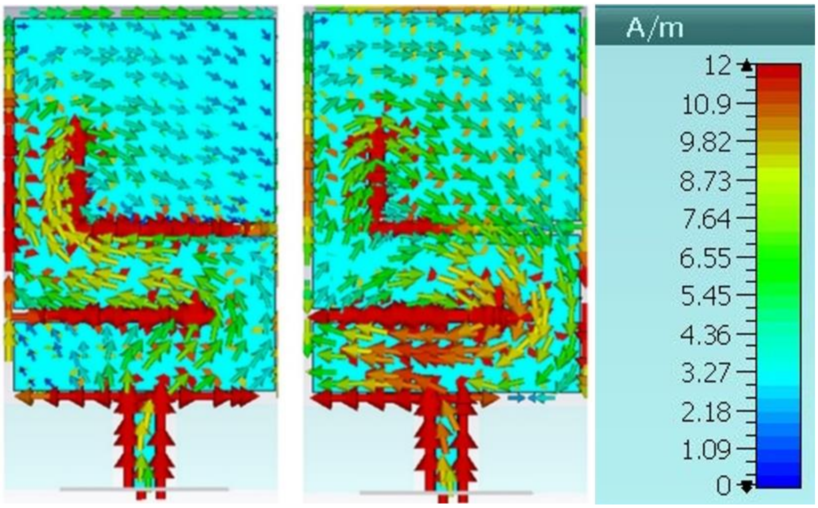

(2.45 GHz) (5.0 GHz)

Fig. 5.6 Plot for electric current distribution

First resonance (f_{r1}) at 2.45 GHz: At this band, resonance current has followed a single path generated at the open end of the horizontal cut and travel through both slot lengths and becomes null near the open end of L-shaped slot. Hence, mathematical value of current path length contributing to first resonance can be calculated from equation 5.5.

$$L_{r1} = (WP2 \times 2) + LP2 + V + WP1 + U \tag{5.5}$$

From the values of slot legths given in Table 5.1, calculated path length L_{r1} is 41.5 mm.. Current length L_{r1} should be half wavelength at the resonance [237], therefore, f_{r1} at this length is given as:

$$f_{r1} = \frac{c}{2\times L_{r1}\times \sqrt{\varepsilon_{reff}}} \approx 2.47\text{GHz} \tag{5.6}$$

Where, effective dielectric constant of a CPW fed antenna is calculated using the equivalent dielectric constant and equation 5.7 [236].

$$\varepsilon_{reff} = 1 + \frac{(\varepsilon_{eq} - 1)}{2} \frac{K(k_6)}{K'(k_6)} \frac{K'(k)}{K'(k)} \approx 2.14$$

(5.7)

Where k_6 can be found from the equation (5. 4) and *k* is given by equation (5.8) [236].

$$k = \frac{WF}{(WF + 2G)} \sqrt{\frac{\left(1 - \frac{(WF + 2G)^2}{W^2}\right)}{\left(1 - \frac{(WF)^2}{W^2}\right)}}$$

(5.8)

Simulated and calculated resonace frequency are agreeing well, and also justifies the calculated equivalent value of dielctric constant.

Second Resonance (f_{r2}) at 5.0 GHz: At the higher band, two current paths are generated from left side of radiating patch in middle of the two slots. Each current path has followed one slot. Current path length at this band can be calculated as:

$$L_{r2} = (WP1 - WN) + (V \times 2) = 21.0 \text{ mm}$$

(5.9)

WN ≈3.5 mm; is the null current length along the horizontal arm of L-slot. Therefore, f_{r2} = 4.89 GHz at the calculated length and simulated result represents the resonance frequency at 5.0 GHz, which is much near to the design methodology. Small variation is probably due the variation in the null current length.

5.2.4 Return Loss

Simulated antenna is fabricated to justify the results. Antenna performance is characterized on phantom gel by the vector network analyzer. Photograph of the antenna with phantom gel during measurement is shown in Fig. 5.7. Measured and simulated reflection coefficient plot for the two operating conditions is drawn in Fig. 5.9.

(a) (b)

Fig. 5.7 Photographs of the antenna during measurement (a) antenna on phantom gel (b) antenna in anechoic chamber for radiation pattern measurement

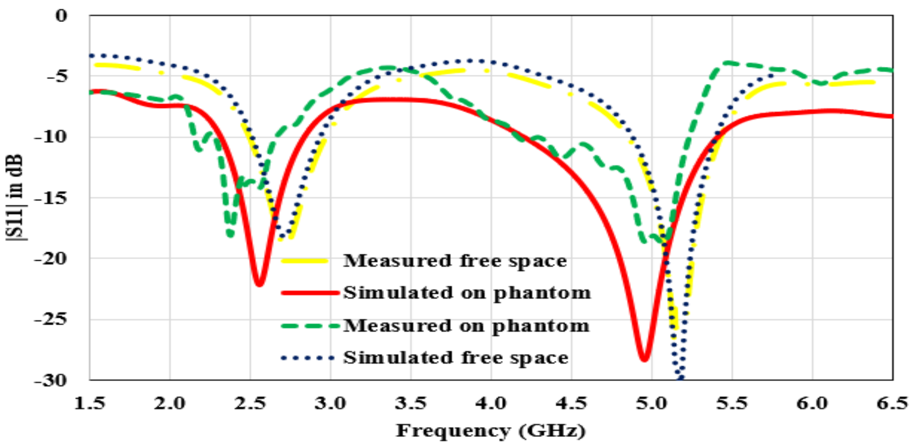

Fig. 5.8 Simulated and measured return loss on phantom and in free space condition

On comparing the results of two conditions, a rightward shift in resonance frequency from 2.5/5.0 GHz to 2.6/5.2 GHz can be observed in free space. In free space effective dielectric constant is reduced as it is depending upon antenna substrate only. Value of measured on-body impedance bandwidth is slightly less than the simulated value for both the bands. This variation is possibly due to the difference in the tissue properties of both setups. Still, antenna has well covered the 10-dB bandwidth from 2.3 GHz - 2.65 GHz (350 MHz) and 4.63 GHz - 5.23 GHz (600 MHz).

5.2.5 Radiation Pattern

Normalized power patterns for the two operating conditions are represented in Fig. 5.9. During on body measurement, fabricated tissue gel is positioned at the bottom of the antenna. In the free space, omnidirectional and dipole like radiation patterns are observed. This is the desired feature for the dual-mode operation of an on-body antenna. After placing the antenna on tissue, some variation occurs in the radiation pattern. At 2.45 GHz, the maximum radiated power is concentrated toward the surface of body at $E_\theta = 280^0$, which is appropriate for on-on body transmission mode. At 5.0 GHz, maximum power is concentrated in the direction opposite to body tissue at $E_\theta = 0^0$ that makes antenna appropriate for off-body communication.

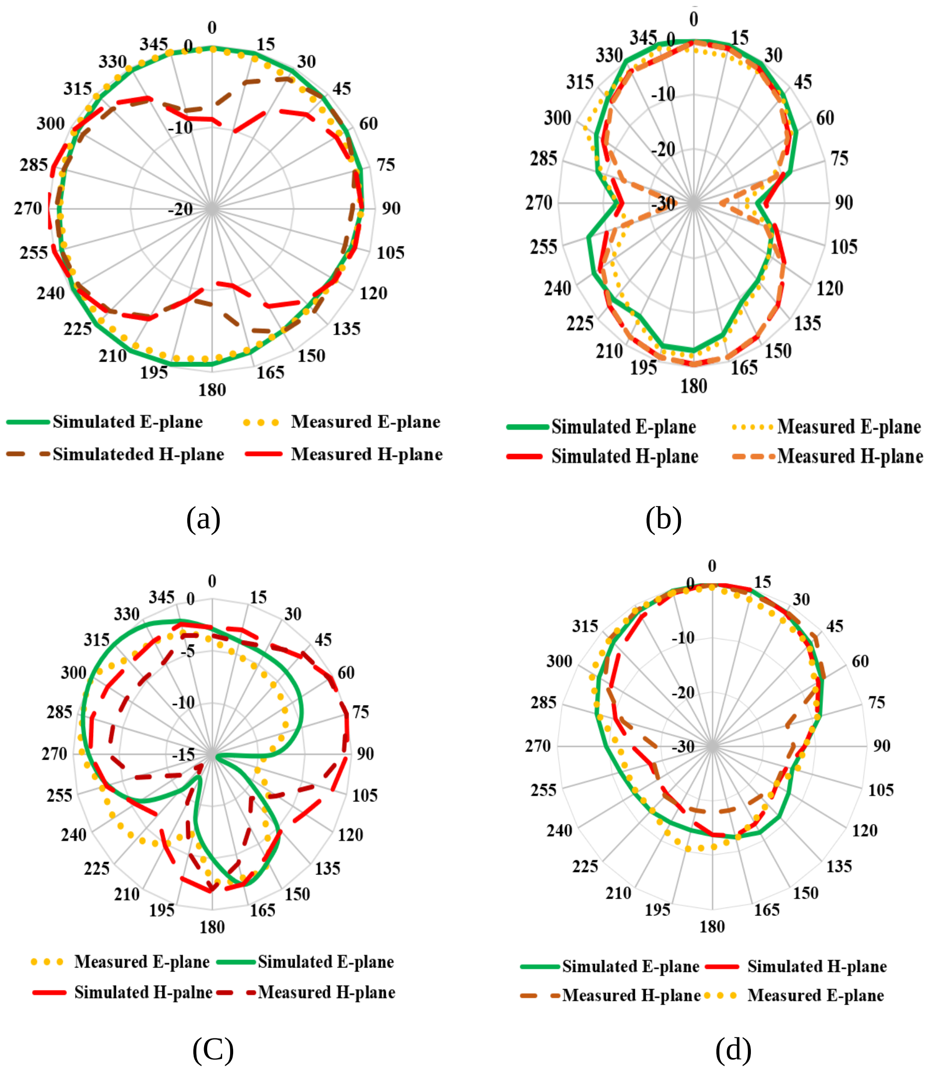

Fig. 5.9 Radiation patterns (a) free space at 2.45 GHz (b) free space at 5.0 GHz (c) on-body at 2.45 GHz (d) on-body at 5.0 GHz

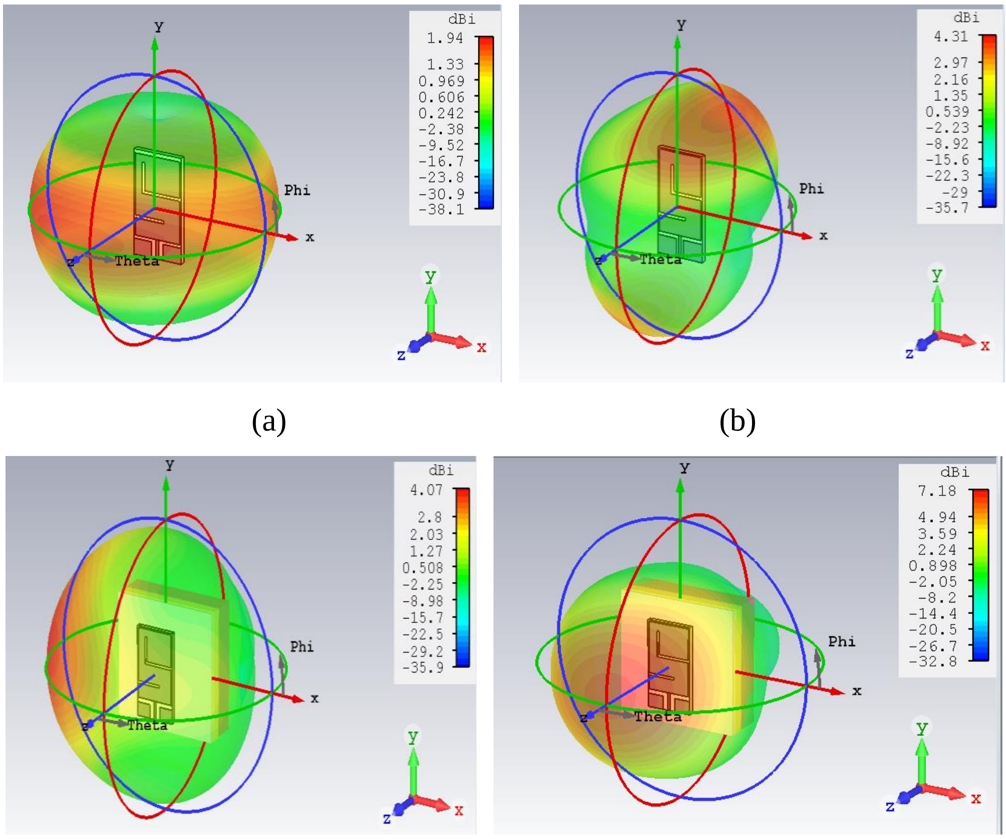

(a) (b)

(c) (d)

Fig. 5.10 3-D directivity plot of proposed structure in free space at (a) 2.45 GHz (b) 5.0 GHz (c) on tissue phantom at 2.45 GHz (d) at 5.0 GHz

To justify the impact of body tissue on the radiation characteristics, simulated 3-D radiation patterns in free space and on-body environment are shown in Fig. 5.10. As antenna is placed on the multilayer tissue, directivity improves from 1.94 dBi to 4.07 dBi at 2.5 GHz and from 4.07 dBi to 7.18 dBi at 5.0 GHz. According to field theory, radiations are reflected back at the interface of two dielectric mediums only if a low permittivity medium is backed by a high permittivity medium. Reflected waves add up with the radiated waves and enhance the antenna directivity. Air-skin interference causes EM waves to reflect away from the body. Thus, on-body pattern has a different radiation pattern and high directivity than free space.

5.2.6 Specific Absorption Rate Analysis

It is important to measure the rate of energy absorption in body tissue when it comes to the immediate effect of electromagnetic radiation. For the designed antenna, SAR is simulated for 0.1W of input power over 10 gram of body tissue and displayed in Fig. 5.11. SAR value at 2.45 GHz is observed as 1.102 W/Kg and at 5.0 GHz as 0.524 W/Kg. These SAR values are less than the safety regulation limit. Antenna performance is compared with some of the existing dual-band antennas reported in the literature and summarized in Table 5.2.

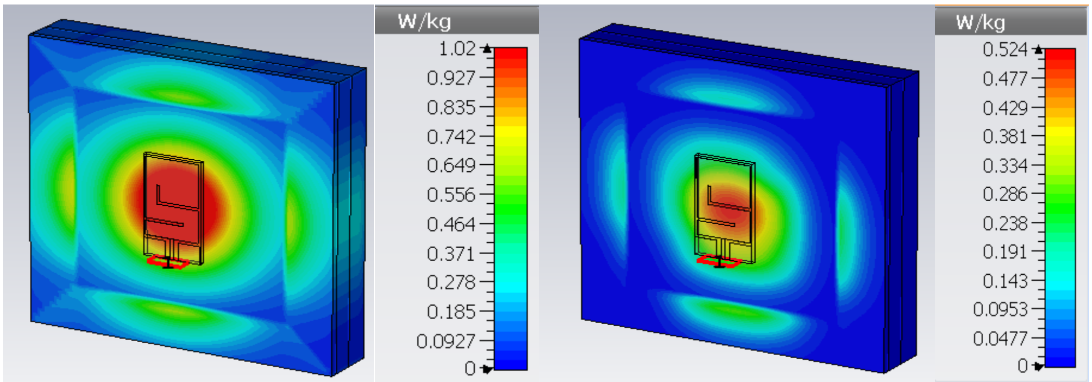

(a) (b)

Fig. 5.11 Simulated SAR at (a) 2.45 GHz and (b) 5.0 GHz

Table 5.2 Comparison of antenna performance with existing literature

Ref.	**Freq. (GHz)**	**Size (mm^2)**	**Bandwidth (MHz)**	**Directivity (dBi)**	**SAR (W/Kg)**	**Efficiency (%) s=gap between body and antenna**
[35]	4.0,5.8	40×20	1000,100	4.0, 6.0	Not specified	22,27 (at s=3mm)
[64]	2,45, 5.8	60×50	130, 270	4.5, 5.6	0.668, 0.155	Not specified
[87]	2.45,5.8	Radius =35mm	84, 247	4.16,4.34	0.248, 0.091	58.6,50.6 (s=10mm)
[76]	2.45	40×38	192	0.52	0.126	23.97 (s=0mm)
[94]	2.45,5.8	30×45	120,160	0.56,-1.59	NA	Not specified
[107]	5.8	41×47	342	6.25	0.54	88.5 (s=2mm)
[113]	5.8	44×24.5	220	5.25	1.39	69 (s=4mm)
[223]	2.45,5.5	50×40	500,1000	1.54,2.54	0.428,1.87	25,27 (s=12mm)
[proposed work]	**2.45, 5.0**	**15×28**	**350, 600**	**4.02, 7.74**	**1.02, 0.524**	**24/55 (at s=3mm)**

Although all the antennas studied have been designed for on-body performance. Still, the proposed structure occupies the smallest area, simplest geometry, high directivity, and good impedance matching while maintaining the safety considerations.

5.3 Wide Band Truncated Patch Antenna with Ring-Shaped Ground

Antenna structures which satisfy the heterogeneous networks are getting more research interest for off-body communication in WBAN system. Considering this feature in mind, a truncated patch antenna that covers triple bands is designed. It covers ISM, LTE and WLAN bands. This allows the sensor node to connect with different off-body networks and enhances the commercial application of WBAN.

5.3.1 Antenna Configuration

Antenna is designed on a printed circuit board of FR-4 material with a thickness of 0.51, $\boldsymbol{\varepsilon}_r$= 4.4, and loss tan = 0.025. During simulation antenna is fed by 0.5 W of input power. Wideband response is realized through a square-shaped ring type coplanar ground and a truncated corner rectangular radiator. To couple maximum power to the radiator, an optimized gap of '$G = 0.425\ mm$' is taken between ground and patch. The value of other geometrical parameters is listed in Table 5.3.

A square-shaped multi-layered phantom model depicting human tissue is modeled for simulating the antenna. It has four layers; bone (10 mm), muscle (8 mm), fat (4 mm), and skin (2 mm). Each side of the phantom model has dimensions of 60 mm.

Table 5.3 Geometrical parameters of the antenna

Geometrical Parameter	value (mm)	Geometrical Parameter	value (mm)
WP	23	L	38
LF	7.5	U	18.5
V	7	LP	23
U2	5.34	U1	6.2
WF	1.2	U4	8.08
U3	4.66	-	-

Antenna impedance and radiation properties vary greatly at the interference of two different dielectric medium. This variation is very high for the antenna substrate and skin layer.

Therefore, a small air gap of '$s = 3\ mm$' is presumed between the tissue surface and antenna substrate. It minimizes the impact of lossy biological tissue on antenna behavior. To validate antenna performance for on-body operation, numerical simulations are completed on the designed tissue model. Fig. 5.12 illustrates the structure of the designed antenna and multi-layered on-body simulation setup.

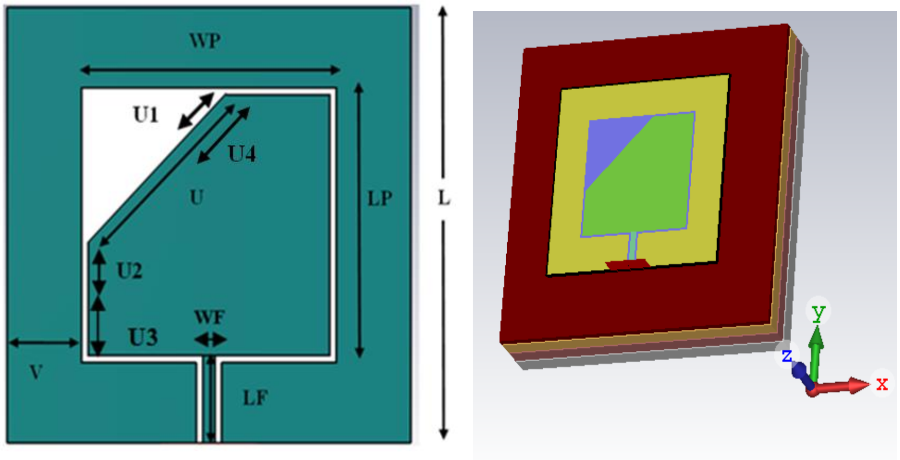

(a) (b)

Fig. 5.12 (a) Antenna geometrical structure (b) Simulation Setup

5.3.2 Evaluation of Antenna Geometry

Coplanar antenna is easy to fit in with the sensor module because the patch and the ground plane share the common surface which reduces the antenna size. Thus, the design process of antenna is initiated with a modified CPW structure. Three antenna geometries are considered to explain the evaluation process, and geometry for each design step is represented in Fig. 5.13.

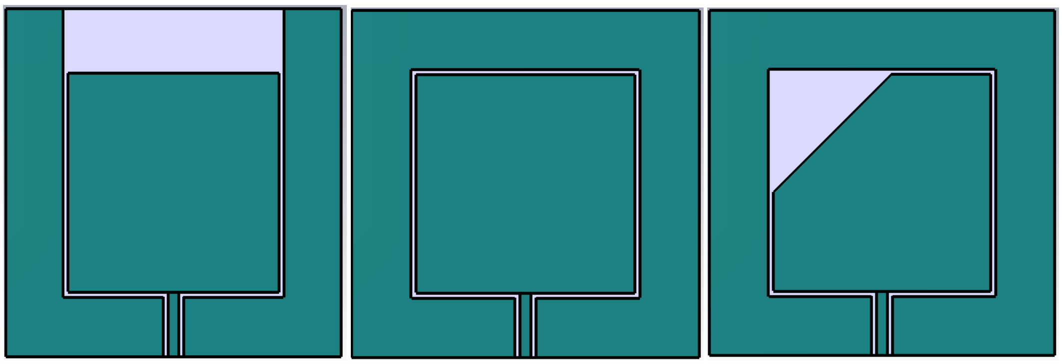

(a) (b) (c)

Fig. 5.13 Geometry of antenna for evaluation steps (a) antenna1 (b) antenna2 (c) antenna3

The return loss plot for three structures of the design procedure is compared in Fig. 5.14. At the first design step, antenna1 is designed with symmetric L-shaped ground and a square patch radiator (Fig. 5.14 (a)). It covers wide impedance bandwidth from 3.3 GHz to 4.1 GHz with center resonance at 3.75 GHz. It is improved to cover multiple bands (ISM, LTE, and WLAN).

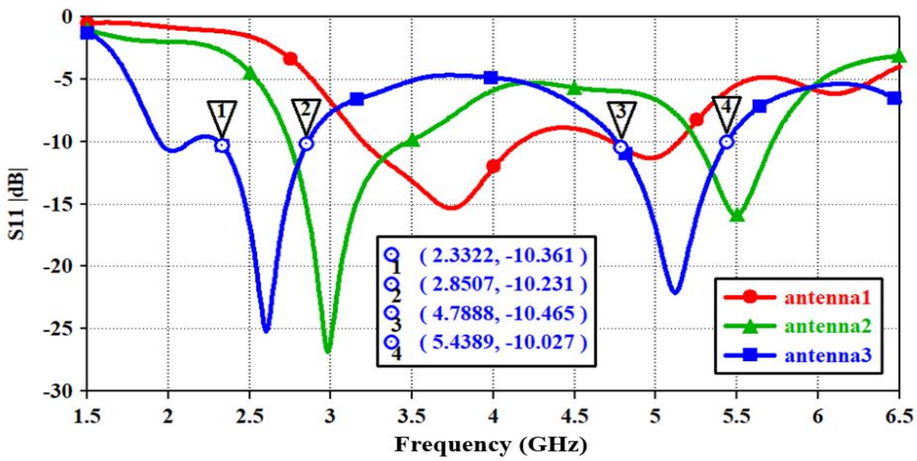

Fig. 5.14 Comparison of reflection coefficcient in three design steps

In antenna 2, ground is modified as ring-shaped ground. It introduced a strong coupling effect in the antenna radiator and resulted in dual excitation at 3.0 GHz and 5.0 GHz frequencies. Coupling at the upper edge of the radiator has increased the current path length and generated resonance at the lower band. Another coupling occurred in the middle of both vertical sides of the patch and contributed to the excitation of upper band resonance.

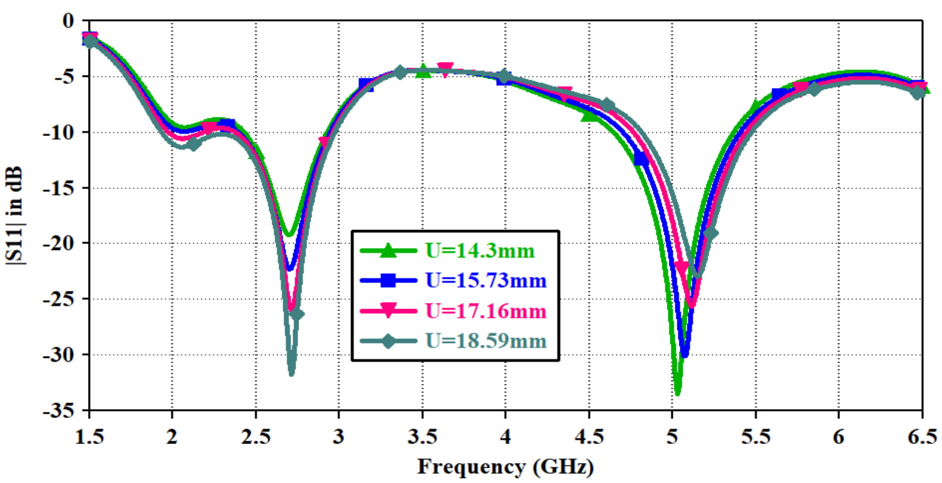

Fig. 5.15 |S11| for varying the truncated corner size

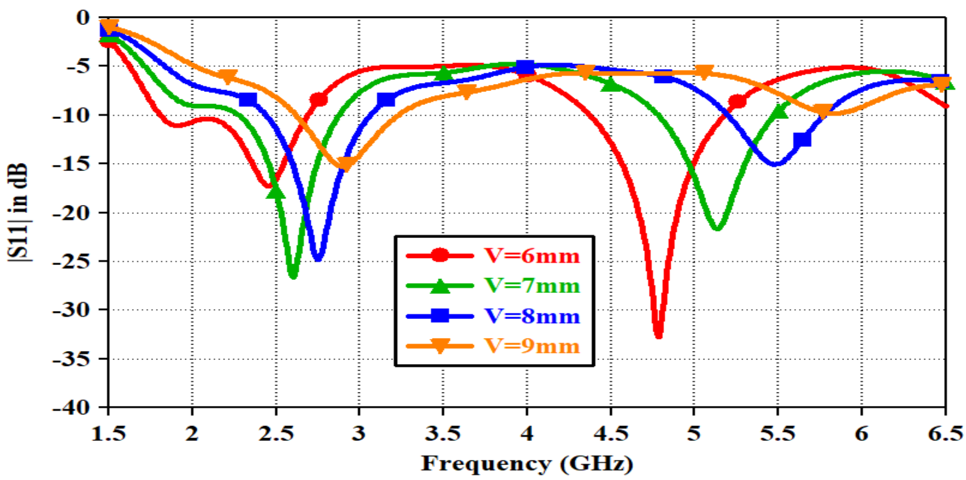

Fig. 5.16 |S11| for varying the width of ground

Finally, antenna 3 is designed by truncating the upper left corner of the antenna 2 radiator. It contributed to shifting of both the frequencies and tuned the antenna to resonance at desired bands. Side of the truncated corner *'U'* is optimized to sustain the best impedance matching. The effect of parametric analysis on the reflection coefficient is shown in Fig. 5.15. The increasing value of *'U'* has shifted the curve downwards and enhances the impedance bandwidth, whereas, at the upper band, resonance is shifting rightward and tunes the higher band at the desired frequency. Therefore, to maintain the good impedance matching at the lower band and upper band optimum value of *'U'* is considered as 18.5 mm in the proposed design. Shape of the ground plane has a prominent role in the antenna design process, thus to study its effect on antenna performance, ground plane width *'V'* is varied. The effect of *'V'* variation on the reflection coefficient is plotted in Fig. 5.16. It can be found that frequency can be lowered by narrowing the ground width but it reduces the impedance matching.

5.3.3 Surface Current Distribution

To justify the coupling effect of ground plane on radiator, surface current plot is displayed at three operating frequencies. Effective dielectric constant (ε_{reff} = 3.43) is calculated using the equations (5.6) and (5.7). Surface current is used to explain the design mothodology for tuning the resonance.

At 2.45 GHz (f_{r1}), surface current distribution shows that extreme current is concentrated at the sides of the radiator. Two λ/2 resonance paths are coupled on two opposite borders of radiator. Depending on antenna substrate thickness and effective dielectric constant, the theoretically calculated value of half-wavelength at 2.45 GHz is 33.05 mm. From the geometry of designed antenna and the path followed by surface current, length of half-wavelength path (L_{r1}) can be calculated with Equation (5.10).

$$L_{r1} = \frac{WP}{2} + U2 + U3 + U - U1 - \frac{WF}{2} = 33.25mm \tag{5.10}$$

By placing this value in equation (5.7) calculated resonance frequency is 2.43 GHz, which is matching well with the simulated results.

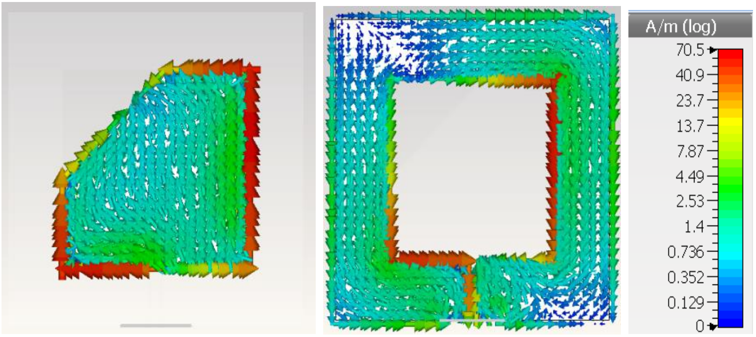

Surface current at patch (a) Surface current at ground

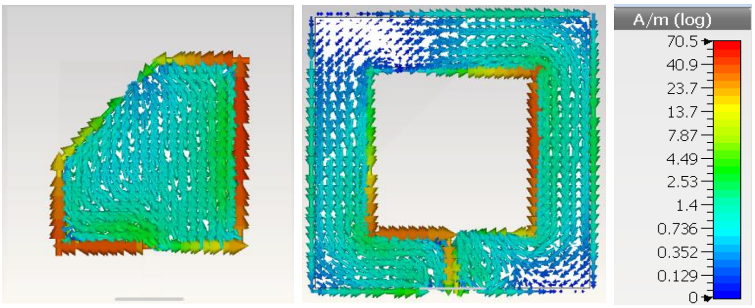

Surface current at patch (b) Surface current at ground

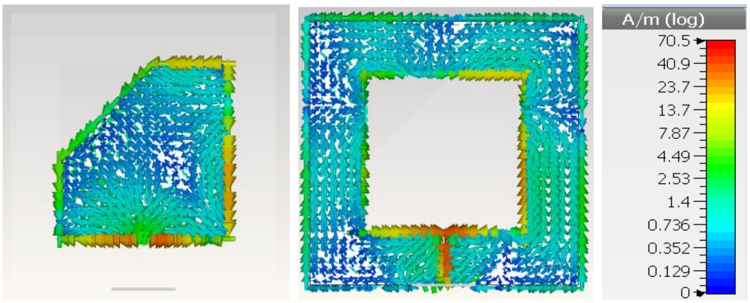

Surface current at patch (c) Surface current at ground

Fig. 5.17 (a) 2.45 GHz (b) 2.6 GHz (c) 5.2 GHz

At 2.6 GHz (f_{r2}), it can be seen that at the truncated corner null current length has slightly increased as compared to first band.

At this resonance frequency, λ/2 path length (L_{r2}) is 31.14 mm. Value of L_{r2} calculated from antenna dimensions is:

$$L_{r2} = \frac{WP}{2} + U2 + U3 + U - U4 - \frac{WF}{2} = 31.37 \text{ mm} \quad (5.11)$$

Using this value of L_{r2} in Equation (5.7), calculated frequency is 2.58 GHz, and in approximation with the theoretical value.

At 5.2 GHz (f_{r3}), we can find from Fig. 5.17(c) that three λ/2 current paths are generated on the edges of the radiator. The first path is coupled at the truncated corner. Another two are excited on both vertical sides near the feed line. The current path size is evaluated from equation 5.12.

$$L_{r3} = \frac{WP}{2} + U3 - \frac{WF}{2} = 15.61\text{mm} \quad (5.12)$$

Resonnace frequency of f_{r3} = 5.18 GHz is satisfied at 15.61 mm and simulated results are closer to the calculated value. Moreover, designed ring shape ground has coupled multiple resonance paths, which contributed to wide bandwidth.

5.3.4 Reflection Coefficient Analysis

Fabricated prototype is measured on vector network analyser. Antenna performance is verified for both the on body and free space operating conditions. Air gap of 3 mm used while simulation is filled with low loss foam spacer that helps to retain the simulated resonance band and impedance matching while testing the antenna. Fig. 5.18 illustrates the measured and simulated |S11| plots for the two operating conditions (on the tissue gel and in free space).

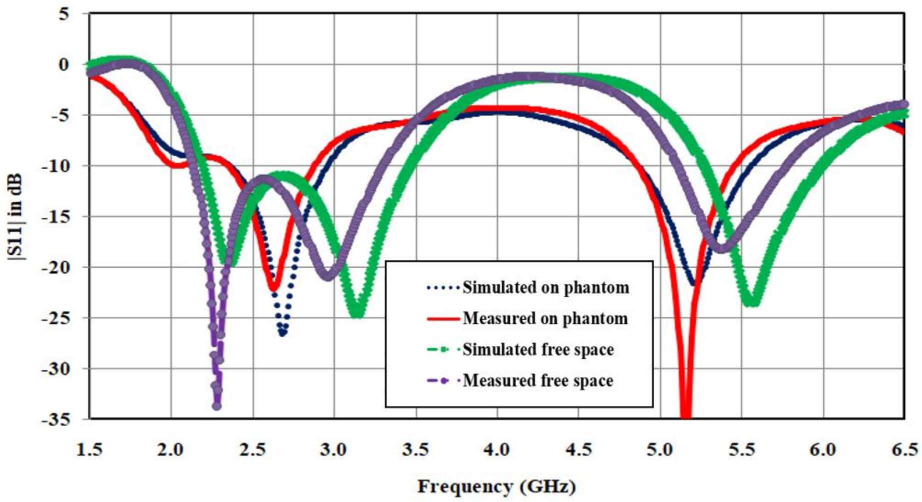

Fig. 5.18 Simulated and measured |S11| plots on the tissue gel and in free space

On-phantom gel, bandwidth is covered from 2.38 GHz to 2.9 GHz and 4.83 GHz to 5.45 GHz corresponding to 2.6 GHz and 5.2 GHz. In free space, 10-dB bandwidth is 1250 MHz (2.1 GHz to 3.35 GHz) and 700 MHz (5.08 GHz to 5.78 GHz) for lower and upper band respectively. Antenna has successfully occupied the ISM, LTE, and WLAN bands (5.1-5.35 GHz) for connecting WBAN with different commercial networks.

5.3.5 Radiation Efficiency and Gain

Simulated radiation efficiency and gain plots for varying antenna and body spacing are plotted in Figures 5.19 and 5.20. In free space, efficiency of 80% (at 2.5 GHz), and 75% (at 5.0 GHz) is achieved. The body tissue has absorbed 65% of power at lower band; when the antenna is located at a minimum gap of $s = 3\,mm$. With the varying gap, power absorbed by the tissue also varies. Simulated absorbed power value at varying gap is listed in Table 5.4. Efficiency of on-body radiator is the function of the power absorbed by tissue layers. Therefore, efficiency for the on-body antenna can be calculated as:

$$\eta_{\text{tissue}} = \frac{P_r}{P_r + P_{abs} + P_l} \tag{5.13}$$

Where, P_{abs} is the power absorbed by tissue, P_r is the antenna radiated power, P_l is the power lost due to ohmic losses and in the substrate material. From the values of Table 5.3 it is clear that as the separation gap is increasing, power absorption is reducing. Thus, radiation efficiency improves with increasing gap.

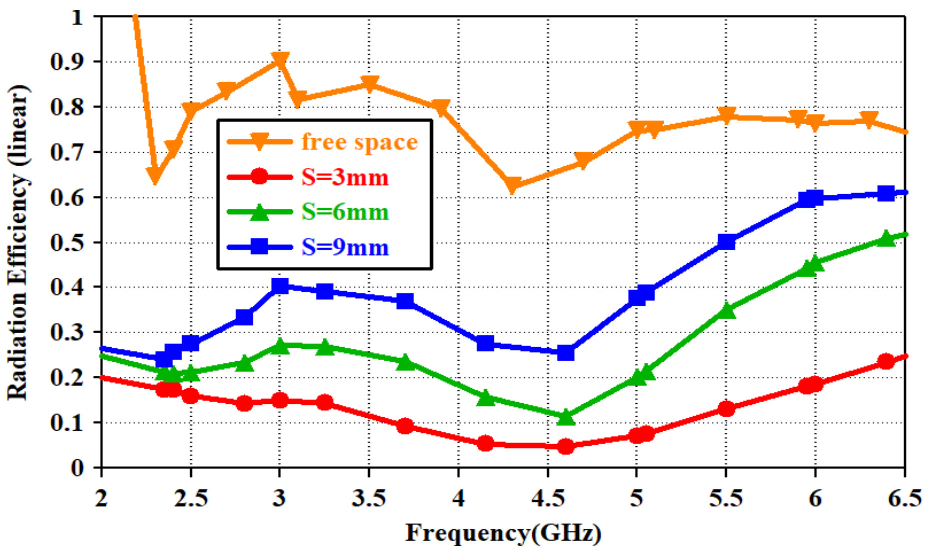

Fig. 5.19 Plot for radiation efficiency

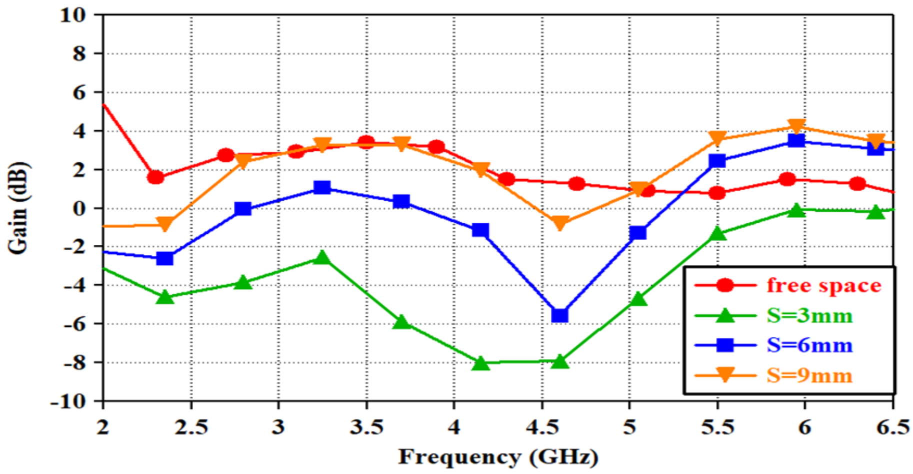

Fig. 5.20. Plot for gain

Fig. 5.20 shows that free space gain of antenna is 2 dB at 2.5 GHz and 1.1 dB at 5.2 GHz. Gain of antenna shifts to -4.1 dB for both the frequencies when antenna is operated nearest to the tissue gel. As the distance is increased, gain curve shifts upwards. At higher frequency, tissue permittivity reduces thus power absorption reduces. Large variance in the air-skin permittivity increases the internal reflections. Therefore, on-body gain is slightly more than free space gain at 5.2 GHz.

Table 5.4 Power distribution with change in the air-skin interface gap

Power (W)	2.48 GHz			5.2 GHz		
	S = 9 mm	S = 6 mm	S = 3 mm	S = 9 mm	S = 6 mm	S = 3 mm
P_{abs} (skin)	0.110	0.135	0.167	0.074	0.135	0.230
P_{abs} (fat)	0.013	0.016	0.018	0.010	0.016	0.024
P_{abs} (muscle)	0.066	0.076	0.092	0.030	0.047	0.070
P_{abs} (bone)	0.024	0.028	0.032	0.006	0.009	0.012
P_l	0.121	0.121	0.121	0.168	0.168	0.168
P_r	0.110	0.086	0.076	0.196	0.116	0.042

5.3.6 Radiation Pattern Analysis

2-D normalized radiation pattern at three frequencies is illustrated in Fig. 5.21. Dipole like radiation pattern has been observed for 2.45 GHz, which is required for on-body receiving mode communication. At 2.6 GHz and 5.2 GHz patch like broadside radiation pattern is obtained. Further, a comparison of antenna performance with some existing papers is given in Table 5.5.

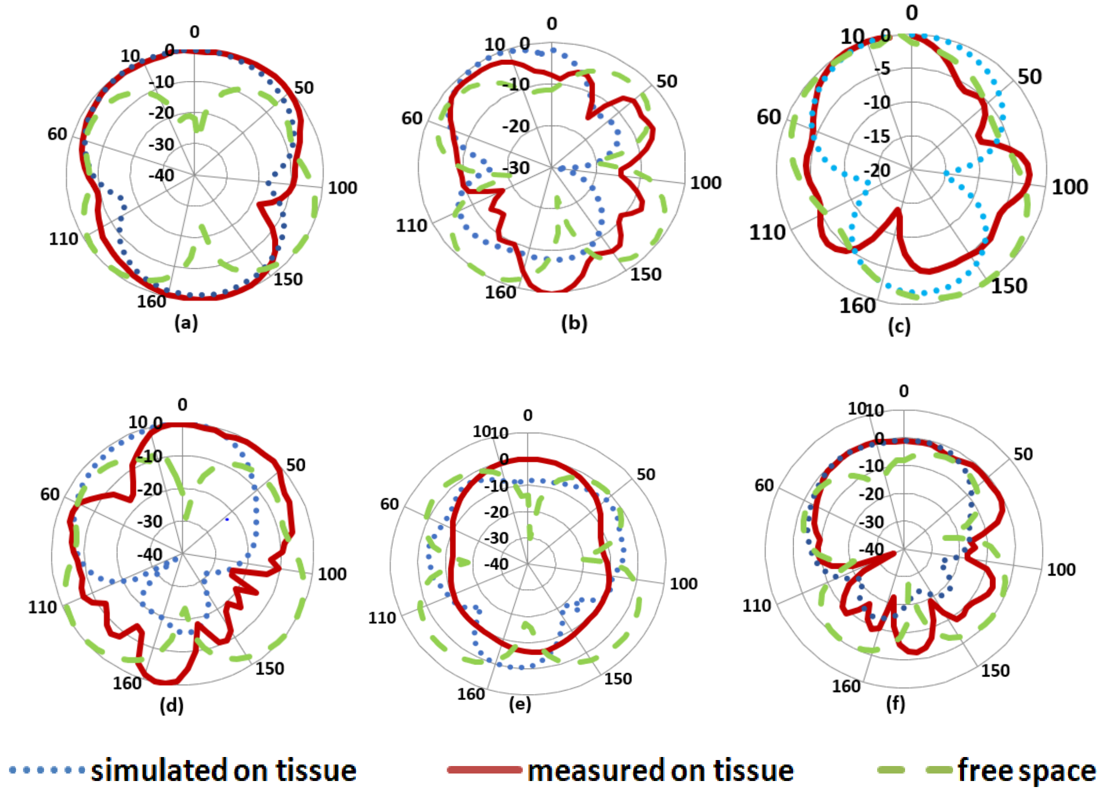

Fig. 5.21 Radiation pattern plots (a, b) E-plane and H-plane at 2.45 GHz (c, d) E-plane, and H-plane at 2.6 GHz (e, f) E-plane and H-plane at 5.2 GHz

Table 5.5 Relative analysis of ground coupled structure with different design techniques studied in literature

Ref. & antenna type	**Size (mm^3)**	**Frequency (GHz)**	**Gain**	**η_{tissue} (%)**	**Bandwidth (MHz)**
AMC integrated [224]	42×63×8	2.45/5.8	5/7.3dB	55/60 (s=5mm)	NA
Slotted circular patch [229]	100×100×2	2.45/5.8	5.93/6.02 dBi	Not specified	119/218
PIFA [230]	40×20×9	2.5/3.5	0.1/4.4 dB	67/58 (s=3mm)	300/420
Metallic back reflector [233]	50×50×4	2.45/5.8	1.2/7.9 dBi	Not specified	100/770
Patch with AMC [234]	70.4×76.14×3.11	1.575/2.45	5.1/5.03 dB	Not specified	31/17
This work Ring shape ground coupled	**38×38×0.6**	**2.45/2.6/5.2**	**2/2.5/1.1 dB**	**21/22/26 (s=6mm)**	**520/620**

The proposed structure showed the largest bandwidth with the smallest geometry to deal with frequency detuning effects in real-time applications. Complex geometrical structures with large vertical heights are used by researchers for gain and efficiency enhancement. It limits the practical application of antenna. Hence, this research is directed toward a planar antenna with broad impedance bandwidth characteristics and good radiation performance.

5.3.7 Specific Absorption Rate (SAR) Analysis

To consider the safety limits, antenna SAR value has been simulated at 100 mW input power for 10 gram of body tissue. Fig. 5.22 shows the simulated SAR results.

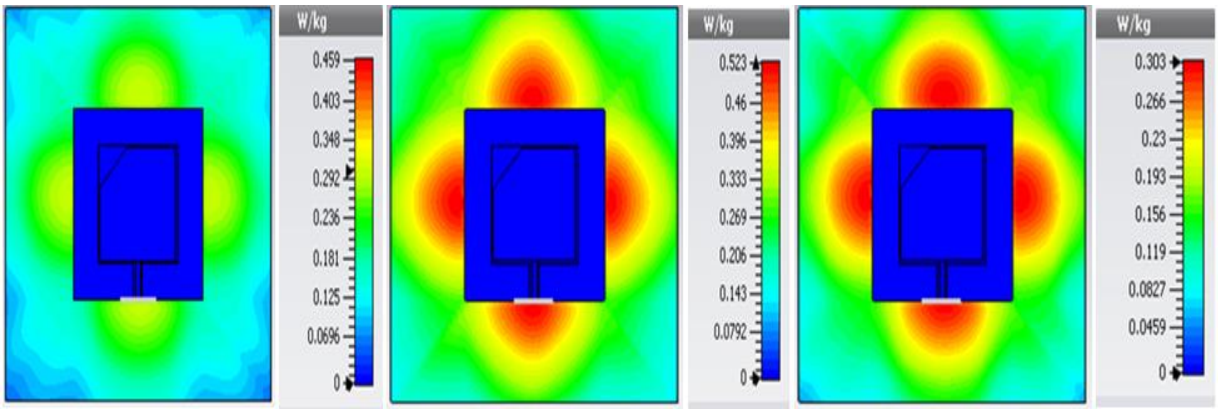

(a) (b) (c)

Fig. 5.22 Simulated SAR value at (a) 2.45 GHz (b) 2.6 GHz (c) 5.2 GHz

Antenna has 0.459 W/kg. SAR at 2.5 GHz, 0.523W /Kg at 2.6 GHz, and 0.303 W/Kg at 5.2 GHz. These values lie in the safety limit at satisfactory input power.

Research Contributions

Open-end slotted compact dual band antenna structure

A horizontal and an L-shaped slots are etched in the rectangular patch to achieve the dual-band resonance for on and off-body communication. Research contributions of this compact dual-mode antenna structure are as follows:

- Antenna occupied very small footprints with dimensions of 15mm×28mm×1.57mm that make antenna suitable to integrate with a compact sensor node. Antenna has covered impedance bandwidth of 350 MHz (14%) and 600 MHz (12%) corresponding to the resonance frequency of 2.45 GHz and 5.0 GHz.

- A three-layered tissue model is designed, and an equivalent dielectric constant for the proposed antenna is evaluated mathematically and verified through numerical simulation.
- Muscle equivalent phantom gel is used to carry out the in vitro test in the laboratory. Good impedance matching and frequency response is achieved for both the on-body and free space operation.
- Omnidirectional and dipole like radiation characteristics are obtained for the dual-mode on-on and on-off body communication with directivity of 4.07 dBi and 7.18 dBi at 2.45 GHz and 5.0 GHz frequencies, respectively.

Ground coupled dual band antenna structure

The designed antenna consisted of a square ring shape coplanar ground and truncated patch.

- Antenna possessed compact geometry of size 38×38×0.51 mm^3 and covered 2.4 GHz to 2.48 GHz (for ISM band), 2.5-2.69 GHz (for LTE band), and 5.1-5.35 GHz (for WLAN bands: U-NII-1: 5.150–5.250 GHz; U-NII-2: 5.250–5.350 GHz).
- Multiple resonance paths are excited due to the designed ground plane, which contributed to wideband performance.
- Experimental evaluation on equivalent tissue phantom and simulated results on tissue model show the robustness of antenna impedance matching and frequency.
- Directional radiation pattern is achieved with the gain value of -2 dB, -1.9 dB, and -0.1 dB at 2.45 GHz, 2.6 GHz and 5.2 GHz when the antenna is placed in extreme proximity of body tissue.
- Low specific absorption rate 0.459 W/kg., 0.523 W/Kg., 0.303 W/kg. at 2.45 GHz, 2.6 GHz, and 5.2 GHz ensured tissue safety.

Publish paper related to this chapter:

1. Gupta, A. Kansal, P. Chawla "Design of a patch antenna with square ring-shaped coupled ground for on-/off body communication." International Journal of Electronics, vol.106, no.12, pp.1214-1228 2019.
2. Gupta, A. Kansal, P. Chawla "Design of a compact dual band antenna for on-/off body communication" IETE Journal of Research, 2020, https://doi.org/10.1080/03772063.2020.1845826

Chapter-6

Role of Antenna in Health Care Systems

6.1 Introduction

In the present-day scenario, antenna has become an integral part of biomedical devices for benefiting the health and improving the standard of life. Antenna has stepped into medical diagnosis and rehabilitation along with data transfer application [238-240]. There are number of health care instruments which are taking the advantages of antenna system. Microwave and magnetic resonance imaging, implantable devices, microwave and radio frequency ablation therapies are some technologies that use antenna. In WBAN, antenna with sensor node is deployed on the body or implanted in body to send diagnosed data to the concerned person or doctor over the internet. Variation in the electrical characteristics of antenna like electromagnetic waves, impedance, and scattering parameters are analyzed to identify various fatal diseases non-invasively. In addition to this, unhealthy cell tissues are treated by the heating effect of near field electromagnetic radiations of antenna. Three types of medical applications of antenna are studied in literature and listed here.

1. Bio-telemetry
2. Diagnosis through magnetic resonance imaging (MRI) and microwave imaging (MWI)
3. Thermal ablation for cancer and cardiological therapy

To represent the role of antenna in health care domain, a compact, UWB, high gain antenna structure for the diagnosis of breast cancer through microwave imaging system. Simulation and measurement performance are analysed to find the variation in back scattered signal. Pre-processing of received signal is performed using GPR algorithm to detect the location 4mm tumour kept inside at 5mm depth at (-4,0) mm location.

6.2 Microwave Imaging (MWI)

Water content in a cancerous cell is much higher than the healthy body cells. High water content increases relative permittivity of unhealthy cells [241,242]. Therefore, back scattered signal also varies significantly on the tumor cells as compared to healthy cells. Fig. 6.1 displays the microwave imaging process on breast tissue [243].

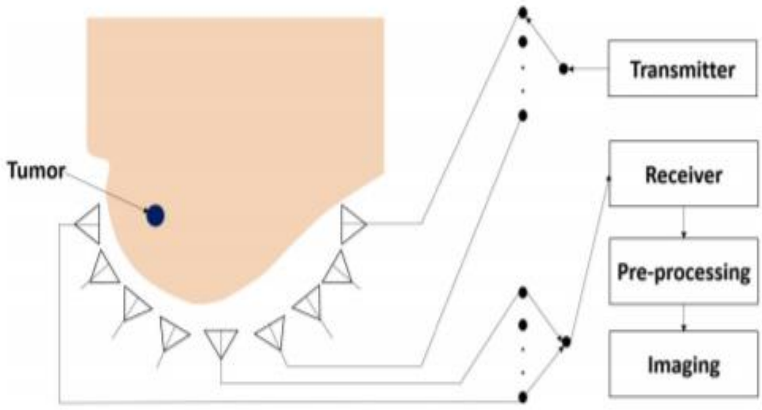

Fig. 6.1 Schematic for cancer detection using microwave imaging [243]

Microwave imaging (MI) is considered as the recent topic of research for the alternative solution of the existing techniques. Researchers are working to improve the performance of MI system in terms of cost reduction, reducing false detection, producing high resolution images and making measurement process simple and comfortable. MI works on the principle of change in back-scattered parameter with the changing electrical properties of body tissue. Malignant cells are exposed under near field EM waves of a single antenna element or array of antennas. Low power signal is intruded in the tissue from different angles and received for image formation by using image reconstructing algorithm like ground-based detection algorithm [244]. Precision of microwave imaging technique is definitely a function of antenna performance. Wideband frequency response with high fidelity is the most vital feature, it allows to vary the penetration depth in heterogeneous working condition [245].

To reduce the size of antenna, along with wider frequency range, gaussian modulated feed line and dark-eyed vivaldi antennas were investigated in [246-248]. However, these structures possessed low gain value of (below 5 dBi) that is not sufficient for health care. To improve the sensitivity of antenna, ellipse-shaped dependent patch was loaded with the radiating patch. It required large physical area ((140×60 mm^2) and also lost resonance at lower cut off frequency [249].

A biconical radiator with cone angle of 45^0 was designed to maintain the bandwidth stability of antenna on bio-tissue. It had unidirectional pattern and null was towards the body. It diminished the antenna sensitivity and limits its utilization for microwave imaging [250]. In [251], UWB antenna was designed by partial ground plane. In this work, single radiating element was used to gather information through s-parameters; however, another important antenna parameter like radiation characteristics, SAR were not examined. In [252], optimization technique was used to enhance the antenna compatibility for microwave imaging.

6.3 Antenna design for Microwave Imaging Application

Proposed UWB antenna for microwave imaging application is designed on Fr4 substrate with ε_r = 4.3 and loss tan=0.2. Geometrical topology of the antenna is shown in Fig. 6.2. Rectangular patch radiator, defected ground structure and dielectric back reflector (RO 3010) is used to design the antenna. Defected ground structure is used to minimize the size, achieving wide bandwidth and dielectric reflector to improve radiation characteristics. Antenna has overall dimension of 24×36×1.85 mm^3. Geometrical dimensions are given in Table 6.1. Step wise design process is shown in Fig. 6.3.

Table 6.1 Geometrical parameters of the proposed antenna

parameter	Value (mm)	parameter	Value (mm)	parameter	Value (mm)	parameter	Value (mm)	parameter	Value (mm)
Wg	24	Wp	6.73	Wf	2.4	Lg1	12.9	Wg1	3.0
Lg	23.1	Lp	9.24	Lf	16.88	Lg2	6.54	Wg2	3.5

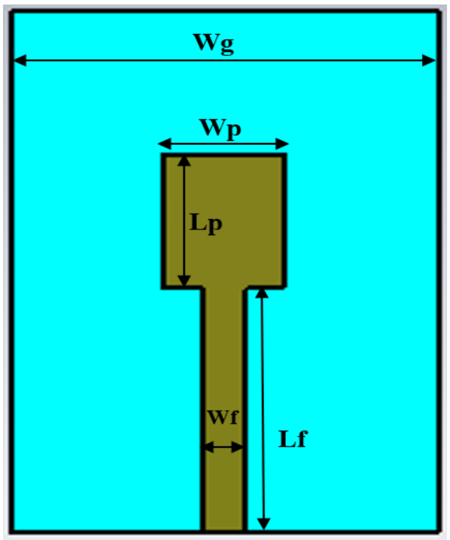

(a)

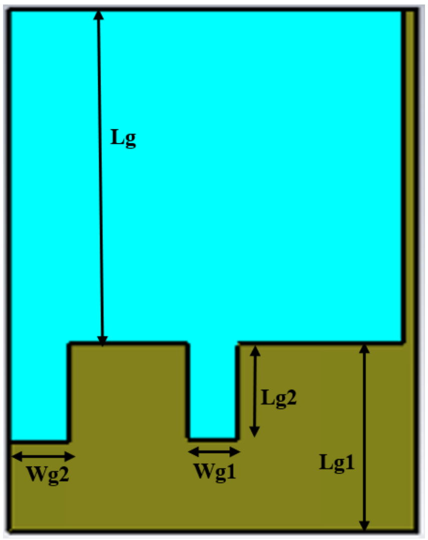

(b)

Fig. 6.2 Antenna geometry (a) front view (b) back view

Initially in step1, partial ground microstrip patch antenna is taken, which is resonating from 3.4 GHz to 6.3 GHz. Reflection coefficient plot for each step is shown in Fig. 6.4. In step2, two rectangular slots are etched on the ground; one in the middle and second on the right upper corner. Etching of these slots generates higher resonating modes that contributes both in impedance matching and wide band resonance towards higher frequencies. 10-dB impedance bandwidth increases from 2.9 GHz (in step1) to 4.7 GHz (in step2). It is clear from the Figure4 that another band is also excited from 8.2 GHz to 11 GHz. Now to achieve the UWB spectrum (in step3), a vertical strip of width 1mm is added on the left side of ground plane. It has strong effect to enhance electrical current length of antenna generates resonance at lower frequency of 3 GHz. This increased current length has introduced more reactive impedance and makes antenna enable to resonate for the desired bandwidth from 3.1 to 10.6 GHz.

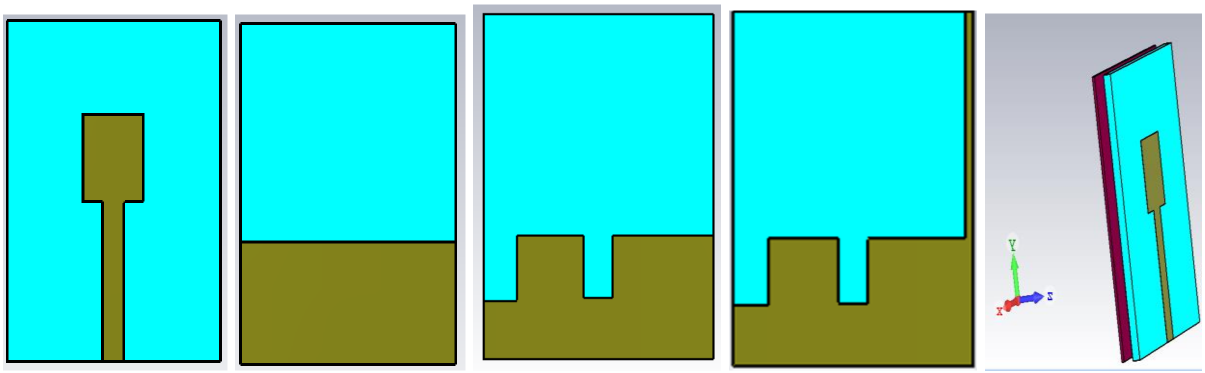

(a) (b) (c) (d) (e)

Fig. 6.3. Step wise topology (a) front view of all steps (b) back view step1 (c) backview step2 (d) backview step3 (e)antenna with dielectric reflector in step4

Although, antenna has sufficiently covered 3-dB bandwidth from 3 GHz to 11 GHz still has poor impedance matching at 4.8 GHz and 7 GHz. Thus, to improve the performance a thin dielectric reflector of 0.25 mm, consists of RO 3010 ($\boldsymbol{\varepsilon}_r$= 10.2, tan δ = 0.0022) is added below the ground plane. It plays prominent role in antenna structure by improving impedance and reducing radiations below the antenna. According to field theory radiations are reflected back at the interface of two dielectric mediums only if a low dielectric medium is backed by high dielectric medium. Reflected waves adds with the radiated waves and enhances the antenna reflection coefficient. Which in turns improves antenna impedance bandwidth and the magnitude of |S11|.

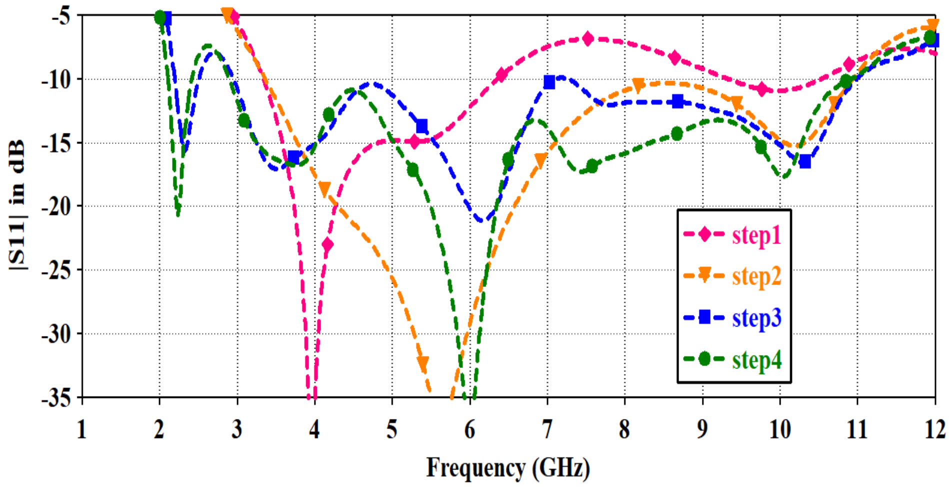

Fig. 6.4 Reflection coefficient for step wise antenna topologies

6.4 Design of Breast phantom and its effect on S11 for tumour detection

The ultimate goal of proposed structure is to detect the tumour inside a breast by identifying the variation in backscattered signal with and without the malignant cells. In order to perform this, a spherical shaped, equivalent breast tissue phantom of 40 mm radius is designed. It consist of 2 mm skin layer ($\boldsymbol{\varepsilon}_r$= 38 and conductivity=1.49 S/m), 38 mm fat layer($\boldsymbol{\varepsilon}_r$= 5.141 and conductivity=0.141 S/m) and a tumour of radius 4 mm, $\boldsymbol{\varepsilon}_r$ =67 and conductivity of 47S/m [173]. Designed phantom model along with simulation setup is shown in Fig. 6.5.

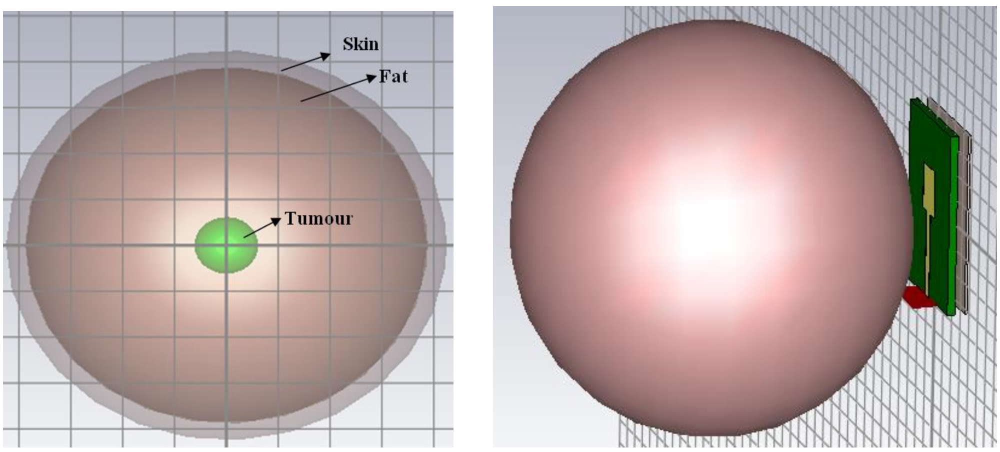

(a) (b)

Fig. 6.5 (a) Breast tissue phantom layers (b) simulation set up with antenna placed parallel to the breast tissue (along z-axis)

As shown in Fig. 6.5(b) antenna is placed exactly parallel to the breast tissue at a distance of 5mm along z-axis. It is well known that unhealthy tumour tissue has high relative permittivity as compared to the healthy tissue. Thus, more power will be reflected towards antenna. Backscattered signal for the two cases (with and without tumour) is shown in Fig. 6.6. It is studied that the only frequency band from 4.5 to 5.5 GHz is not affected by the presence of tumour. Rest of the entire UWB spectrum is altered due to the tumour. Details of the changes occurred in the magnitude of S11 at different frequency bands of the transmitted UWB pulse is mentioned in Table 6.2. It can be stated that an UWB pulse transmitted to a cancerous breast tissues and then received by the same antenna (monostatic radar) itself provides the information of existence of malignant cells.

Table 6.2 Comparison of S11 variation of antenna with and without presence of tumour w.r.t Fig. 6.6

Frequency band (GHz)	Frequency at which |S11| is analyzed (GHz)	|S11| in free space (dB)	|S11| on breast tissue without tumour (dB)	|S11| on breast tissue with tumour (dB)	Difference in magnitude of |S11| (without and with tumour)	Existence of tumour
3.0-4.5	3.5	-17	-16.49	-14.07	2.42	Weekly traceable
	4.0	-14.76	-18.8	-10.45	8.4	traceable
4.5-6.5	5.0	-14.75	-14.75	-14.51	0.24	Not traceable
	6.0	-33	-30.16	-23	7.16	traceable
6.5-8.5	6.8	-12.84	-12.97	-21	8.03	traceable
	8.0	-14.00	-14.34	-12.21	2.14	Weekly traceable
8.5-10.5	9.4	-13.80	-16.23	-12.12	4.11	traceable
	10	-13.84	-17.62	-10.76	6.86	traceable

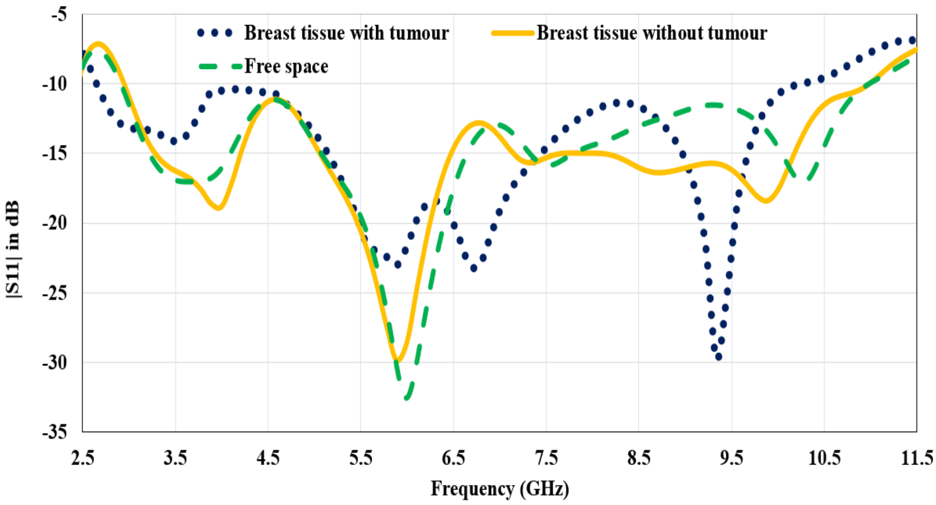

Fig. 6.6 Antenna backscattered signal with and without presence of tumour

6.5 Experimental validation of the simulated results

In order to validate the simulated results, a prototype of the simulate antenna is fabricated and experimentally tested for three different cases (free space, on breast tissue without tumour and on breast tissue with tumour). Due to issue of safety permission, realistic human body/patient is not used for the measurement purpose. Phantom tissue is prepared using polyethene for skin layer, petroleum jelly for fat layer (ε_r = 2.36, conductivity=0.0012S/m) and mixture of wheat flour (10g) and water (5.5g) for tumour (ε_r = 23, conductivity=2.57 S/m) [251]. Snapshots of the prepared breast tissue along with inserted tumour is shown in Fig. 6.7 (a and b). Antenna fabricated prototype and measurement setup in free space is represented in Fig. 6.7 (c and d).

(a) (b) (c) (d)

Fig. 6.7 Photographs of the measurement setup (a) breast phantom with tumour (b) breast phantom without tumour (c)Fabricated antenna prototype (d) results on VNA

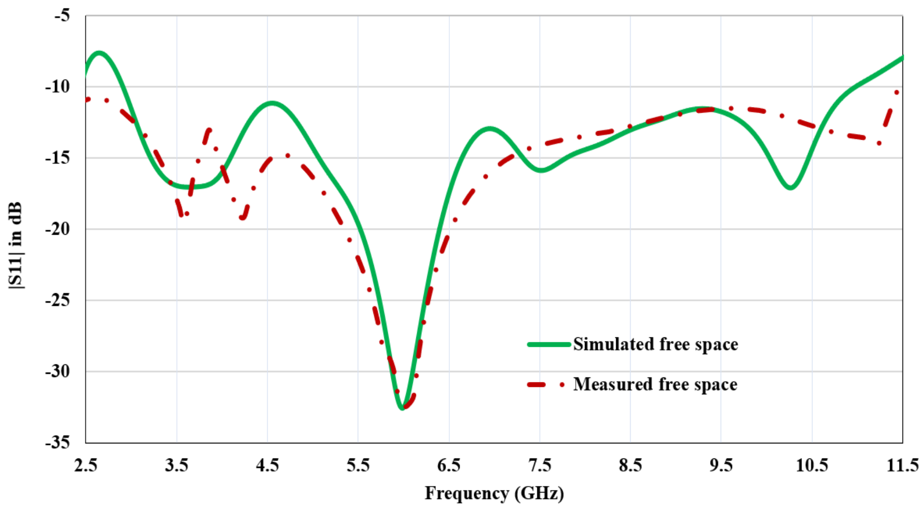

Fig. 6.8 Comparison of simulated and measured backscattered signals in free space

In the free space scenario, Fig. 6.8, simulated and measured results are agreed well to each other with negligible discrepancies. Required ultra-wide band (3.1 to 10.6 GHz) is effectively covered by the fabricated prototype. It is evident from the Fig. 6.9, that antenna has shown significant difference in the backscattered signals when measured with and without the tumour. At 4 GHz, 5.8 GHz and 9.5 GHz difference of 4 dB, 7 dB and 11dB in the value of backscattered signal with and without tumour can be observed. This justifies that antenna can easily detect the existence of malignant cells inside the breast.

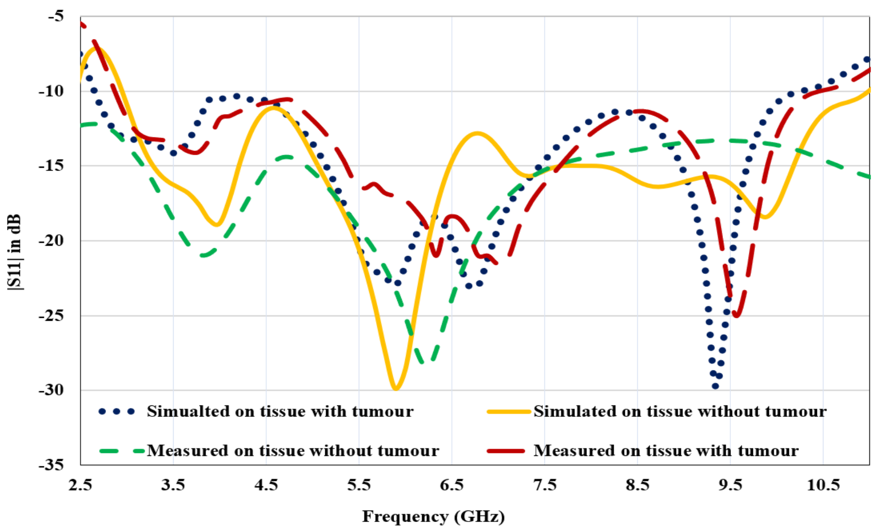

Fig. 6.9 Comparison of simulated and measured backscattered signals on breast tissues

6.6 Evaluation of tumour depth using ground penitrating radar (GPR) algorithm

To get sharper and clear image of the tumour, bckscattered signal from free space and unhealthy tissue are subtarcted. Then difference signal is preprocessed to find the depth of tumour. Fig. 6.10 shows the preprocessing steps used for time domain conversion and attaining impulse response.

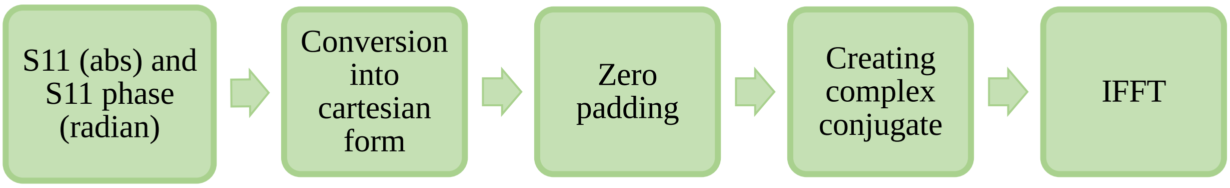

Fig. 6.10 Block diagram for preprocessing of backscttered signal

Preprocessing of the S11: frequency domain S11 is preprocessed to convert into time domain by using IFFT (Inverse Fast Fouries transform). IFFT is preferred as it requires less mathematical operation and easy way to synthesize the signal in discrete frequency domain and to convert into time domain.

Imitially, Reflection coefficient (|S11|) obtained from CST simulation is in polar form (|(f)|phase(f)), it must be converted into cartesian form ($z=|(f)|e^{j(f)}$). To create the complex conjugate, frequency range (f) is required from ($-f_{stop}$ to $+f_{stop}$) but S11 is achievd only for the positive frequencies from 2.5-11.5 GHz. To complete the frequeny spectrum, zero padding is done from 0 to f_{start}. Zero padding is performed as:

$$\text{Number of zeros to be padded} = {f_{start}}/{(\Delta f - 1)} \qquad (6.1)$$

Here, f_{start} =2.5 GHz, Δf =8.99 MHz, Δf depends upon the frequency samples prodced for each antenna position. In this paper, 1001 number of samples were obtained between 2.5 GHz to 11.5 GHz. Thus, the number of zeros added between 0 and 2.5 GHz is 313. On performing zero padding, |S11(f)| is attained for (0 to f_{stop}).

Further to get |S11(f)| samples from ($-f_{stop}$ to $+f_{stop}$), complex conjugate is reconstructed by using hermitian property which states that ($-f_{stop}$,0) is the conjugate symmetry of (0,f_{stop}). Now, total number of frequency coefficients are 2628 that is calculated using (2×

(313+1001)). Then, IFFT is performed to get 2628 samples in time domain (of Impulse response). Maximum frequency of the backscattered signal is 11.5 GHz and acording to sampling theorem, data is sampled at the frequency of ($fs=3\times11.5\times10^9$ Hz). Time resolution of the sampled signal is given by ($\Delta t = 1/fs$).

Finally, depth of tumour is identified using GPR algorithm. Depth resolution is evaluated using:

$$\Delta \mathrm{d} = \frac{\Delta t}{2} / \nu \tag{6.2}$$

where, ν is the speed of electromagnetic wave (3×10^8m/s). Depth vector equation is given by:

$$\mathrm{z} = (0{:}\,2628) \times \Delta d \tag{6.3}$$

As mentioned above, antenna is placed at a gap of 5 mm from the tissue. Thus for imaging data is considered from the depth of 5 mm to 25 mm. Data from 0 to 5 mm and 20 mm to 25 mm is windowed.

$$\text{Windowed signal } = \begin{cases} \mathrm{S11} & d_{min} < diff < d_{max} \\ 0 & otherwise \end{cases} \tag{6.4}$$

Where $diff$ is the difference of backscattered signal with and without tumour; $d_{min} = Z_{min}/\Delta \mathrm{d}$ and $d_{max} = Z_{max}/\Delta \mathrm{d}$. Then from the resulting data microwave image for depth identification is reconstructed in the Fig. 6.11 and the tumour depth at 5mm an be clearly identified.

Microwave image shown in Fig. 6.11 is based on simulation based scanning, measurement work is limited to the antenna performance analysis in the free space and biological enviornment. Mechanical rotating setup along with data acquisition system is required for real time microwave imaging and future prospective of this work will be concentarated toward implementation of proposed MWI antenna.

In Table 6.3 comparison of proposed MWI system with the existing systems is listed. Antenna of the proposed system is smallest structure with widest bandwidth. Single antenna is used to detect the tumour location, that makes MWI system simple, low cost and portable.

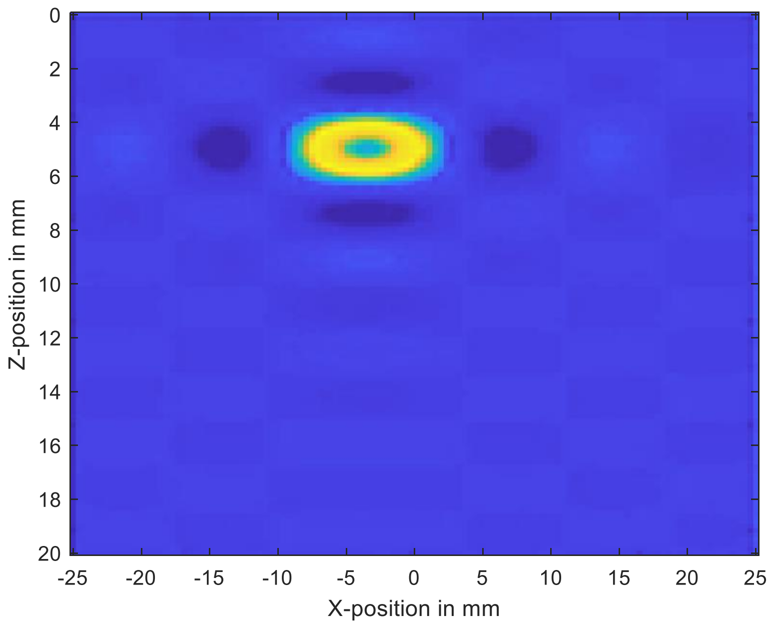

Fig. 6.11 Microwave image representing depth of tumour

Table 6.3 Comparison of proposed MWI system with the existing systems

Ref	Size (m^3)	bandwidth	Imaging domain	discussion
[246]	76×78× 3.2	5.35 GHz	Blind deconvolution with point spread optimization algorithm	Not specify the imaging algorithm
[251]	34×36× 1.6	2.3 GHz	Monostatic, GPR algorithm	Detected deep and multiple tumours but suffers with low bandwidth that reduces accuracy
[253]	30×28 mm^2	2.5 GHz	Multistatic, distorted born iterative mathod	Not biocompatible, used array of 32 antennas that redues its feasibility also in real time scenario.
[254]	40×50 mm^2	1.8 GHz	Multistatic radar with 5 antennas	Lack of scattering parameter analysis for location identification
Proposed strucure	**24×36×1.85**	**8 GHz**	**Monostatic radar, GPR algorithm**	**Detected location of 4mm radius tumour at the depth of 5mm**

Research Contribution

Antennas are extremely sensitive for medical diagnosis and thermal ablations. In this chapter, an UWB antenna is designed and analyzed for microwave imaging of breast tissue. Microwave imaging has inherent potential of differentiating healthy and malignant tissue. The most vital component of this system is antenna, which can influence the performance of whole system. Therefore, in this chapter, An UWB antenna is designed and implemented for breast tumour identification in the early stages. To achieve the desired performance, antenna is customized with a dielectric reflector. Heterogenous breast tissue phantom is designed to analyse the antenna response in the presence ana absence of tumour. A tumour of 4 mm radius placed at the depth of 5 mm inside the breast phantom. Single antenna (monostatic radar-based approach) is used to receive backscattered signal. Antenna is traced along the surface of body. Changes in signal magnitude with changing dielectric properties of tissue due to cancerous cell is evaluated, pre-processed using GPR algorithm for depth estimation and plotted as 2-D image using MATLAB.

Published work related to this Chapter:

1. A Gupta, A. Kansal, P. Chawla "A Survey and classification on Applications of antenna in health care domain: signal transmission, diagnosis and treatment." Sadhana Journal, https://doi.org/10.1007/s12046-021-01586-4
2. A Gupta, A. Kansal, P. Chawla, K. Singh "An Active and Low-Cost Microwave Imaging System design for Detection of Breast Cancer Using Back Scattered Signal" Current Medical Imaging, https://doi.org/10.2174/1573405617666210129114536

Chapter-7

Conclusions and Future Work

7.1 Introduction

This chapter summarizes the research work presented in the previous chapters of this thesis. Research conclusions of the designed antenna to the body area network are described briefly. In addition to this, a general discussion on thoughts and scope for future work is presented.

7.2 Conclusions

Antenna is the key component of the wireless body area network and the bio-medical system. Health care devices have become the inherited part of body area networks with the help of antennas. This work is started with the background of wireless body area network including communication standard, architecture, frequencies, and design issues need to consider for designing WBAN antennas. This thesis is paying attention to the two major aspects of antenna technology: designing conformal and dual mode antenna structures for wireless body area networks and highlighting the potential of antenna technology in healthcare system designs.

To cover the first feature, five antenna configurations are designed and characterized for WBAN application.

A compact and conformal MIMO antenna is presented for on-body communication. An open-end slotted antenna covering 2.45 GHz band is designed and fabricated. The proposed dual radiator MIMO antenna has occupied the size of 28 × 25 × 0.51 mm^3 Inverted U-shaped parasitic stub has reduced the mutual coupling to -30 dB that helped to maintain diversity performance. Stable and reliable performance is achieved against bending conditions.

Design and performance analysis of two on-body flexible antenna designs have been demonstrated. A CPW fed antenna with back reflector plate is designed and characterized for on-off body communication. Back reflector plate has excited dual-band resonance and reduces the power coupling to body tissue. High gain efficiency is observed after the addition of reflector. Impedance bandwidth of 310/330 with gain of 3/4 dB at 2.45/5.8 GHz is achieved in this antenna. The chosen substrate material is soft, flexible material, and its effectiveness is evaluated by bending the antenna. In second design, a conformal defected ground patch antenna with Artificial Magnetic Conductor (AMC) is introduced for on-body communication at 2.45 GHz. Initially, a DGS based antenna with a shorting pin is designed.

It resonates effectively on body tissue, but most of the near field EM radiations are absorbed by the tissue. Thus, to reduce the effect of tissue loading on antenna performance, an I-shaped AMC based structure is added. Better impedance matching, high efficiency, and good bandwidth are achieved when antenna is integrated with AMC structure.

The design and operational mechanism of two on-body antenna structures have been demonstrated for dual-mode on-/off body communication. Size of the first antenna is miniaturized to $0.120\lambda o \times 0.224\lambda o$. It has covered a wide bandwidth of 350 MHz and 600 MHZ at 2.45 GHz and 5.0 GHz resonance frequency. Second dual mode antenna is ground plane is modified to couple more power to the radiator. Multiple resonance paths are excited that enhances antenna bandwidth. Both structures have satisfied the safety guidelines.

Another key feature of this thesis is to describe an overside of the different roles of antenna in medical systems and design of a compact antenna structure for breast cancer detection by microwave imaging. Based on the near and far-field sensing, antenna applications are classified into three categories: Data transfer from in/on-body to off-body devices, disease detection by investigating the changes in antenna parameters with the healthy and unhealthy body, and treatment of malfunctioning cells by exposing them to the near field electromagnetic waves. Proposed defected ground antenna is designed to operate over the frequency range of 3.1 GHz to 10.6 GHz UWB spectrum. Antenna performance is verified experimentally on an artificially fabricated breast tissue and tumour. Malignant tissue has different dielectric properties than the normal tissue, that causes deviation in the scattered antenna power. Maximum deviation of 8dB is observed in measured backscattered signal. Deviation in backscattered signals is collected at different locations of breast tissue and processed to reconstruct the microwave image of breast tissue interior.

7.3 Future Scope

In this work, research is oriented towards the design of low profile, flexible antenna structures for the on-on body, and on-off body communication mode of wireless body area network. Antenna technology has incredible potential in providing health care services under the bio-instrumentation and WBAN architecture. It is not easy to overcome the design challenges of all the applications in one thesis. Therefore, there is enough scope for the development and improvement of the current work.

1. In this thesis, only microstrip patch antennas are designed. Other types of antennas like Yagi-Uda, surface integrated waveguide antennas can be used for the performance enhancement of wearable devices.

2. One can attempt to design on-body antenna for delivering power to the implantable device. It will increase the life span of the implant, reduce the size of the sensor node, and save the cost and pain of replacing the battery.
3. Antenna designed in this thesis are linearly polarized that may suffer from time-varying orientation mismatch during body movements; therefore, work can be improved by adding circular polarization and pattern diversity features.
4. More experimental work can be done to find the communication link range of designed antenna as their performance is affected by a dense indoor environment.
5. Besides data transfer, research can be emphasized to extract information from antenna parameters like reflection coefficient, impedance matching, and electric field distribution for designing new medical systems.
6. In the current work, the industrial, scientific, and medical band is adopted for transferring data from the human body to the external control unit. Most recent literature shows that high-frequency mm-wave technology is becoming an integral part of WBAN. It is necessary to make WBAN compatible with future networks. There is a lot of scope and unaddressed challenges for designing on-body antenna at mm-wave. In addition to antenna designing, new safety measures and standards should be addressed for ensuring safety against electromagnetic radiation at high frequencies.
7. New techniques can be incorporated to reduce the coupling of radiations with the body for improving the radiation efficiency.
8. There is a scope to integrate research with chemical engineering fields for fabricating low loss flexible substrates for antenna. The robustness of antenna can be improved with evaluations of new materials.
9. An array size of the MIMO antenna can be increased for improving communication reliability.

REFERENCES

References

[1] M. Chen, S. Gonzalaez, A. Vasilakos, H. Cao and C.M.V. Leung, "Body area networks: A survey," *Mobile Networks and Applications*, vol.16, no. 2, pp. 171-193, 2011.

[2] A. Meharouech, J. Elias, and A. Mehaoua, "Moving towards body-to-body sensor networks for ubiquitous applications: A survey," *Journal of Sensor and Actuator Networks*, vol. 8, no. 2, pp. 27, 2019.

[3] R. Schmidt, T. Norgall, J. Morsdorf, J. Bernhard, and T. V. Grun, "Body Area Network BAN- a key infrastructure element for patient-centered medical applications," *Biomed. Tech. (Berl.)*, vol. 47, pp.365–368, 2002.

[4] A. van Halteren, R. Bults, K. Wac, N. Dokovsky, G. Koprinkov, I. Widya, D. Konstantas, V. Jones, and R. Herzog, "Wireless Body Area Networks for healthcare: The MobiHealth project," in *Wearable eHealth Systems for Personalised Health Management: State of the Art and Future Challenges, Amsterdam, The Netherlands*: IOS Press, 2004, pp.108.

[5] R. S. H. Istepanian, E. Jovanov, and Y. T. Zhang, "Guest editorial introduction to the special section on M-health: Beyond seamless mobility and global wireless health-care connectivity," *IEEE Trans. Inf. Technol. Biomed.,* vol. 8, no. 4, pp. 405–414, 2004.

[6] D. Rathee, S. Rangi, S. Chakarvarti, V. Singh, "Recent trends in wireless body area network (WBAN) research and cognition based adaptive WBAN architecture for healthcare," *Health and Technology*, vol. 4, no. 3, pp. 239-244, 2014.

[7] M. Ghamri, B.Jako, R. Sheratt, W.Harwin, R. Piechockik and C. Soltanpur, "A survey on wireless body area networks for e-healthcare systems in residential environments", *Sensors*, vol.16, no. 831, pp. 1-33, 2016.

[8] E. Jovanov, C.C. Poon, G.Z. Yang, and Y.T. Zhang, "Guest editorial body sensor networks: From theory to emerging applications," *IEEE Transactions on Information Technology in Biomedicine*, vol. 13, no. 6, pp. 859-863, 2009.

[9] E. Jovanov, C.C. Poon, G.-Z. Yang, and Y.T. Zhang, "Guest editorial body sensor networks: from theory to emerging applications," *IEEE Transactions on*

antennas Information Technology in Biomedicine, vol.13, no.6, pp. 859-863, 2009.

[10] S. Movassaghi, M. Abolhasan, J. Lipman, D Smith and A. Jamalipour, "Wireless body area networks: A survey." *IEEE Communications Surveys & Tutorials*, vol. 16, no. 3, pp.1658-1686, 2014.

[11] D. Kurup, G.Vermeeren, E. Tanghe, W. Joseph and L. Martens, "In-to-out body antenna-independent path loss model for multi-layered tissues and heterogeneous medium," *Sensors*, vol.15, no.1, pp. 408-421, 2014.

[12] Y. Xiao and J. Rosdahl, "Throughput and delay limits of IEEE 802.11", *IEEE Communications Letters*, vol. 6, no. 8, pp. 355-357, 2002.

[13] S. Ullah, H. Higgins, B. Braem, B. Latre, C. Blondia, I. Moerman, S. Saleem, Z. Rahman and K. S. Kwak, "A comprehensive survey of wireless body area networks," *Journal of Medical Systems*, vol. 36, no.3, pp. 1-30,2010.

[14] S. M. Malladi and S. Vadivel, "Designing and deploying a Hospital Management Application in Google cloud and performance study of the application," *International Conference on Cloud Computing Technologies, Applications and Management (ICCCTAM)*, Dubai, pp. 43-51, 2012.

[15] M. Gamella, A. Koushanpour and E. Katz, "Biofuel cells–activation of micro-and macro-electronic devices," *Bioelectrochemistry*, vol. *119*, no.1, pp.33-42, 2018.

[16] Y.D. Lee and W. Y. Chung, "Wireless sensor network based wearable smart shirt for ubiquitous health and activity monitoring," *Sensors and Actuators B: Chemical*, vol.140, no. 2, pp.390-395, 2009.

[17] J. Alberto, C. Leal, C. Fernandes, P.A. Lopes, H. Paisana, A.T. Almeida and M. Tavakoli, "Fully untethered battery-free biomonitoring electronic tattoo with wireless energy harvesting," *Scientific reports*, vol. 10, no.1, pp.1-11, 2020.

[18] T. Tamura, M. Huang and T Togawa, "Current developments in wearable thermometers," *Advanced Biomedical Engineering*, vol. *7*, pp.88-99, 2018.

[19] Y. Kumar, S.C. Yen, A. Tay, W. Lee, F. Gao, Z. Zhao, J. Li, B. Hon, T. Tian-Ma Xu, A. Cheong and K. Koh, "Wireless wearable range-of-motion sensor system for upper and lower extremity joints: a validation study," *Healthcare technology letters*, vol. 2, no.1, pp.12-17, 2015.

[20] J. Kim and Y. Rahmat-Samii, "Implanted antennas inside a human body: Simulations, designs, and characterizations," *IEEE Trans. Microw. Theory Tech.*, vol.52, no.8, pp. 1934–1943, 2004.

[21] M.S. Wegmueller, A. Kuhn, J. Froehlich, M. Oberle, N. Felber, N. Kuster and W. Fichtner, “An attempt to model the human body as a communication channel”, *IEEE Transactions on biomedical engineering*, Vol.54, No.10, pp-1851-1857, 2007.

[22] V. Karthik and T.R. Rao, “Investigations on SAR and thermal effects of a body wearable microstrip antenna,” *Wireless Personal Communications*, vol. 96, no.3, pp. 1-17, 2017.

[23] G. Galatee, B. Nicolas, T. Jeremie, M. Elham, U. Leena, B. Toni and V. Johanna, “Embroidered antenna-microchip interconnections and contour antennas in passive in UHF RFID textile tag,” *IEEE Antennas and Wireless Propagation Letters*, vol.16, pp. 1205-1208, 2016.

[24] M.C. Gosselin, E. Neufeld, H. Moser, E. Huber, S. Farcito, L. Gerber, M. Jedensjö, I. Hilber, F. Di Gennaro, B. Lloyd and E. Cherubini, “Development of a new generation of high-resolution anatomical models for medical device evaluation: Virtual Population 3.0.,” *Phys. Med. Biol.*, vol. 59, no. 18, pp. 5287–5303, 2014.

[25] A. Kumar, R. K. Badhai, P. Suraj, “Design of printed symmetrical CPW-fed monopole antenna for on-body medical diagnosis applications,” Journal of Cmputational Electronics, vol. 17, pp. 1741-1747, 2018.

[26] X. Zhu, Y. Guo, and W. Wu, “Miniaturized dual band and dual-polarized antenna for 146 MBAN applications,” *IEEE Trans. Antennas Propag.,* vol. 62, no.7, pp. 2805–2817, 2018.

[27] Z. H. Jiang, D. E. Brocker, P. E. Sieber, and D. H. Werner, “A compact, low-profile metasurface-enabled antenna for wearable medical body-area network devices,” *IEEE Trans. Antennas Propag.,* vol. 62, no.8, pp. 4021–4030, 2014.

[28] T. Karacolak, R. Cooper and E. Topsakal, “Electrical properties of rat skin and design of implantable antennas for medical wireless telemetry,” *IEEE Transactions on Antennas and Propagation*, vol. 57, no.9, pp. 2806-2812, 2009.

[29] J. Nuutinen, R. Ikäheimo and T. Lahtinen, “Validation of a new dielectric device to assess changes of tissue water in skin and subcutaneous fat,” *Physiological measurement*, vol.*25, no.* 2, pp. 447-454, 2004.

[30] I. Gani and H. Yoo, “Multi-band antenna system for skin implant,” *IEEE Microwave and Wireless Components Letters*, vol. 26, no.4, pp. 294-296, 2016.

[31] A. Sharma, E. Kampianakis and M. S. Reynolds, “A dual-band HF and UHF antenna system for implanted neural recording and stimulation devices,” *IEEE Antennas and Wireless Propagation Letters*, vol. 16, pp. 493-496, 2017.

[32] T. Karacolak, A. Z. Hood, and E. Topsakal, “Design of a dual-band implantable antenna and development of skin mimicking gels for continuous glucose monitoring,” *IEEE Trans. Microwave Theory Techniques*, vol.56, no.4, pp. 1001–1008, 2008.

[33] J. Ung and K. Tutku, “A dual-band meandered dipole antenna for medical telemetry applications,” *Prog. Electromagn. Res.*, vol. 63, pp. 85–94, 2016.

[34] M. Patel and J. Wang, “Applications, challenges, and prospective in emerging body area networking technologies,” *IEEE Wirel. Commun.*, vol.17, no.1, pp. 80–88, 2010.

[35] Z. Duan, L. J. Xu and W. Geyi, “Metal frame repeater antenna with partial slotted ground for bandwidth enhancement of wristband devices,” *IET microwave antennas propagation*, vol.11, no.10, pp. 1438-1444, 2017.

[36] J. Tak, S. Lee and J. Choi, “All-textile higher order mode circular patch antenna for on-body to on-body communications,” *IET Microwaves, Antennas & Propagation*, vol. 9, no.6, pp. 576-584, 2015.

[37] G. Varshney, V.S. Pandey, R. S. Yaduvanshi and L. Kumar, “Wide band circularly polarized dielectric resonator antenna with stair-shaped slot excitation,” *IEEE Transactions on Antennas and Propagation*, vol. 65, no. 3, pp.1380-1383, 2016.

[38] Q. Bai and R. Langley, “Crumpling of PIFA textile Antenna,” *IEEE Trans Antennas Propag.*, vol. 60, no.1, pp. 63-70, 2012.

[39] M. Asili, R. Green, S. Seran and E. Topsakal, “A small implantable antenna for MedRadio and ISM bands,” *IEEE Antennas and Wireless Propagation Letters*, vol. 11, pp. 1683-1685, 2012.

[40] M.B. Abbasi, S. Nikolaou, M.A. Antoniades, M.N. Stevanovic, P. Vyronides, “Compact EBG backed planar monopole for BAN wearable applications,” *IEEE Trans. Antennas Propag.*, vol.65, no.2, pp. 453-462, 2017.

[41] L. Poffelie, A. Yimdjo, P.J. Soh, S. Yan and G.A.E. Vandenbosch, “A high-fidelity all-textile UWB antenna with low back radiation for off-body WBAN applications,” *IEEE Transactions on Antennas and Propagation*, vol. 64, no.2, pp. 757-760, 2016.

[42] D. Singh, and V.M. Srivastava, “An analysis of RCS for dual-band slotted patch antenna with a thin dielectric using shorted stubs metamaterial absorber,” *AEU-International Journal of Electronics and Communications*, vol. *90*, no.1, pp.53-62, 2018.

[43] D. Singh, A. Thakur, and V.M. Srivastava, “Miniaturization and gain enhancement of microstrip patch antenna using defected ground with EBG,” *Journal of Communication*, vol. *13, no.*12, pp.730-736, 2018.

[44] A. Gupta and V. Kumar, “Design of a tri-band patch antenna with back reflector for off-body communication,” *Wireless Personal Communications*, vol. 11, pp. 1-13, 2020.

[45] M. Usuler, B. Cetindere and S.C. Basaran, “Compact implantable antenna design for MICS and ISM band biotelemetry applications,” *Microwave and Optical Technology Letter*, vol.62, no. 4, pp. 1581-1587, 2020.

[46] G. Varshney, S. Gotra, S. Chaturvedi, V. S. Pandey and R.S. Yaduvanshi, “Compact four-port MIMO dielectric resonator antenna with pattern diversity,” *IET Microwaves, Antennas & Propagation*, vol. 13, no. 12, pp.2193-2198, 2019.

[47] C.R. Liu, Y.X. Guo and S.Q. Xiao, “Capacitively loaded circularly polarized implantable patch antenna for ISM band biomedical applications,” *IEEE Trans Antennas Propag.,* vol. 62, no.5, pp. 2407-2417, 2014.

[48] S. Hout and J.Y. Chung, “Design and characterization of a miniaturized implantable antenna in a seven-layer brain phantom,” *IEEE Access*, vol. 7, pp. 162062-162069, 2019.

[49] L. Luo, B. Hu, J. Wu, T. Yan and L. J. Xu, “Compact dual band antenna with slotted ground for implantable applications,” *Microwave and Optical Technology Letter*, vol. 61, pp. 1314-1319, 2019.

[50] IEEE Standard for Safety Levels with Respect to Human Exposure to Radiofrequency Electromagnetic Fields, 3 kHz to 300 GHz, *IEEE Standard C95.1, 2005*.

[51] IEEE Standard for Safety Levels with Respect to Human Exposure to Radiofrequency Electromagnetic Fields, 3 kHz to 300 GHz, *IEEE Standard C95.1*, 1999

[52] J. Kim and Y.R. Samii, "SAR reduction of implanted planar inverted F antennas with non-uniform width radiator," *IEEE International Symposium on Antennas and Propagation, Albuquerque, New Mexico,* 2006.

[53] M. Zada, I.A. Shah and H. Yoo, "Metamaterial-loaded compact high-gain dual-band circularly polarized implantable antenna system for multiple biomedical applications," *IEEE Trans. Antennas Propag.,* vol.68, no.2, pp. 1140 – 1144,2020.

[54] C. Y. Poon, B. P. Lo, M.R. Yuce and A. Alomainy, "Body Sensor Networks: In the era of bid data and beyond," *IEEE Reviews in Biomedical Engineering*, vol. 8, no. 1, pp. 4-16, 2015.

[55] S.I. Kwak, D.U. Sim, J.H. Kwon and Y.J. Yoon, "Design of PIFA with metamaterials for body-SAR reduction in wearable applications," *IEEE Transactions on Electromagnetic Compatibility*, vol.59, no.1, pp. 297-300,2017.

[56] I. Gill and R.F. Garcia, "Wearable PIFA antenna implemented on jean substrate for wireless body area network," *Journal of Electromagnetic Waves and Applications*, vol.31, no.11, pp. 1194-1204, 2017.

[57] P.J. Soh, G.A.E. Vandenbosch, S.L. Ooi and N.H.M. Rais, "Design of a broadband all-textile slotted PIFA," *IEEE Transactions on Antennas and Propagation*, vol. 60, no.1, pp. 379-384, 2012.

[58] W.N. Liu, J.K. Xiao, S. Zhang and Y. Li, "A novel PBG planar inverted-F antenna for wearable system," *Journal of Electromagnetic Waves and Applications*, vol. 20, no.5, pp. 615-622, 2012.

[59] F.X. Liu, T. Kaufmann, Z. Xu and C. Fumeaux, "Wearable applications of quarter-wave patch and half-mode cavity antennas," *IEEE Antennas and Wireless Propagation Letters,* vol. 14, pp. 1478-1481, 2014.

[60] T. Alves, B. Poussot and J.M. Laheurte, "PIFA-top-loaded-monopole antenna with diversity features for WBAN applications," *IEEE Antennas and Wireless Propagation Letters,* vol.10, pp. 693-696, 2011.

[61] C.H. Lin, K. Saito, M. Takahashi and K. Ito, "A compact planar inverted-F antenna for 2.45 GHZ on-body communications," *IEEE Transactions on Antennas and Propagation,* vol. 60, no.9, pp. 4422-4426, 2012.

[62] G.A. Casula, A. Michel, P. Nepa, G. Montisci and G. Mazzarella, "Robustness of wearable UHF-band PIFAs to human-body proximity," *IEEE Transactions of Antennas and Propagation,* vol. 64, no.5, pp. 2050-2055, 2016.

[63] K. Zhang, C. Liu, X. Yang, X. Liu and H. Guo, "An ingestible capsule system for in-body core temperature monitoring," *Microwave and Optical Technology Letters*, vol. 59, no.10, pp. 2670-2675, 2017.

[64] G. Gao, B. Hu, S. Wang and C. Yang, "Wearable planar inverted-F antenna with stable characteristic and low specific absorption rate," *Microwave and Optical Technology Letters*, vol.60, no.4, pp. 876-882, 2018.

[65] P.J. Soh, G.A.E. Vandenbosch, S.L. Ooi and M.R.N. Husna, "Wearable dual-band sierpinski fractal PIFA using conductive fabric," *Electronics Letters*, vol. 47, no.6, pp. 365-367, 2011.

[66] S. Yan, V. Volskiy and G.A.E. Vandenbosch, "Compact dual-band textile PIFA for 433-MHz/2.4-GHz ISM bands," *IEEE Antennas and Wireless Propagation Letters*, vol.16, pp. 2436-2439, 2017.

[67] G.P. Gao, C. Yang, B. Hu, R.F. Zhang and S.F. Wang, "A wearable PIFA with an all-textile metasurface for 5 GHz WBAN applications," *IEEE Antennas and Wireless Propagation Letters*, vol. 18, no.2, pp. 288-292, 2019.

[68] J. Shang, Y. Yu and L.J. Xu, "Compact dual-band implantable planar inverted-F antenna with bandwidth enhancement," *Microwave and Optical Technology Letters*, vol. 62, no.1, pp. 322-328, 2020.

[69] Q.H. Wu, X.W. Xuan, W. Wang, K. Li and H.B. Zhao, "A miniaturized implantable planar inverted-F antenna for biotelemetry applications at 2.45 GHz industrial, scientific, and medical band," *Microwave and Optical Technology Letters*, vol. 62, no.1, pp. 391-396, 2020.

[70] A. Al-Sehemi, A. Al-Ghamdi, N. Dishovsky, N. Atanasov and G. Atanasova, "On-body investigation of a compact planar antenna on multilayer polymer composite for body-centric wireless communications," *International Journal of Electronics and Communications*, vol. 82, pp. 20-29, 2017.

[71] M. Särestöniemi, C. Pomalaza-Ráez, C. Kissi, M. Berg, M. Hämäläinen and J. Iinatti, "WBAN channel characteristics between capsule endoscope and receiving directive UWB on-body antennas," *IEEE Access*, vol. 8, pp. 55953-55968, 2020.

[72] S. Yan, P. J. Soh, and G. A. E. Vandenbosch, "Wearable dual-band magneto-electric dipole antenna for WBAN/WLAN applications," *IEEE Transaction Antennas Propagation*, vol. 63, no. 9, pp. 4165–4169, 2015.

[73] Y. Li, Y.X. Guo and S. Xiao, "Orientation insensitive antenna with polarization diversity for wireless capsule endoscope system," *IEEE Transactions on Antennas and Propagation,* vol.65, no.7, pp. 3738-43, 2017.

[74] B. Moradi, R. Fernández-García and I. Gil, "Wearable high-performance meander ring dipole antenna for electronic-textile applications." *The Journal of The Textile Institute,* vol. 111, no.2, pp.178-182, 2020.

[75] A. H. Ismael, H. Yang and W. Chen. "Wearable triband E-shaped dipole antenna with low SAR for IoT applications." *Electronics,* vol. 8, no.6, pp. 665, 2019.

[76] A. Al-Sehemi, A. Al-Ghamdi, N. Dishovsky, N. Atanasov, and G. Atanasova. "Miniaturized wearable antennas with improved radiation efficiency using magneto-dielectric composites," *IETE Journal of Research,* pp. 1-11, 2019.

[77] A. Ammar, S. Lui, K.S. Keng, S. Moshfegh, A. Soto-Breceda, W. Tong, J.M. Redoute, D. J. Garrett, Y. T.Wong, and S. Prawer, "Wide dipole antennas for wireless powering of miniaturised bioelectronic devices," *Sensing and Bio-Sensing Research*, vol.27, pp. 100311, 2020.

[78] S. A. Balakrishnanand E. F. Sundarsingh, "Conformal self-balanced EBG integrated printed folded dipole antenna for wireless body area networks," *IET Microwaves, Antennas & Propagation,* vol. 13, no.14, pp. 2480-2485, 2019.

[79] D. G. Kang, J. Tak, and J. Choi, "Low- profile dipole antenna with parasitic elements for WBAN applications," *Microwave and Optical Technology Letters*, vol. 58, no.5, pp. 1093-1097, 2016.

[80] A.T. Mobashsher and A.M. Abbosh, "Compact 3-D slot-loaded folded dipole antenna with unidirectional radiation and low impulse distortion for head imaging applications," *IEEE Trans. Antennas Propag.*, vol.64, no.7, pp. 3245–3250, 2016.

[81] H.Y. Lin, M. Takahashi, K. Saito and K. Ito, "Performance of implantable folded dipole antenna for in-body wireless communication," *IEEE Trans. Antennas Propag.*, vol.61, no.3, pp.1363–1370, 2013.

[82] M.L. Scarpello, D. Kurup, H. Rogier, D. V. Ginste, F. Axisa, J. Vanfleteren, W. Joseph, L. Martens and G. Vermeeren, "Design of an implantable slot dipole conformal flexible antenna for biomedical applications," *IEEE Trans. Antennas Propag.*, vol.59, no.10, pp. 3556–3564, 2011.

[83] H. M. Bernety, H. Zhang, D. Schurig, and C.M. Furse, "Field focusing for implanted medical devices," *IEEE Journal of Electromagnetics, RF and Microwaves in Medicine and Biology*, pp.1-11, 2020.

[84] Y. Hong, J. Tak and J. Choi, "Dual-band dual-mode patch antenna for on–on–off WBAN applications," *IET Electronics Letter*, vol.50, no.25, pp. 1895–1896, 2014.

[85] J. Tak, Y. Hong, and J. Choi, "Textile antenna with EBG structure for body surface wave enhancement," *Electronics Letters*, vol.51, no.15, pp. 1131-1132, 2015.

[86] W. A. Ali, A. M. Mansour and D. A. Mohamed, "Compact UWB wearable planar antenna mounted on different phantoms and human body," *Microwave Optical and Technology Letter*, vol.58, no.10, pp. 2531-2536, 2016.

[87] B. V. Roy, B. Simorangkir, Y. Yang, L. Matekovits and K. P. Esselle, "Dual-band dual-mode textile antenna on PDMS substrate for body-centric communications," *IEEE Antennas and Wireless Propagation Letters,* vol.16, pp. 1-4, 2017.

[88] M. N. Shakib, M. Moghavvemi, and B. W. Mahadi, "Design of a tri-band off-body antenna for WBAN communication," *IEEE Antennas and Wireless Propagation Letters*, vol.16, pp. 210-213, 2017.

[89] H. Lee, J. Tak and J. Choi, "Wearable antenna integrated into military berets for indoor/outdoor positioning system," *IEEE Antennas and Wireless Propagation Letters*, vol. 16, pp. 1919-1922, 2017.

[90] S. Bhattacharjee, S. Maity, S. R. B. Chaudhuri and M. Mitra, "A compact dual-band dual-polarized omnidirectional antenna for on-body applications," *IEEE Transactions on Antennas and Propagation*, Aug. vol.67, no.8, pp. 5044-5053, 2019.

[91] W. Wang, X. W. Xuan, P. Pan, Y. J. Hua, H. B. Zhao and K. Li, "A low-profile dual-band omnidirectional Alford antenna for wearable WBAN applications," *Microwave and Optical Technology Letters, vol.* 62, no. 5, pp. 2040-2046, 2020.

[92] G. Wolgast, C. Echrenburg, A. Israelsson, J. Halender, E. Johanson and H. Manefjord, "Wireless body area network for heart attack detection [Education Corner]," *IEEE Antennas and Propagation Magazine*, vol.58, no.5, pp. 84-92, 2016.

[93] M. Grilo, M. H. Seko, and F. S. Correra, "Wearable textile patch antenna fed by proximity coupling with increased bandwidth," *Microwave Optical and Technology Letter*, vol. 58, no.8, pp. 1906-1911, 2016.

[94] J. Tak, S. Woo, J. Kwon, and J. Choi, “Dual-band dual-mode patch antenna for on- /off-body WBAN communications”, *IEEE Antennas and Wireless Propagation Letters*, vol.15, pp. 348-351, 2016.

[95] J. Zhang, S. Yan, and G. A. E. Vandenbosch, “A miniature feeding network for aperture-coupled wearable antennas,” *IEEE Transactions on Antennas and Propagation*, vol. 65, no. 5, pp. 2650-2654, 2017.

[96] D. Ferreira, P. Pires, R. Rodrigues and R. F.S. Caldeirinha, “Wearable textile antennas examining the effect of bending on their performance,” *IEEE Antennas & Propagation Magazine*, vol.59, no.3, pp. 54-59, 2017.

[97] A. Arif, M. Zubair, M. Ali, M. U. Khan and M. Q. Mehmood, “A compact, low-profile fractal antenna for wearable on-body WBAN applications,” *IEEE Antennas and Wireless Propagation Letters*, vol.18, no.5, pp. 981-985, May 2019.

[98] A. Ashyap, S. H. Dahlan, Z. Z. Abidin, M. H. Dahri, H. A. Majid, M. R. Kamarudin, S. K. Yee, M. H. Jamaluddin, A. Alomainy and Q. H. Abbasi, “Robust and efficient integrated antenna with EBG-DGS enabled wide bandwidth for wearable medical device applications,” *IEEE Access*, vol. 8, pp. 56346-56358, 2020.

[99] G. Gao, R. Zhang, C. Yang, H. Meng, W. Geng and B. Hu, “Microstrip monopole antenna with a novel UC-EBG for 2.4 GHz WBAN applications,” *IET Microwaves, Antennas & Propagation*, vol. 13, no.13, pp. 2319-2323, 2020.

[100] A. Singh and P.K. Jain, “FDTD analysis of the dispersion characteristics of the metal PBG structures,” *Progress in Electromagnetics Research*, vol. 39, pp.71-88, 2012.

[101] G.A. Conway and W. G. Scanlon, “Antennas for over-body-surface communication at 2.45 GHz,” *IEEE Transactions on Antennas and Propagation*, vol. 57, no.4, pp. 844-855, April 2009.

[102] I. Elfergani, A. Iqbal, C. Zebiri, A. Basir, J. Rodriguez, M. Sajedin, A.O. Pereira, W. Mshwat, R. Abd-Alhameed and S. Ullah, “Low-profile and closely spaced four-element MIMO antenna for wireless body area networks,” *Electronics*, vol. 9, no.2, pp. 258, 2020.

[103] A. Ashyap, Z.Z. Abidin, S.H. Dahlan, H.A. Majid and G. Saleh, “Metamaterial inspired fabric antenna for wearable applications,” *International Journal of RF and Microwave Computer-Aided Engineering*, vol. 29, no.3, e21640, 2019.

[104] A. Anbalagan, E.F. Sundarsingh and V. S. Ramalingam, "Design and experimental evaluation of a novel on-body textile antenna for unicast applications," *Microwave and Optical Technology Letters*, vol. 62, no.2, pp. 789-799, 2020.

[105] X.Y. Liu, Z.T. Wu, Y. Fan and E.M. Tentzeris, "A miniaturized CSRR loaded wide-beamwidth circularly polarized implantable antenna for subcutaneous real-time glucose monitoring," *IEEE Antennas and Wireless Propagation Letters*, vol.16, pp. 577-580, 2017.

[106] R. Moro, S. Agneessens, H. Rogie and M. Bozzi, "Circularly-polarised cavity-backed wearable antenna in SIW technology," *IET Microwaves, Antennas & Propagation*, vol.12, no.1, pp.127-131, Jan. 2018.

[107] D. Chaturvedi and S. Raghavan, "Circular quarter-mode SIW antenna for WBAN application," *IETE Journal of Research*, vol. 64, no.4, pp.482-488, 2018.

[108] D. Chaturvediand S. Raghavan, "A triangular-shaped quarter-mode substrate integrated waveguide-based antenna for WBAN applications," *Defence Science Journal*, vol.68, no.2, pp. 190-196, 2018.

[109] B. Mandal and S.K. Parui, "Wearable tri-band SIW based antenna on leather substrate," *Electronics Letters*, vol.21, no. 20, pp. 1563-1564, 2015.

[110] Y. Hong, J. Tak, and J. Choi, "An all textile SIW cavity-backed circular ring slot antenna for WBAN applications," *IEEE Antennas and Wireless Propagation Letters*, vol.15, pp. 1995-1999, 2015.

[111] S. Agneessens, "Coupled eighth-mode substrate integrated waveguide antenna: small and wideband with high-body antenna isolation," *IEEE Access*, vol. 6, pp. 1595-1602, 2018.

[112] S. Lee and J. Choi, "All-textile corrugated ground SIW horn antenna for millimetre-wave WBAN applications," *Journal of Electromagnetic Engineering and Science*, vol.19, no.4, pp. 221-226, 2019.

[113] D. Chaturvedi and S. Raghavan, "A half-mode SIW cavity-backed semi-hexagonal slot antenna for WBAN application," *IETE Journal of Research*, vol.65, no.5, pp. 582-588, 2018.

[114] D. Chaturvedi and S. Raghavan, "A dual-band half-mode substrate integrated waveguide-based antenna for WLAN/WBAN applications," *International Journal of RF and Microwave Computer Aided Engineering*, vol.28, no.5, e21239, 2018.

[115] M. M. Jawad, N. Malik, N. A. Murad, M. R. Ahmad, M. Esa and Y. M. Hussein, "Design of substrate integrated waveguide with Minkowski-Sierpinski fractal antenna for WBAN applications," *Bulletin of Electrical Engineering and Informatics*, vol.9, no.6, pp. 2455-2461, 2020.

[116] B. S. Abirami and E. F. Sundarsingh, "EBG-backed flexible printed Yagi–Uda antenna for on-body communication," *IEEE Transactions on Antennas and Propagation*, vol. 65, no.7, pp. 3762-3765, 2017.

[117] V. Aruna, M. G. N. Alsath, S. Kirubaveni and M. Maheswari, "Flexible and beam steerable planar UWB Quasi-Yagi antenna for WBAN," *IETE Journal of Research*, vol.1, pp.1-11, 2019.

[118] X. Y. Wu, L. Akhoondzadeh-Asl, and P. S. Hall, "Printed Yagi–Uda array for on-body communication channels at 60 GHz," *Microwave and Optical Technology Letters*, vol.53, no.12, pp. 2728-2730, 2011.

[119] N. Chahat, M. Zhadobov and R. Sauleau, "Yagi-Uda Textile Antenna for On-Body Communications at 60 GHz," *7th European Conference on Antennas and Propagation (EuCAP)*, pp. 411-413, 2013.

[120] A. R. Guraliuc, N. Chahat, C. Leduc, M. Zhadobov and R. Sauleau, "End-fire antenna for BAN at 60 GHz: Impact of Bending, On-Body Performances, and Study of an On to Off-Body Scenario," *Electronics*, vol.3, no.2, pp. 221-233, 2014.

[121] K. Agarwal, Y.X. Guo and B. Salam, "Wearable AMC backed near-end fire antenna for on-body communications on latex substrate," *IEEE Transactions on Components, Packaging and Manufacturing Technology*, vol.6, no.3, pp. 346-358, 2016.

[122] K. Kamardin, M. Kamal, A. Rahim, N. A. Samsuri, M. E. Jalil, and H. A. Majid, "Transmission enhancement using textile artificial magnetic conductor with coplanar waveguide monopole antenna," *Microwave Optical and Technology Letter*, vol.57, no.1, pp. 197-200, 2015.

[123] C.L. Tsai, K. Chen and C. Yang, "Implantable wideband low-specific-absorption-rate antenna on a thin flexible substrate," *IEEE Antennas and Wireless Propagation Letters*, vol.15, pp. 1048-1052, 2016.

[124] H. Baharami, “Flexible, polarization-diverse UWB antennas for implantable neural recording systems,” *IEEE Transactions on Biomedical Circuits and Systems*, vol.10, no.1, pp. 38-48, 2016.

[125] Z. H. Jiang, Z. Cui, T. Yue, Y. Zhu and D. H. Werner, “Compact, highly efficient, and fully flexible circularly polarized antenna enabled by silver nanowires for wireless body-area networks,” *IEEE Transactions on Biomedical Circuits and Systems*, vol.11, no.4, pp. 920-932, 2017.

[126] S. Sukhija and R. K. Sarin, “Low-profile patch antennas for biomedical and wireless applications,” *Springer Journal of Comp. Electronics*, vol. 16, no.2, pp. 354-368, 2017.

[127] C. Mendos and C. Peixeiro “A dual-mode single- band micro strip antenna for body area network,” *IEEE Antennas and Wireless Propagation Letters*, vol.16, pp. 3055- 3058, 2017.

[128] B. Hu, G.Ping, L.he, X. D. Cong and J.N. Zhao, “Bending and on-arm effects on a wearable antenna for 2.45 GHz body area network,” *IEEE Antennas and Wireless Propagation Letters*, vol.16, pp. 378-381, 2016.

[129] A. Alemaryeen and S. Noghanian, “On-body low-profile textile antenna with artificial magnetic conductor,” *IEEE Transactions on Antennas and Propagation*, vol. 67, no.6, pp. 3649-3656, 2019.

[130] I. Khan, P.S. Hall, A. A. Serra, A. R. Guraliuc and P. Nepa, “Diversity performance analysis for on-body communication channels at 2.45 GHz,” *IEEE Transactions on Antennas and Propagation*, vol. 57, no.4, pp. 956-963, 2009,

[131] R.S. Alrawashdeh, Y. Huang, M. Kod, A.A.Sajak, “A broadband flexible implantable loop antenna with complementary split ring resonators,” *IEEE antennas and wireless propagation letters*, vol. 14, pp. 1506-1509, 2015.

[132] L. Qu, H. Piao, Y. Qu, H.H. Kim and H. Kim, “Circularly polarized MIMO ground radiation antennas for wearable devices,” *IET Electronics Letters*, vol. 54, no.4, pp. 189-190, Feb. 2018.

[133] A. Ruaro, J. Thaysen and K. B. Jakobsen, “Wearable shell antenna for 2.4 GHz hearing instruments,” *IEEE Transactions on Antennas and Propagation*, vol.64, no.6, pp. 2127-2135, 2016.

[134] M. Mantash and T. A. Denidni, “Finger-worn end-fire antenna for mm wave applications,” *Microwave Optical and technology Letter*, vol.59, no.10, pp. 2591-2593, 2017.

[135] X. Hu, S. Yan and G. A.E. Vandenbosch, “Wearable button antenna for dual-band WBAN applications with combined on and off-body radiation patterns,” *IEEE Transactions on Antennas and Propagation*, vol.65, no.3, pp. 1384-1387, 2017.

[136] V. Kaim, B.K. Kanaujia and K. Rambabu, “Design of a miniaturised broadband 3× 3 mm antenna for intraocular retinal prosthesis application,” *Electronics Letters*, vol. 54, no.20, pp. 1150-1152, 2018.

[137] P. Sambandam, M. Kanagasabai, R. Natarajan, M.G.N. Alsath and S.k. Palaniswamy, “Miniaturized button like WBAN antenna for off body communication,” *IEEE Transactions on Antennas and Propagation*, vol. 68, no.1, pp.1324-1331, 2020.

[138] B. Rana, J. Shim and J. Chung, “An implantable antenna with broadside radiation for a brain–machine interface,” *IEEE Sensors Journal*, vol.19, no.20, pp. 9200-9205, 2019.

[139] A.O. Kaka, M. Toycan and S.D. Walker, “Circularly polarized implantable antenna characterization for retinal prosthesis systems,” *Turkish Journal of Electrical Engineering & Computer Sciences*, vol. 26, no. 3, pp. 1180-1189, 2018.

[140] A. Vorobyov, C. Hennemann, A. Vasylchenko, J. Decotignie and J. Baumgartner, “Folded loop antenna as a promising solution for a cochlear implant,” In *8th European Conference on Antennas and Propagation (EuCAP 2014)*, The Hague, 2014, pp. 1735-1738.

[141] Y. Cho and H. Yoo, “Miniaturised dual-band implantable antenna for wireless biotelemetry,” *Electronics Letters*, vol. 52, no.12, pp. 1005-1007, 2016.

[142] A. Sharma, K. Eleftherios and M.S. Reynolds, “A dual-band HF and UHF antenna system for implanted neural recording and stimulation devices,” *IEEE Antennas and Wireless Propagation Letters*, vol. 16, pp. 493-496, 2017.

[143] V.K. Gupta and D. Thakur, “Design and performance analysis of a CPW- fed circularly polarized implantable antenna for 2.45 GHz ISM band,” *Microwave and Optical Technology Letters*, vol.62, no.12, pp. 3952-3959, 2020.

[144] A.K. Skrivervik and F. Merli, "Design strategies for implantable antennas," *Proceedings of the Antennas and Propagation Conference, Loughborough, UK*, 2011.

[145] T. Karacolak, R. Cooper, J. Butler, S. Fisher, and E. Topsakal, "In vivo verification of implantable antennas using rats as model animals," *IEEE Antennas and Wireless Propagation Letters*, vol.9, pp. 334-337, 2010.

[146] A. Goel, P. Gupta and M. Agrawal, "Joint ICI cancellation and PAPR reduction in OFDM systems without side information," *Wireless Personal Communications*, vol. 71, no. 4, pp. 2605-2623, 2013.

[147] Z. Yang, L. Zhu and S. Xiao, "An implantable circularly polarized patch antenna design for pacemaker monitoring based on quality factor analysis," *IEEE Trans. Antennas Propag., vol.*66, no.10, pp. 5180-5192, 2018.

[148] Z. Xia, H. Li, Z. Lee, S. Xiao, W. Shao, X. Ding and X. Yang, "A wideband circularly polarized implantable patch antenna for ISM band medical applications," *IEEE Trans. Antennas Propag.*, vol.68, no.3, pp. 2399 – 2404, 2020.

[149] P.M. Izdebski, H. Rajagopalan and Y.R. Samii, "Conformal ingestible capsule antenna: A novel chandelier meandered design Pro," *IEEE Trans. Antennas propag*., vol.57, no.4, pp. 900–909, 2009.

[150] S. Gabriel, R.W. Lau and C. Gabriel, "The dielectric properties of biological tissues: III. Parametric models for the dielectric spectrum of tissues," *Phys. Med. Biol.*, vol.41, no.11, pp. 2271–2293, 1996.

[151] H. Rajagopalan and Y.R. Samii, "Wireless medical telemetry characterization for ingestible capsule antenna designs," *IEEE Antenna Wireless Propagation*, vol.11, pp. 1679-82, 2012.

[152] S.H. Lee, J. Lee, Y.J. Yoon, S. Park, C. Cheon, K. Kim and S. Nam, "A wideband spiral antenna for ingestible capsule endoscope systems: Experimental results in a human phantom and a pig," *IEEE Transactions on Biomedical Engineering*, vol. 58, no.6, pp. 1734-41, 2011.

[153] F.E. Hatmi, M. Grzeskowiak, S. Protat and O. Picon, "Link budget of magnetic antennas for ingestible capsule at 40 MHz," *In 6th European Conference on Antennas and Propagation (EUCAP),* Prague, 2012, pp. 1-5.

[154] X. Cheng, J. Wu, R. Blank, D.E. Senior, Y.K. Yoon, "An omnidirectional wrappable compact patch antenna for wireless endoscope applications," *IEEE Antennas Wireless Propag*. Lett., vol.11, pp. 1667–1670, 2012.

[155] M. Miah, C. Icheln, K. Haneda and A.N. Khan, "Antenna systems for wireless capsule endoscope: Design, analysis and experimental validation," *arXiv preprint arXiv:1804.01577*. 2018.

[156] L.J. Xu, Y.X. Guo and W. Wu, "Bandwidth enhancement of an implantable antenna," *IEEE Antennas and Wireless Propagation Letters*, vol.24, no.14, pp. 1510-1513, 2014.

[157] J.J. Baek, S.W. Kim and Y.T. Kim, "Camera-integrable wide-bandwidth antenna for capsule endoscope," *Sensors*, vol.20, no.1, pp. 232, 2020.

[158] Z. Bao, Y.X. Guo and R. Mittra, "An ultrawideband conformal capsule antenna with stable impedance matching," *IEEE Transactions on Antennas and Propagation*, vol.65, no.10, pp. 5086-94, 2017.

[159] C. Liu, Y.X. Guo and S. Xiao, "Circularly polarized helical antenna for ISM-band ingestible capsule endoscope systems," *IEEE Trans. Antennas Propag.*, vol. 62, no.12, pp. 6027–6039, 2014.

[160] M. Idrees, "An overview on MRI physics and its clinical applications," *International Journal of Current Pharmaceutical & Clinical Research*, vol. *4, no.* 4, pp.185-193, 2014.

[161] T.S. Ibrahim, R. Lee, B.A. Baertlein, A.M. Abduljalil, H.Zhu and P.L. Robitaille, "Effect of RF coil excitation on field inhomogeneity at ultra-high fields: A field optimized TEM resonator," *Magnetic Resonance Imaging*, vol.19, no.10, pp. 1339-1347, 2001.

[162] R.L. Barry, S.J. Vannesjo, S. By, J.C. Gore and S.A. Smith, "Spinal cord MRI at 7T," *Neuro Image*, vol.168, pp. 437-451, 2017.

[163] R.M. Shulman and B. Hunt, "Cardiac implanted electronic devices and MRI safety in 2018—the state of play," *European Radiology*, vol.28, pp. 4062–4065, 2018.

[164] S. Li, Q.X. Yang and M.B. Smith, "RF coil optimization: Evaluation of B1 field homogeneity using field histograms and finite element calculations," *Magnetic Resonance Imaging*, vol.12, pp. 1079-1087, 1994.

[165] T. Truonga, B.D. Clymerb, D.W. Chakeresa and P. Schmalbrocka, "Three-dimensional numerical simulations of susceptibility-induced magnetic field

inhomogeneities in the human head," *Magnetic Resonance Imaging*, vol.20, pp. 759–770, 2002.

[166] A.J.E. Raaijmakers, M. Italiaander, I.J. Voogt, P.R. Luijten, J.M. Hoogduin, D.W.J. Klomp and C.V. Berg, "The fractionated dipole antenna: a new antenna for body imaging at 7 Tesla," *Magnetic Resonance in Medicine*, vol.75, no. 1366–1374, 2016.

[167] A.I. Imran and T.A. Elwi, "A cylindrical wideband slotted patch antenna loaded with Frequency Selective Surface for MRI applications," *Engineering Science and Technology, an International Journal*, vol.20, no.3, pp. 990–996, 2017,

[168] J. Hoffmann, G. Shajan, J. Budde, K. Scheffler and R. Pohmann, "Human brain imaging at 9.4 T using a tunable patch antenna for transmission," *Magnetic Resonance in Medicine*, vol.69, pp. 1494–1500, 2013.

[169] B. Xu, Y. Li and Y. Kim, "Classification of finger movements based on reflection coefficient variations of a body-worn electrically small antenna," *IEEE Antennas and Wireless Propagation Letters*, vol.16, no. 1812-1815, 2017.

[170] Y. Li and Y. Kim, "Classification of human activities using variation in impedance of single on-body antenna," *IEEE Antennas and Wireless Propagation Letters*, vol.16, pp. 541-544, 2017.

[171] A. Serra, P. Nepa, G. Manara, G. Corsini, and J.L. Volakis, "A single on-body antenna as a sensor for cardiopulmonary monitoring," *IEEE Antennas and Wireless Propagation Letters*, vol.9, pp. 930-933, 2010.

[172] R. Caliskan, S.S. Gultekin, D. Uzer and O. Dundar, "A microstrip patch antenna design for breast cancer detection," *Procedia Social and Behavioral Sciences*, vol.195, pp. 2905-2911, 2015.

[173] T. Islam, M. Samsuzzaman, M.R. Faruque, J. Singh, M.T. Islam, "Microwave imaging-based breast tumor detection using compact wide slotted UWB patch antenna," *Optoelectronics and Advanced Materials – Rapid Communications*, vol. 13, no. 7-8, pp. 448-457, 2019.

[174] A. Attaran, W.B. Handler and B.A. Chronik, "12 mm radius loop antenna and linear active balun for near field measurement of magnetic field in MRI-conditional testing of medical devices," *IEEE Transactions on Electromagnetic Compatibility*, vol. 62, no.1, pp.186-193, 2019.

[175] G. Solomakha, J.T. Svejda, C.V. Leeuwen, A. Rennings, A.J. Raaijmakers, S. Glybovski and D. Erni “Self-matched leaky-wave antenna for ultrahigh-field MRI with low SAR,” *arXiv preprint arXiv:2001.10410*, 2020.

[176] E.T. Wilhelm, L.Winter, H. Han, E. Oberacker, A. Kuehne, H. Waiczies, S. Schmitter, L. Boehmert, C. Prinz, H.D. Trefna and T. Niendorf, “Wideband self-grounded bow- tie antenna for thermal MR,” *NMR in Biomedicine*, vol. 33, no.5, e4274, 2020.

[177] A. Leeor, R. Lattanzi, K. Lakshmanan, R. Brown, C.M. Deniz, D.K. Sodickson and C.M. Collins, “Transverse slot antennas for high field MRI,” *Magnetic Resonance in Medicine*, vol. 80, no.3, pp. 1233-1242, 2018.

[178] B. Mohammed, A.M. Abbosh, S. Mustafa and D. Ireland, “Microwave system for head imaging,” *IEEE Transactions on Instrumentation and Measurement*, vol.63, no.1, pp. 117-123, 2014.

[179] R. Thomas and C.L. Brace, “Interstitial microwave treatment for cancer: historical basis and current techniques in antenna design and performance,” *International Journal of Hyperthermia,* vol. 33, no.1, pp. 3-14, 2017.

[180] G. Qian, N. Wang, Q. Shen, Q. Sheng, J. Zhao, M. Kuang, G. Liu and M. Wu, “Efficacy of microwave versus radiofrequency ablation for treatment of small hepatocellular carcinoma: experimental and clinical studies*,” European radiology*, vol. 22, no.9, pp. 1983-1990, 2012.

[181] J.W. Zimmerman, H. Jimenez, M.J. Pennison, I. Brezovich, D. Morgan, A. Mudry, F.P. Costa, A. Barbault and B. Pasche, “Targeted treatment of cancer with radiofrequency electromagnetic fields amplitude-modulated at tumor-specific frequencies,” *Chinese Journal of Cancer*, vol. 32, no.11, pp. 573-81, 2013.

[182] N.V. Violi, R. Duran, B. Guiu, J. Cercueil, C. Aubé, A. Digklia, I. Pache, P. Deltenre, J.F. Knebel, A. Denys, “Efficacy of microwave ablation versus radiofrequency ablation for the treatment of hepatocellular carcinoma in patients with chronic liver disease: a randomised controlled phase 2 trial,” *The Lancet Gastroenterology & Hepatology*, vol. 3, no.5, pp. 317-325, 2018.

[183] M.B. Glassberg, S. Ghosh, J.W. Clymer, R.A. Qadeer, N.C. Ferko, B. Sadeghirad, G.W.J. Wright and J.F. Amaral, “Microwave ablation compared with radiofrequency ablation for treatment of hepatocellular and liver metastases: a

systematic reside and meta-analysis," *Onco Targets and therapy*, vol.12, pp. 6407, 2019.

[184] A.S. Wright, L.A. Sampson, T.F. Warner, D.M. Mahvi, J. Lee and T. Fred, "Radiofrequency versus microwave ablation in a hepatic porcine model," *Radiology*, vol. 236, no.1, pp. 132–139, 2005.

[185] R. Ortega-Palacios, C.J. Trujillo-Romero, M.F.J. Rubio, A. Vera, L. Leija, J.L. Reyes, M.C. Ramírez-Estudillo, F. Alvarez, M.A. Vega-López, "Feasibility of using a novel 2.45 GHz double short distance slot coaxial antenna for minimally invasive cancer breast microwave ablation therapy: computational model, phantom, and in vivo swine experimentation," *Journal of healthcare engineering*, 2018, https://doi.org/10.1155/2018/5806753.

[186] S. Labonte, A. Blais, S.R. Legault, H.O. Ali and L. Roy, "Monopole antennas for microwave catheter ablation," *IEEE Trans Microwave Theory Tech.*, vol.44, no.10, pp. 1832–1840, 1996.

[187] W. Hurter, F. Reinbold and W. Lorenz, "A dipole antenna for interstitial microwave hyperthermia," *IEEE Trans Microwave Theory Tech*., vol. 39, no.6, pp.1048–1054, 1991.

[188] I. Longo, G.B. Gentili, M. Cerretelli and N. Tosoratti, "A coaxial antenna with miniaturized choke for minimally invasive interstitial heating," *IEEE Trans Biomed Eng*., vol.50, no.1, pp. 82–88, 2003.

[189] C.L. Brace, "Dual-slot antennas for microwave tissue heating: parametric design analysis and experimental validation," Med Phys., vol.38, no.7, pp. 4232–4240, 2011.

[190] D. Liu and C.L. Brace, "CT imaging during microwave ablation: analysis of spatial and temporal tissue contraction," *Med Phys.*, vol.41, no.11, pp. 113303, 2014.

[191] C. Rossmann, E. Garrett-Mayer, F. Rattay and D. Haemmerich, "Dynamics of tissue shrinkage during ablative temperature exposures," *Physical Measure*, vol.35, no.1, pp. 55-67, 2014.

[192] V. Lopresto, R. Pinto, G.A. Lovisolo and M. Cavagnaro, "Changes in the dielectric properties of vivo bovine liver during microwave thermal ablation at 2.45 GHz," *Phys Med Biol.*, vol.57, no.8, pp. 2309, 2012.

[193] J.M. Bertram, D. Yang, M.C. Converse, J.G. Webster and D.M. Mahvi , “A reside of coaxial-based interstitial antennas for hepatic microwave ablation,” *Crit Rev Biomed Eng.,* vol.34, no.3, pp. 187-213, 2006.

[194] S.A. Shock, K. Meredith, T.F. Warner, L.A. Sampson, A.S. Wright, T.C. Winter, D. M. Mahvi, J.P. Fine and F. T. Lee, “Microwave ablation with loop antenna: in vivo porcine liver model,” *Radiology,* vol.231, no.1, pp. 143–149, 2004.

[195] B.T. McWilliams, E.E. Schnell, S. Curto, T.M. Fahrbach and P. Prakash, “A directional interstitial antenna for microwave tissue ablation: theoretical and experimental investigation,” *IEEE Trans Biomed Eng.,* vol.62, no.9, pp. 2144–2150, 2015.

[196] K. Ito, K. Saito, M. Takahashi, “Small antennas for medical applications,” *International Workshop on Antenna Technology (IWAT 2007*), Cambridge, March 2007, pp. 116-119.

[197] K. Ito, “Recent small antennas for medical applications,” *Int Workshop on IWAT* '08, Chiba, March 2008, pp. 1-4.

[198] K. Saito, H. Yoshimura, K. Ito, Y. Aoyagi and H. Horita, “Clinical trials of interstitial microwave hyperthermia by use of coaxial-slot antenna with two slots,” *IEEE Transaction Microw Theory*., vol. 52, no.8, pp. 1987-91, 2015.

[199] H. Acikgoz and I. Turer, “A novel microwave coaxial slot antenna for liver tumor ablation,” *Advanced Electromagnetics*, vol.3, no.1, pp. 20-25, 2013.

[200] C.W. Cheol, S. Lim and Y.J. Yoon, “Evaluation of transmit-array lens antenna for deep-seated hyperthermia tumor treatment,” *IEEE Antennas and Wireless Propag. Lett*., vol. 19, no.5, pp. 866-870, 2020.

[201] M.W. Little, D. Chung, P. Boardman, F.V. Gleeson and E.M. Anderson, “Microwave ablation of pulmonary malignancies using a novel high-energy antenna system,” *Cardiovascular and Interventional Radiology*, vol. 36, no.2, pp. 460-465, 2013.

[202] S. Etoz and C.L. Brace, “Analysis of microwave ablation antenna optimization techniques,” *International Journal of RF and Microwave Computer-Aided Engineering*, vol. 28, no.3, e21224, 2018.

[203] H. Acikgoz and R. Mittra, “Microwave coaxial antenna for cancer treatment: reducing the backward heating using a double choke,” *In 2015 International Symposium on Antennas and Propagation*, pp.1-4.

[204] S. Pisa, M. Cavagnaro, P. Bernardi and J.C. Lin, "A 915-MHz antenna for microwave thermal ablation treatment: physical design, computer modelling and experimental measurement," *IEEE transactions on biomedical engineering*, vol. 48, no.5, pp. 599-601, 2001.

[205] M. Lee and T. Son, "Helical Slot Antenna for the Microwave Ablation." *International Journal of Antennas and Propagation,* 2019, https://doi.org/10.1155/2019/2126879.

[206] C. Hancock, N. Dharmasiri, C.I. Duff and M. White, "New microwave antenna structures for treating gastro-oesophageal reflux disease (GERD)," *IEEE Transactions on Microwave Theory and Techniques*, vol. 61, no.5, pp. 2242-2252, 2013.

[207] G.P. Gao, C. Yang, B. Hu, R.F. Zhang, and S.F. Wang, "A wide-bandwidth wearable all-textile PIFA with dual resonance modes for 5 GHz WLAN applications*," IEEE Transactions on Antennas and Propagation*, vol. 67, no.6, pp. 4206- 4211, 2019.

[208] H. Lago, P. J. Soh, M.F. Jamlos, N. Shohaimi, S. Yan and G.A.E. Vandenbosch, "Textile antenna integrated with compact AMC and parasitic elements for WLAN/WBAN applications," *Applied Physics A*, vol.122, no.12, pp. 1059, 2016.

[209] A.K. Biswas and U. Chakraborty, "Compact wearable MIMO antenna with improved port isolation for ultra-wideband applications," *IET Microwaves, Antennas & Propagation,* vol. 13, no.4, pp. 498-504, 2019.

[210] A.K. Biswas and U. Chakraborty, "Investigation on decoupling of wideband wearable multiple-input multiple output antenna elements using microstrip neutralization line," *RF and Microwave computer Aided Engineering,* e21723, pp.1-11, 2019.

[211] S. Chouhan, D. K. Panda, P. K. Khushwah and P.K. Mishra, "Octagonal-shaped wideband MIMO antenna for human interface device and S-band application," *International Journal of Microwave and Wireless Technologies*, vol.11, no.3, pp. 287-296, 2019.

[212] S. Gotra, G. Varshney, V. S. Pandey and R. S. Yaduvanshi, Super-wideband multi-input–multi-output dielectric resonator antenna. *IET Microwaves, Antennas & Propagation, vol. 14, no.1, pp.21-27, 2019.*

[213] A. Kiourti and K. S. Nikita, “A reside of implantable patch antennas for biomedical telemetry: Challenges and solutions,” *IEEE Antennas and Propagation Magazine*, vol. 54, pp. 210–227, 2012.

[214] K. D. Prasad and D. Handa, “Antenna and Wave Propagation. 3rd ed. Satya Parkashan: New Delhi, India, 2003.

[215] K. Zhao, S. Zhang, Z. Ying, T. Bolin and S. He, “SAR study of different MIMO antenna designs for LTE application in smart mobile handsets,” *IEEE Transactions on Antennas and Propagation*, vol. 61, no. 6, pp. 3270-3279, 2013.

[216] D. Wen, Y. Hao, M. Munoz, H. Wang and H. Zhou, “A compact and low-profile MIMO antenna using a miniature circular high-impedance surface for wearable applications,” *IEEE Transactions on Antennas and Propagation*, vol. 66, no.1, pp. 96-104, 2018.

[217] G. Singh, “Double negative left-handed metamaterials for miniaturization of rectangular microstrip antenna,” *J. Electromagnetic Analysis and Applications*, Vol. 2 No. 6, pp. 347-351, 2010.

[218] M. Wang, Z. yang, J. Wu, J. Bao, J. Liu, L. Cai, T. Dang, H. Zheng and E. Li, “Investigation of SAR reduction using flexible antenna with metamaterial structure in wireless body area network,” *IEEE Transactions on Antennas and Propagation*, vol. 66, no.6, pp. 3076-3085, 2018.

[219] S. Dwivedi and P. K. Jain, "Electromagnetic Analysis of a Disk-Loaded Coaxial Waveguiding Structure for MILO," *IEEE Transactions on Plasma Science*, vol. 40, no. 4, pp. 1032-1041, 2012.

[220] B. Hazarika, B. Basu and J. Kumar, “A multi-layered dual band on-body conformal integrated antenna for WBAN communication,” *Int. J. Electron. Commun. (AEÜ)*, vol. 95, pp. 226-235, 2018.

[221] U. Illahi, J. Iqbal, M. I. Sulaiman, M.M. Alam, M.M. Su’Ud, M.H. Jamaluddin and M.N. Yasin, “Design of new circularly polarized wearable dielectric resonator antenna for off-body communication in WBAN applications,” *IEEE Access*, vol.7, pp. 150573-150582, 2019.

[222] A. Iqbal, A. Basir, A. Smida, N.K. Mallat, I. Elfergani, J. Rodriguez and S. Kim, “Electromagnetic bandgap backed millimeter-wave MIMO antenna for wearable applications,” *IEEE Access*, vol. 7, pp. 111135-111144, 2019.

[223] A.Al-Sehemi, A. Al-Ghamdi, N. Dishovsky, N. Atanasov and G. Atanasova, “Design and performance analysis of dual-band wearable compact low- profile

antenna for body-centric wireless communication," *International Journal of Microwave and Wireless Technologies*, vol.10, no.10, pp. 1175-1185, 2018.

[224] A. Mersani, O. Lotfi, and J.M. Ribero, "Design of a textile antenna with artificial magnetic conductor for wearable applications," *Microwave Optical and Technology Letter*, vol. 60, pp. 1343-1349, 2018.

[225] F. Capolino. (2009). Theory and phenomena of metamaterials. Taylor & Francis.

[226] N. Jaglan, S.D. Gupta, B. K. Kanaujia and S. Srivastava "Band notched UWB circular monopole antenna with inductance enhanced modified mushroom EBG structures," *Wireless Networks*, vol. 24, no.2, pp. 383-393, 2016.

[227] Z.H. Jiang, M.D. Gregory and D.H. Werner. "A broadband monopole antenna enabled by an ultrathin anisotropic metamaterial coating," *IEEE Antennas Wirel Propag Lett.*, vol.10, pp. 1543-1546, 2011.

[228] C.R. Simovski, P.D. Maagt and I.V. Melchakova "High-impedance surfaces having stable resonance with respect to polarization and incidence angle," *IEEE Trans Antennas Propagation*, vol.53, no.3, pp. 908-914, 2005.

[229] L. Zhou, S. Fang and X. Jia, "Dual-band and dual-polarised circular patch textile antenna for on-/off-body WBAN applications." *IET Microwaves, Antennas & Propagation*, vol.14, no.7, pp. 643-648, 2020.

[230] S. Bhattacharjee, M. Midya, M. Mitra, and S.R.B. Chaudhuri, "Dual band-dual polarized planar inverted F-antenna for MBAN applications," *International Journal of Microwave and Wireless Technologies*, vol. 11, no.1, pp. 76-86, 2019.

[231] R. Verma and N.P. Singh, "GRA based network selection in heterogeneous wireless networks," *Wireless personal communications*, vol. 72, no. 2, pp.1437-1452, 2013.

[232] M. K. Magill, G. A. Conway and W. G. Scanlon, "Circularly polarized dual-mode wearable implant repeater antenna with enhanced into-body gain," *IEEE Transactions on Antennas and Propagation*, vol.68, no.5, pp. 3515-3524, 2020.

[233] C. Zhao and W. Geyi, "Design of a dual band dual mode antenna for on/off body communications," *Microwave and Optical Technology Letters*, vol.62, no.1, pp. 514-520, 2020.

[234] K.N. Paracha, S.K.A. Rahim, P.J. Soh, M.R. Kamarudin, K.G. Tan, Y.C. Lo and M.T. Islam, "A low profile, dual-band, dual polarized antenna for indoor/outdoor wearable application," *IEEE Access*, vol.7, pp. 33277-33288, 2019.

[235] Y. Yoon and B. Kim, "A new formula for effective dielectric constant in multi-dielectric layer microstrip structure," *IEEE 9th tropical meeting on electrical performance of electronic packaging,* 2010.

[236] R. Garg, I. Bahl and M. Bozzi, "Microstrip Lines and Slotlines," 3rd ed., *Archtech House Publication,* 1996.

[237] C.A. Balanis, "Antenna Theory Analysis and Design," *Hobonken, New Jersy, 3rd ed, A John Wiley & Sons, Inc. Publication,* 2005.

[238] T. Singh, M.N. Stevanovic and B. Kolundzija, "Survey and classification of antennas for medical applications," *In 13th European Conference on Antennas and Propagation (EuCAP)*, Krakow, Poland 2019, pp. 1-5.

[239] K. Ito,"Recent antenna technology for medical applications," *In the Second European Conference on Antennas and Propagation, EuCAP* ,2007, pp.10-11.

[240] I. Malhotra, R.K. Jha and G. Singh, "Terahertz antenna technology for imaging applications: A technical review." *International Journal of Microwave and Wireless Technologies*, vol. *10, no.*3, pp. 271-290, 2018.

[241] M. Lazebnik, L. McCartney, D. Popovic, C.B. Watkins, M.J. Lindstrom, J. Harter, S. Sewall, A. Magliocco, J. H. Booske, M. Okoniewski and S.C. Hagness, "A large-scale study of the ultrawideband microwave dielectric properties of normal breast tissue obtained from reduction surgeries," *Physics in medicine and biology*, vol.52, no.10, pp. 2637-2656, 2007.

[242] S.K. Davis, V. Veen, B.D. Hagness and F. Kelcz, "Breast tumour characterization based on ultrawideband microwave backscatter," *IEEE Transactions on Biomedical Engineering,* vol.55, pp. 237-246, 2008.

[243] E.I. Misilmani, T. Naous, Al Khatib, K.Y. Kabalan, "A survey on antenna designs for breast cancer detection using microwave imaging," *IEEE Access*, vol. 8, pp. 102570-94, 2020.

[244] O. Koistinen, H. Valmu, A. Raisanen, J. Talvela and M. Halikainen, "A Radiometer for Ground-Based Detection of Stratospheric Ozone at 110 GHz," *22nd European Microwave Conference*, Helsinki, Finland, pp. 1231-1233, 1992.

[245] M. Islam, M. Samsuzzaman, M. Islam, S. Kibria, M.J.S. Singh, "A homogeneous breast phantom measurement system with an improved modified microwave imaging antenna sensor," Sensors, Vol.18, no.1, pp. 2962, 2018.

[246] Z. Mahmud, M. Islam, N. Misran, S. Kibria and M. Samsuzzaman, "Microwave imaging for breast tumour detection using unipolar AMC based CPW fed microstrip patch," *IEEE Access*, vol.6, pp. 44763–44775, 2018.

[247] H. Kanj and M. Popovic, "Miniaturized microstrip-fed dark eyes antenna for near-field microwave sensing," *IEEE Antennas and Wireless Propagation Letters*, vol. 4, pp.397–401, 2005.

[248] G. Pandey, H. Verma and M. Meshram, "Compact antipodal vivaldi antenna for UWB applications," *Electronics Letters*, vol.51, pp. 308–310, 2015.

[249] I.T. Nassar and T.M. Weller, "A novel method for improving antipodal vivaldi antenna performance," *IEEE Transactions on Antennas and Propagation*, vol. 63, pp. 3321–3324, 2015.

[250] S.S. Tiang, M.S. Hathal, T.F. Zanoon, M.F. Ain, M.Z. Abdullah, "Radar sensing featuring biconical antenna and enhanced delay and sum algorithm for early-stage breast cancer detection," *Progress in Electromagnetics Research*, vol. 46, pp. 299-316, 2013.

[251] V. Selvaraj, D. Baskaran, P.H. Rao, P. Srinivasan and R. Krishnan, "Breast tissue tumour analysis using wideband antenna and microwave scattering," *IETE Journal of Research*, vol.23, pp. 1-11, 2018.

[252] B. Wu, Y. Ji and G. Fang, "Design and measurement of compact tapered slot antenna for UWB microwave imaging radar," *In Electronic Measurement & Instruments*, 9^{th} International Conference, 2009; 2-226-222-229 (IEEE).

[253] M. J. Burfeindt, N. Behdad, B.D. Van Veen, S. C. Hagness, "Quantitative Microwave imaging of realistic numerical breast phantoms using an enclosed array of multiband, miniaturized patch antennas," *IEEE Antennas Wireless Propag. Lett.*, vol. 11, pp. 1626-1629, 2012.

[254] M. koutsoupidou, I. S. Karanasiou, C. G. Kakoyiannis, E. Groumpas, C. Conessa, N. Joachimowicz, "Evaluation of a tumor detection microwave system with a realistic breast phantom," *Microwave and Optical Technology Letters*, vol. 59, pp. 6-10, 2017.

LIST OF PUBLICATIONS

Published Papers

1. A. Gupta, A. Kansal, P. Chawla “Design of a patch antenna with square ring-shaped coupled ground for on-/off body communication.” International Journal of Electronics, vol.106, no.12, pp.1214-1228, 2019.
2. A. Gupta, A. Kansal, P. Chawla “Design of A Wearable MIMO Antenna Deployed with An Inverted U-Shaped Ground Stub for diversity performance enhancement.” International Journal of Microwave and Wireless Technologies, vol.13, no.1, pp.76-86. 2020.
3. A. Gupta, A. Kansal, P. Chawla “Design and performance analysis of L-shaped ground and radiator antenna with a metallic reflector for WBAN.” International journal of Electronics, 2020. https://doi.org/10.1080/00207217.2020.1793408
4. A. Gupta, A. Kansal, P. Chawla “Design of a compact dual band antenna for on-/off body communication” IETE Journal of Research, 2020. https://doi.org/10.1080/03772063.2020.1845826
5. A. Gupta, A. Kansal, P. Chawla “A Survey and classification on Applications of antenna in health care domain: signal transmission, diagnosis and treatment.” Sadhana Journal, vol. 46:68, 2021, https://doi.org/10.1007/s12046-021-01586-4
6. A. Gupta, A. Kansal, P. Chawla, K. Singh “An Active and Low-Cost Microwave Imaging System design for Detection of Breast Cancer Using Back Scattered Signal” Current Medical Imaging, 2021, https://doi.org/10.2174/1573405617666210129114536

Communicated Paper

7. A. Gupta, A. Kansal, P. Chawla “A compact antenna structure with AMC reflector for on-body communication” International Journal of Electronics, TETN-2021-0476.
8. A. Gupta, A. Kansal, P. Chawla “Implementation of Defected Ground Circular Polarized Antenna for WLAN” International Journal of Electronics Letter, TETL-2021-0477.